Probing many-body localization with ultracold atoms in optical lattices
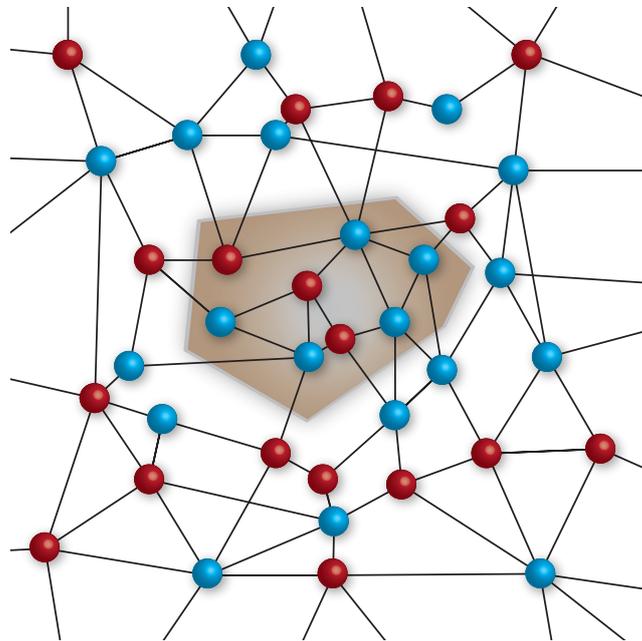
Pranjal Bordia

München 2017

Probing many-body localization with ultracold atoms in optical lattices

Dissertation der Fakultät für Physik
der Ludwig-Maximilians-Universität München

vorgelegt von

Pranjal Bordia

geboren in Udaipur, Indien

München, 05. April 2017

Contents

viii   Table of Contents

Zusammenfassung

Diese Doktorarbeit befasst sich mit der Realisierung nicht-ergodischer Zustände ultrakalter Atome in quasi-periodischen optischen Gittern mit einem zweikomponentigen, wechselwirkenden, fermionischen Gas aus Kalium-40-Atomen in einer und zwei Dimensionen. Die Ergebnisse zeigen hochangeregte, nicht-thermalisierende Zustände in isolierten Quantensystemen. Unsere Beobachtungen lassen sich mit dem Phänomen der Vielteilchenlokalisierung erklären – einer nicht-ergodischen Phase der Materie, deren Eigenschaften mittels dynamischer Observablen detektiert werden können.

Zur Untersuchung einer solchen Phase präparieren wir zunächst einen Nichtgleichgewichtszustand und beobachten wie dessen Merkmale während der Zeitentwicklung verloren gehen. So können mehrere Parameterbereiche und Zeitskalen identifiziert werden, in denen lokale Quanteninformationen aufgrund der Unordnung erhalten bleiben und von Parameterbereichen unterschieden werden, in denen lokale Informationen mit Hilfe von Wechselwirkungen in hochgradig nichtlokale Quantenkorrelationen umgewandelt werden. Wir zeigen, wie die Beschreibung isolierter Quantensysteme in allen Experimenten systematisch zusammenbricht, da das System (notwendigerweise) an eine badähnliche Struktur gekoppelt ist. Des Weiteren wird gezeigt, dass Lokalisierung auch in periodisch getriebenen Quantensystemen existieren kann, von denen bis vor kurzem angenommen wurde, dass sie sich immer entsprechend einem Zustand unendlicher Temperatur verhalten. Wir ermöglichen die experimentelle Erforschung ungeordneter Systeme in zwei Dimensionen und zeigen die Existenz einer nicht-trivialen Dynamik, die als Zusammenspiel von Wechselwirkungen, Störungen und Dimensionen auftritt. Nach der Untersuchung eines mutmaßlichen Übergangs zeigen wir weitere Signaturen einer neuen Art langsamer Relaxation, die möglicherweise auf Unordnung im Anfangszustand züruckzuführen ist. Wir schließen die Diskussion mit einigen theoretischen Ergebnissen zur Untersuchung der Quantendynamik in Abwesenheit von Transport und diskutieren vielversprechende zukünftige Experimente.

Abstract

This thesis reports on first experiments on the observation of ergodicity breaking in a two-component, interacting fermionic gas of Potassium-40 subject to quasi-periodic optical lattices in one and two dimensions, demonstrating the breakdown of thermalization in highly excited states of isolated quantum systems. Our observations can be explained by the phenomenon of many-body localization, a non-ergodic phase of matter, whose properties can be detected with non-equilibrium probes.

To probe such a phase, we first design a far-from-equilibrium initial state and then monitor how much the system remembers of this design during time evolution. This allows us to identify regimes and timescales where disorder can protect local quantum information and distinguish such cases from regimes where interactions amalgamate local information into highly nonlocal quantum correlations. We then describe how this treatment systematically breaks down in all real-world systems as the system is (necessarily) coupled to some bath-like structure. Following very recent developments, we are further able to show that order can exist even in driven quantum systems, which were earlier thought to exhibit no interesting features, corresponding to an infinite temperature state. We also extend the experimental realm to explore two dimensions and show that the dynamics emerge as a distinct interplay of interactions, disorder, and dimensions. Upon probing a putative MBL transition, we further show signatures of a new kind of slow relaxation, potentially arising due to randomness in the initial state. We close with some theoretical results on probing quantum dynamics ensuing in the absence of transport and a discussion of exciting areas for future experiments.

Introduction

Ground states of quantum many-body systems and their low-energy excitations host myriad exciting quantum phenomena [1], including superconductivity [2], superfluidity [3–5], quantum Hall effects [6, 7] and Bose-Einstein condensation [8–10]. Understanding the nature of these phases forms the basic tenet of many-body physics. Conventionally, these phases have been described utilizing the notions of *equilibrium* statistical physics. This allows for the classification of quantum phases according to patterns of local orders emerging via Spontaneous Symmetry Breaking (SSB) [11] and more recently, according to various classes of topological orders [12–14]. Both of these classifications come with some general constraints. Most topological insulators, e.g. the integer quantum Hall insulator, possess a bulk gap. For systems exhibiting true long-range local order via SSB such as ferromagnets, the Mermin–Wagner theorem [15–17] prohibits their existence at finite temperatures in lower dimensions.

Different quantum phases are disconnected from each other via Quantum Phase Transitions (QPTs), where the system undergoes macroscopic rearrangements at *zero temperature* as a parameter in the Hamiltonian is tuned [18, 19]. An exemplary case is the Bose-Hubbard Model which exhibits a QPT as the ratio of kinetic energy to on-site repulsion is tuned [20]. For large kinetic energies, the system is in a symmetry broken superfluid (SF) state, while for large on-site repulsion the system is in a Mott-insulating (MI) phase. These two phases have very different qualitative properties. In a QPT, it is useful to identify a quantity called the order parameter, which undergoes a singular (non-analytic) change at the phase transition. Multiple order parameters can characterize the phase, such as the energy gap between the ground and the first excited state or the incompressibility of the MI phase. At zero temperature, this order parameter has a non-zero value in the MI phase, and becomes *exactly zero* outside it. The SF, on the other hand, is characterized as a compressible, gap-less state with long-range order. Hence, the two phases have qualitatively very different properties.

Recent progress on Many-Body Localization (MBL) [21–23] shows that several of these ideas are incomplete. The existence of MBL states implies the existence of genuinely new, and distinct phases of quantum matter in *highly excited states* and in *lower-dimensions*, whose signatures are not captured by equilibrium thermodynamics, but instead by *non-equilibrium dynamics*. MBL generalizes the idea of localization of single particles due to quenched disorder (Anderson Localization (AL) [24]) to interacting particles and describes a non-ergodic phase present in highly excited states. Further, MBL itself can be

of different kinds and can exhibit phases with SSB or topological order [25–27]. Such phenomena strongly violate the expectation from the Mermin-Wagner type arguments, generally ruling out SSB in lower dimensions as well as realizing the possibility of topological order even in a *gapless bulk*. In an MBL system, the localization of excitations, allows order to persist in highly excited states, contrary to the predictions of equilibrium thermodynamics.

The transition from a thermalizing phase to an MBL phase itself has attracted enormous interest [28–37]. On one side of the transition, ergodicity prevails, and the system has notions of temperature and thermodynamics, and eigenstates are expected to follow the Eigenstate Thermalization Hypothesis (ETH) [34, 38]. In such an ergodic time evolution, *local* degrees of freedom becomes fully entangled with the rest of the system, leading to an effectively classical description, with only slow hydrodynamic modes surviving at long times [39]. On the other side of the transition, quantum correlations can persist locally for arbitrarily long times. Since the transition lies outside the purview of traditional statistical mechanics, a variety of novel tools have been developed to understand such an ETH violating phase [22, 23, 40]. Further, dynamical order parameters characterize these phases, instead of thermodynamic ones, and there are indications that these even change abruptly across the transition [41, 42].

All the references mentioned above about MBL are theoretical. In many ways, this is naturally connected to a *necessary* requirement for the existence of the phase: that there should be no underlying bath in the system. In traditional condensed matter systems, lattice phonons provide such a bath and lead to Mott's variable range hopping phenomena [43] instead of AL. Moreover, such phonons are highly effective at high temperatures at delocalizing the otherwise localized states (both AL and MBL). In general, any dissipative coupling to the outside world is expected to thermalize the MBL phase eventually [21]. This implies that perfect MBL can only exist in perfectly isolated systems, which, unfortunately, do not exist. This is reminiscent of QPTs, which are exactly defined only at zero temperature [18] and hence, do not exist in the real world. However, properties of quantum systems at low enough temperatures can be understood by their zero temperature quantum phases and QPTs up to a certain *frequency scale*. In the same spirit, even though perfectly isolated systems do not exist, the properties of almost isolated systems can be understood by their isolated limits up to a certain *time scale*.

Synthetic quantum systems provide ideal test beds for such theories due to their high degree of isolation and versatile control of almost all the microscopic parameters. Experimental platforms such as ultracold atoms [44], ions [45], hybrid quantum circuits utilizing superconducting q-bits [46] and nitrogen-vacancy centers [47] are continuously separated from their surroundings to both increase their potential to perform digital computations [45], as well as to provide exciting areas to explore foundational questions in quantum physics [48]. In these systems, the timescales of internal dynamics are well separated from the timescales at which they couple to the environment. Up to such times, they are expected to show one of the two generic behaviors: thermalization via entanglement with the rest of the system [49–52] or many-body localization.

Ultracold atoms in optical lattices

Owing to the remarkable progress in laser cooling of neutral atoms in vacuum chambers [53–55], multiple groups were able to reach quantum degeneracy in bosonic atomic alkali gases [56] in the mid-90s, followed by DeMarco and Jin reaching degeneracy with an ultracold fermionic gas of Potassium-40 [57]. These bulk gases were then successfully used as constituents for assembling lattice models. Following the proposal of Ref. [58], a landmark experiment showed a QPT from a Mott-insulator to a superfluid in 2001 in the group of T. Hänsch [59]. This work demonstrated the potential of ultracold atoms to perform quantum simulations of many-body lattice Hamiltonians by allowing the realization of (almost) an ideal Bose-Hubbard model.

To achieve this, the bosonic atoms were trapped in periodic potentials formed by laser light called an optical lattice. The resulting system allowed a wide tuning range for the parameters of the Hamiltonian. This, coupled with long coherence times compared to the natural timescales of the system, facilitated the realization of an almost ideal non-dissipative quantum system. An outbreak of experimental results followed, including realizations of the fermionic Mott-insulator [60, 61]. These systems of fermions in optical lattices in the strongly correlated regime opened up possibilities for further simulations of condensed matter phenomena [62]. Two hallmark experiments [63, 64], one with a quasi-periodic potential and one with a real-random potential, demonstrated that neutral ultracold atoms can be employed to probe effects of disorder in a controlled manner. With a new platform to probe Anderson localization, new observables could be employed to probe the effects of disorder. Such experiments were able to directly show an exponentially localized density distribution, a distinctive feature of Anderson localization. Moreover, interactions could be readily introduced in these systems, and hence, they provided a novel platform for exploring interacting many-body disordered systems [65–68].

Ultracold atoms are thus being described as quantum simulators, in many ways according to the line of thought of R. Feynman [69]. In many niches, these new systems possess a natural advantage over even established methods. For example, they are natural systems to study dynamics, especially in higher dimensions in a controlled manner. In the context of MBL, this becomes even more relevant, as some of the most successful methods, such as the stochastic method [70] and matrix-product-state type algorithms [71], find it extremely challenging to capture the dynamics in highly excited energy states in higher dimensions. On the experimental side, in real materials, the effects of the underlying phonon bath is usually too strong to leave signatures of MBL. In this thesis, we describe how ultracold fermions in quasi-periodic optical lattices can be used to probe many-body localization in a highly coherent manner, with almost complete control over the interaction and the disorder. This is achieved by preparing an artificial density-wave and monitoring its relaxation dynamics. We describe the requirements to create such a phase of matter and demonstrate its features. Our experiments reveal dynamics in regimes which are often not accessible to state-of-the-art numerical simulations.

Contents of this thesis

We remark that unlike the results of many previous experiments with ultracold atoms, the fundamental physics which describe our experiments is itself currently not fully understood and little is known with certainty. Therefore, not only is the relevant physics being *demonstrated* in such artificial systems for the first time, but in many ways, we are even *knowing* them for the first time. On the one hand, this makes the subject extremely exciting, but at the same time, care must be taken to read the current interpretations, as it is necessarily subject to the best of my comprehension of the performed experiments and the limitations of experimental data.

In this thesis, the current theoretical understanding is summarized, and the experimental progress on probing many-body localization with ultracold atomic gases in one and two dimensions is reported. The results are explained with a particular emphasis on understanding the role of real experimental platforms. As much as possible, the details of the experiments which might be too technical, are provided in separate chapters, for a clear presentation of experimental results. Moreover, the field of MBL originally developed with a strong theoretical purview and only with the recent advances in isolating quantum systems have experiments started to explore this interesting regime. Therefore, many of the theoretical notions are translated to what we understand will be more easily accessible to experimentalists. To achieve this in an orderly fashion, this thesis is divided into 10 Chapters. The initial chapters are devoted to explaining the necessary theoretical concepts required to interpret the experimental results. The later chapters describe the experimental results along with their interpretations and limitations.

Chapter 2 is devoted to taking the textbook notions of thermodynamics and statistical mechanics to the realm of interacting isolated systems, under the purview of the Eigenstate Thermalization Hypothesis (ETH). In generic interacting systems, ETH represents an extreme form of the *equivalence of ensembles* and allows the usage of the machinery built for traditional statistical mechanics directly to isolated quantum systems, without necessitating the notion of an underlying bath or ensemble averaging. **Chapter 3** explains the basics of *Anderson localization*, providing simple illustrations to describe localization of single particles in disordered lattices [24].

While Chapter 2 espouses that interactions in isolated systems cause thermalization, Chapter 3 proposes that disorder can make the system highly non-ergodic. In **Chapter 4**, these two mechanisms are put to compete against one another. This leads to Many-body localization (MBL) wherein interactions can indeed turn a system thermal, but only if the disorder is weak. On the other hand, if the disorder is strong enough, the system fails to thermalize and becomes MBL. We describe many exotic properties of this phase such as the absence of transport due to localization and a slow growth of quantum correlations (which saturate to sub-thermal values).

The experimental apparatus is introduced in **Chapter 5**. For all experiments, we have used fermionic Potassium-40 atoms (^{40}K). The atoms are laser cooled in a dual-species Magneto-Optical Trap with bosonic Rubidium-87 (^{87}Rb) in a vacuum chamber, followed by a magnetic transfer to another vacuum chamber with a lower background pressure. Subsequently, they are evaporatively cooled in a magnetic trap. They are then transferred

into an optical dipole trap and evaporatively cooled further. In the final stage, the ^{87}Rb atoms are removed, leaving behind a pure fermionic ^{40}K gas, which is then loaded into optical lattices of various configurations. We then argue how this turns the system into almost ideal lattice models. Importantly, the preparation of a far-from-equilibrium state is described, necessary for probing the dynamical structure of the different Hamiltonians. For the read-out, a specific band-mapping sequence is described. This finishes the necessary theoretical, and experimental background and the following chapters will utilize them to describe and interpret experimental results.

Chapter 6 describes the first experiments performed in our group to probe MBL, wherein an underlying quasi-periodic potential serves as the disorder. Results on how an isolated system, pulled far away from equilibrium may *not* relax to a thermal state are presented. This is captured quantitatively with the relaxation of the density-wave and benchmarked against numerical simulations, providing additional support for the experimental prowess. Our results explore the role of energy density, interactions, and disorder, providing an almost complete description of the Hamiltonian in highly excited states. Most results are supported by numerical calculations, which show very good agreement.

Chapter 7 explores the effect of a controllable bath-like effect by coupling identical MBL systems with each other, providing benchmarks in regimes not directly accessible to numerical simulations. We show that this technique can be used to distinguish interacting and non-interacting systems. It suggests that non-thermal but interacting systems (including MBL) in d dimensions should generically get *destabilized* and transform into thermal systems in $d+1$ dimensions under such a coupling. Further, non-interacting, non-thermal systems (including AL) remain *stable* under such a coupling and retain their features.

Having explored features in *static* systems up to now, in **Chapter 8**, a more general class of systems are described, whose Hamiltonians are periodic in time, called Floquet systems. The generalization of ETH in the Floquet-setting is presented, generically leading to a heat death. An exception is provided by MBL systems, protected from heating due to locality but it was theoretically argued to hold only if the drive frequency is high enough. We show evidence for such a drive-induced delocalization at finite frequency. Interestingly, the experiment reveals a new regime, which remains exceedingly stable even at low frequencies, and is still not fully understood. The role of the functional form of the drive is highlighted, as well as the non-universality in the emerging descriptions.

To go beyond all these cases built on the one-dimensional MBL case, **Chapter 9** describes a *two-dimensional* system with quasi-periodic potentials along both directions. The two orthogonal directions are separable in the non-interacting case, which allows us to set clear benchmarks. The relaxation is then explored, in the case of interacting systems and special emphasis is put on probing the dynamics near a possible MBL critical point. We also report the impact of interaction and energy-density on the ensuing dynamics.

All the results mentioned above are related to particle transport. Finally, in **Chapter 10**, some theoretical calculations are presented which might make it possible to study quantum dynamics that ensue even in the *absence* of transport. These are based on generalizations of out-of-time-ordered measurements, requiring time-reversal of the Hamiltonian. However, it does not require two identical copies of the quantum system.

Publications

From the works which report the results obtained during my time as a graduate student, the following are described in this thesis:

- Michael Schreiber, Sean S. Hodgman, **Pranjal Bordia**, Henrik P. Lüschen, Mark H. Fischer, Ronen Vosk, Ehud Altman, Ulrich Schneider, and Immanuel Bloch. *Observation of many-body localization of interacting fermions in a quasirandom optical lattice.* Science, 349(6250):842–845, 2015 [72]

- **Pranjal Bordia**, Henrik P. Lüschen, Sean S. Hodgman, Michael Schreiber, Immanuel Bloch, and Ulrich Schneider. *Coupling identical one-dimensional many-body localized systems*. Physical Review Letters, 116:140401, Apr 2016 [73]

- **Pranjal Bordia**, Henrik P. Lüschen, Ulrich Schneider, Michael Knap and Immanuel Bloch. *Periodically driving a many-body localized quantum system*. Nature Physics (2017), doi:10.1038/nphys4020 [74]

- **Pranjal Bordia**, Henrik P. Lüschen, Sebastian Scherg, Sarang Gopalakrishnan, Michael Knap, Ulrich Schneider, and Immanuel Bloch. *Probing Slow Relaxation and Many-Body Localization in Two-Dimensional Quasi-Periodic Systems*, Preprint on arXiv:1704.03063 [75]

- **Pranjal Bordia**, Fabien Alet, Pavan Hosur. *On probing quantum dynamics in interacting localized systems*, in prep.

The following are not described in this thesis:

- Henrik P. Lüschen, **Pranjal Bordia**, Sean S. Hodgman, Michael Schreiber, Saubhik Sarkar, Andrew Daley, Mark Fischer, Ehud Altman, Immanuel Bloch, and Ulrich Schneider. *Signatures of Many-Body Localization in a Controlled Open Quantum System*, Physical Review X, 7, 011034, March 2017, [76]

- Henrik P Lüschen, **Pranjal Bordia**, Sebastian Scherg, Fabien Alet, Ehud Altman, Ulrich Schneider, Immanuel Bloch, *Evidence for Griffiths-Type Dynamics near the Many-Body Localization Transition in Quasi-Periodic Systems*, Preprint on arXiv:1612.07173 [77]

Emergence of Thermodynamics in Isolated Quantum Systems

Short summary: The chapter introduces the notion of thermalization in closed and isolated quantum systems and overviews the basic ideas developed under the umbrella of the Eigenstate Thermalization Hypothesis. In particular, their implication on the experimental observables is discussed.

2.1   Introduction

All micro(and macro)-scopic systems are coupled to their surroundings. This coupling could be very weak but is nonetheless, non-zero. The surroundings are themselves, in principle, some quantum system consisting of a large number of particles. To describe this, one can often approximate the surroundings to have a "bath-like" effect on the system, i.e. it acts like a Markovian source-drain (for particles/energy, etc.) and effectively provides a temperature to the system. Using this assigned temperature and assuming ergodicity, one can obtain the results of statistical mechanics, providing the necessary link to connect the microscopic variables to macroscopic observables, as a natural result of probabilistic chances when a large collection of particles is considered. However, several recently developed quantum systems, such as ultracold atoms, are not very well coupled to their surroundings and one is quite interested in timescales on which they are effectively completely isolated. One can ask if even such isolated quantum systems thermalize and if yes, what is the notion of temperature, ergodicity, and thermalization in such systems?

The Eigenstate Thermalization Hypothesis (ETH) seeks to provide answers to such questions and describes a set of ideas which posit how, when and why isolated quantum systems can be accurately described by using the concepts of *equilibrium* statistical mechanics. In particular, one seeks to answer questions such as, how fast a far-from-equilibrium state can approach a state which appears to be in *equilibrium* and *thermalized* and what it means to say that the system thermalizes. Isolating many of these notions is useful to compare and contrast them.
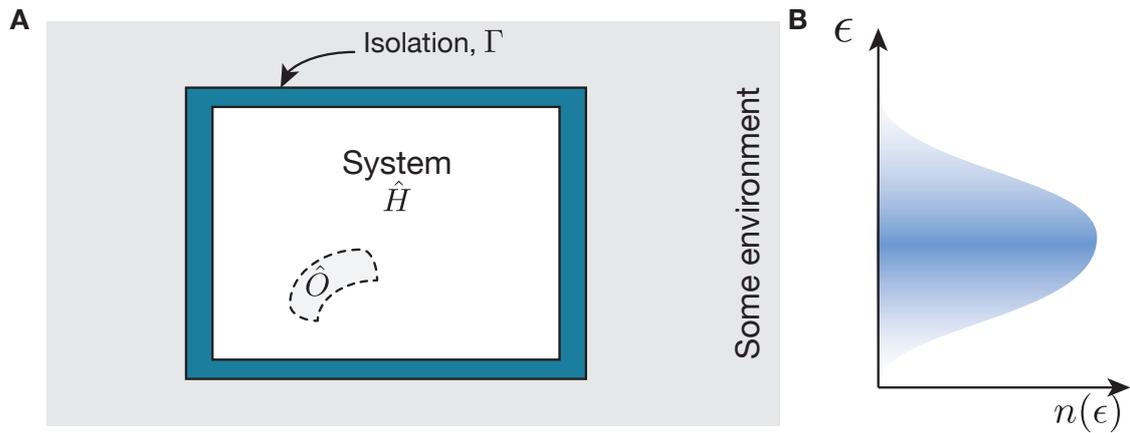
Figure 2.1: Isolated quantum systems, A: Schematic illustrating a quantum system $\hat{H}$, such as ultracold quantum gases in optical lattices, which can be approximated as well isolated from all other systems (e.g. environment) at certain timescales. This isolation can be parametrized with some (necessarily non-zero) dissipative coupling $\Gamma > 0$ and the system is said to be isolated for all times which are much smaller compared to the inverse of such a coupling $t \ll 1/\Gamma$. **Energy density in a many-body system, B:** Typical plot of the density of states $n(\epsilon)$ of a many-body system with a bounded energy density, ϵ. Almost all of the states lie in the middle of the spectrum (darker blue). Finite energy density states are depicted with blue color. Towards the end of the spectrum they fade to zero energy density states (white color).

2.2   Isolated quantum systems

As remarked earlier, all systems are coupled to some other system in the universe. In this sense, the only (maybe also not) isolated system would be the universe. This is not a useful notion. In general, to define a practical notion of an isolated quantum system one would like to assume some (a very weak but non-zero) coupling to the environment, $0 < \Gamma \ll 1$, see Fig. 2.1 **A**. From the standard notions of statistical mechanics described above, the system is expected to thermalize on timescales which are much larger than the inverse coupling, i.e. $t \gg 1/\Gamma$. It means that the system, once taken out of equilibrium at some point, will return to thermal equilibrium at those timescales. However, the interesting question is what happens to the system at timescales which are much shorter than the inverse coupling scale, i.e. $t \ll 1/\Gamma$ and whether the system still thermalizes, without the coupling to the environment, already on timescales much smaller than the inverse coupling? Hence, the expected hierarchy of timescales would be the following:

$$t_{\text{isolated}} \ll t_{\text{crossover}} \sim 1/\Gamma \ll t_{\text{thermal}} \tag{2.1}$$

At times $t < t_{\text{isolated}}$, the system is called isolated and is describable by unitary Hamiltonian evolution, where one would like to ask about thermalization without a bath at $t \sim t_{\text{isolated}}$. The crossover to the regime of $t \sim t_{\text{crossover}}$ is also explored in this thesis by implementing a controlled coupling Γ, see Chapter 7. At long times $t \sim t_{\text{thermal}}$, thermalization is always expected via an external bath.
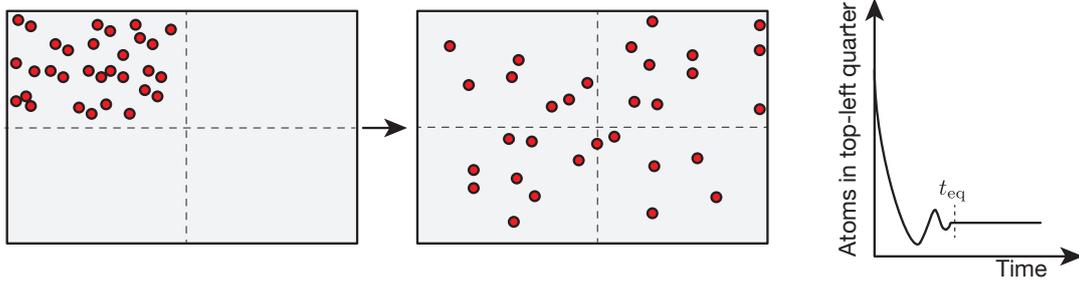
Figure 2.2: Equilibration of an observable: An observable of the system is said to be equilibrated when the expectation value of the observable does not change appreciably with time. This is illustrated with the following example. Consider a gas of atoms initialized on the top left quarter of a box, and we monitor the number of atoms in that quarter as a function of time. After long times the gas would expand to occupy the whole box and the atom numbers in any area, including the top-left quarter, would become stationary. This would happen after some time t_{eq}, which will depend on details, such as the system size, the measured observable and the initial state. After this period, this observable has equilibrated. Additionally, if the equilibrated value of the observable is also the same as expected from a thermal distribution, the observable is said to have a thermal expectation value. In this sense, equilibration is a prerequisite for thermalization.

2.3 Equilibration

The notion is adapted from Ref. [52]. Imagine that a system is not prepared in an eigenstate, but instead in a far-from-equilibrium state. In particular, it is not a thermal state either (i.e. not Boltzmann distributed), but a generic superposition of many eigenstates. For example, one can take a gas of atoms in a box, and put it in the top left quarter of the box, see Fig. 2.2.

One would like to time evolve this state and say that the system equilibrates if the system evolves in such a way that the expectation values of all observables do not change with time appreciably for almost all times. Note that it does not have to become stationary to the value obtained from a *thermal* distribution at the same energy, but only become stationary so that the fluctuations are very small. If it happens, one can also define a timescale for this and call it the equilibration time, t_{eq}. This means for example that the released gas then occupies the entire box and afterwards almost *never* goes back to the top left quarter again, and the number of atoms in the top left quarter of the box does not change with time. The equilibrated value of an observable may or may not be the same as the expectation from a thermal ensemble. If, however, it is, the observable is said to follow the thermal expectation value. In this sense, equilibration is a prerequisite for thermalization. Note that different observables can have very different equilibration times t_{eq} and this has important observable consequences on the system. At this point, it appears that all time-independent systems, which are not fine-tuned, have observables which show equilibration (including MBL systems); however, the distinctions can lie in *how* they equilibrate and *if* they thermalize.

2.4   Thermalization

We call the system thermal, if the equilibrated state is such that the expectation value of all observables can be accurately determined by assuming a single temperature T and calculating *all* observables from this with a Boltzmann density matrix, fully recovering the results of statistical mechanics. This definition of thermalization would permit that as long as one can find one observable that does not show the same behavior as expected from thermal behavior, the system is non-thermal. This statement will be utilized to demonstrate the non-thermal behavior of the MBL state with a very simple local observable. However, showing *thermalization* of a large system is very challenging, as it is in general prohibitively difficult to measure the density matrix of a large system [78]. While such results have partly been demonstrated in experiments [79, 80], they are limited to small system sizes $N < 10$, as it becomes exponentially hard (in the system size) to demonstrate this for larger systems.

2.5   High energy density

The notion is adapted from Garrison and Grover [81]. Consider a large system of size L and total number of particles N. The density of particles ρ, is assumed to be fixed:

$$\rho = \lim_{N,L\to\infty} N/L = c > 0 \tag{2.2}$$

Other parameters are assumed to be finite (i.e. internal states of the particle/sub-lattice structure on a site). To each eigenstate $|\phi_i\rangle$, an energy density ϵ_i is associated:

$$\epsilon_i = \lim_{N\to\infty} E_i/N \tag{2.3}$$

where, $E_i = \langle\phi|\hat{H}|\phi\rangle$ is the eigenenergy of the state and ϵ_i is assumed to be bounded and continuous. Let $\epsilon_{\min}$ and $\epsilon_{\max}$ denote the minimum and the maximum energy density over all the eigenstates. The notions which follow are believed to be true for all eigenstates ϕ_i, with an energy density ϵ_i not close to the minimum or the maximum,

$$|(\epsilon_{\min} - \epsilon_i)(\epsilon_{\max} - \epsilon_i)| > 0 \tag{2.4}$$

These are the blue regions in Fig. 2.1 **B**. Physically this means that one wants to consider only those eigenstates which are far away from the ends of the spectrum. Note that the above definition takes care of both gapped and gapless systems as the definition requires a finite density of excitations and a finite energy gap between the ground state and the first excited state is not important.

In the literature, one also finds terms such as "infinite temperature", "finite energy density", "highly excited state", "extensive energy densities", "far away from the ground state", etc. and they could all be interchangeably used without changing the physics and mean the same, above defined property.

2.6   The Eigenstate Thermalization Hypothesis

ETH provides one (possibly generic) way to answer the questions mentioned above and provides a mechanism for thermalization in isolated quantum systems. Some of the initial ideas were developed by Deutsch [49] in 1991, whereby it was shown that an integrable non-interacting gas of atoms defies the common ideas of quantum statistical mechanics, but adding even small perturbations restores the results of quantum statistical mechanics. In 1994, Srednicki [50] showed that under certain conditions an isolated quantum system with many particles in a specific initial state will always approach thermal equilibrium and used the term "eigenstate thermalization". That is, thermalization is present at the level of individual eigenstates, and no ensemble averaging is required to obtain statistical mechanics. This is highly non-trivial. Obviously, the micro-canonical ensemble is used to describe isolated systems, but it requires the assumption of ergodicity to obtain the expectation values of observables. In the case of eigenstate thermalization, this entire procedure of ensemble averaging is not necessary, and just a single state is enough and hence, one does not need the ergodic hypothesis. It is, of course, another matter, that it is usually impossible to obtain the individual eigenstates of quantum many-body systems.

These results were further elaborated and illustrated with numerical calculations by Rigol et.al. in Refs. [51, 82], who proposed that if thermalization happens, the mechanism is indeed ETH and is expected to describe thermalization at *finite energy densities* [83]. The exclusion of states near the ground state is necessary since they are known to be ergodicity breaking. Hence, instead, the discussion is about thermalization at finite energy-densities.

Why are the *low-lying eigenstates* excluded?

A very natural question to ask is why the low-lying eigenstates with zero energy density are excluded. Note that this is not only the ground state(s) but infinitely many states close to it which are zero energy density states. For example, consider the Mott-insulator ground state and consider exciting just one of the atoms. This still results in a zero energy density state. Such states are excluded from the discussion.

This is because such zero energy density states are special and we know of explicit cases where they break ergodic behavior. For example, take a spontaneous symmetry breaking (SSB) ground state such as a ferromagnet. Here, the system explicitly breaks ergodicity as once it has chosen (randomly) an alignment; it does not explore the other equally energetically allowed alignments as it has zero matrix element to tunnel in a large system. Hence, if one measures the local magnetization, it becomes non-zero, even though a microcanonical average is zero. Further, the low-energy excitations are long-wavelength magnons of the system (just spin-waves), which still will not render this to zero. This local polarization can only be destroyed at very high temperatures with infinitely many excitations. These are the states which are the bulk of the system and will be the basis to scrutinize ETH.

ETH

ETH holds true, if the expectation value of an operator $\hat{O}$, calculated from the micro-canonical ensemble at an energy density, is identical to the one calculated from *any* single eigenstate at the same energy density. This implies that the expectation value of such operators are the same in nearby eigenstates, even though the eigenstates themselves are orthogonal. In this case, the expectation value of an operator in a finite energy density state $|\psi\rangle$ is precisely equal to the one obtained from a thermal ensemble, i.e.

$$\langle\psi|\hat{O}|\psi\rangle = \frac{tr(\hat{O}e^{-\hat{H}/(k_B T)})}{tr(e^{-\hat{H}/(k_B T)})} \tag{2.5}$$

where, k_B is Boltzmann constant and the temperature T is chosen such that Eq. 2.5 holds true when $\hat{O} = \hat{H}$. Additionally, the off-diagonal elements between two distinct eigenstates, $|\phi\rangle$ and $|\psi\rangle$ with $\langle\phi|\psi\rangle = 0$, are vanishing,

$$\langle\psi|\hat{O}|\phi\rangle = 0 \tag{2.6}$$

In this sense, ETH is an *extreme* case of the micro-canonical ensemble where thermalization happens at the level of a *single* eigenstate. Naturally, there have to be certain constraints on the operators one can choose for such a result to hold, as it is visibly not true for highly non-local operators, such as the projection operators. In general, ETH does not propose the operators for which it is true, and hence, by itself, it is incomplete. In this
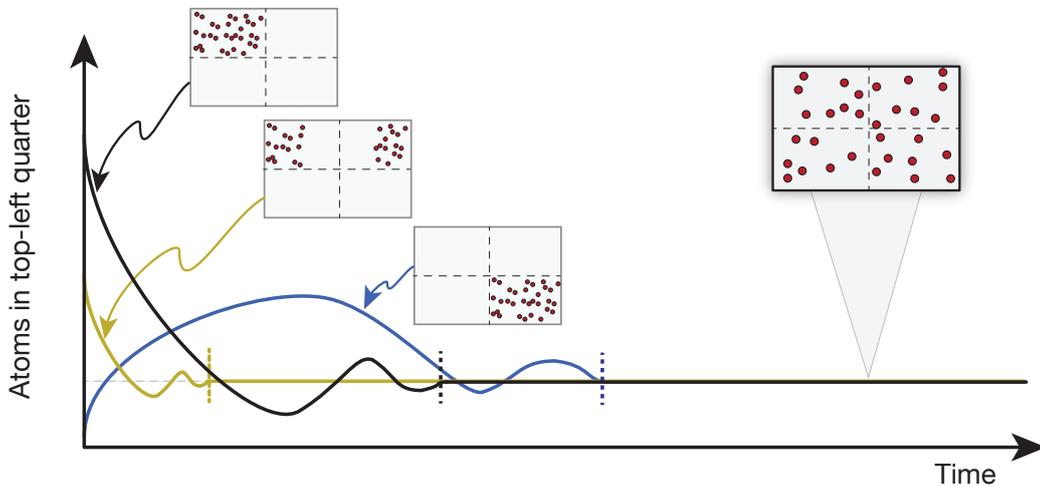
Figure 2.3: Thermalization and initial state independence: In systems which thermalize, the expectation value of an observable at long times is identical for any initial condition, as long as certain extensive quantities such as the total energy and the total particle number remain the same. For example, as shown in this cartoon figure, one can release the gas in any configuration in the box, and in a thermal system, not only will they equilibrate, they will equilibrate to the same value of the observable. This "loss of memory" of the initial state to always reach the same final state at long enough times is one of the main defining features of a thermal system. The time to thermalize (dashed lines), however, will depend on the observable, the initial state and the microscopic details of the Hamiltonian.

context, Ref. [81] proposes and gives numerical evidence that the equations are true for *all* operators within a subsystem *A* when the volume of the subsystem *A* satisfies $V_A \ll V$, where *V* is the volume of the full system. It also gives some evidence, that even when the volume of the subsystem V_A is a non-zero but restricted fraction of the total volume, all operators *not* explicitly involving energy conservation take their thermal values. The experimental consequences of ETH and thermalization are far reaching. They imply that *all* generic isolated systems are already thermal and a measurement of *any* observable of the above kind, even in an eigenstate, would result in the value one would expect from statistical mechanics.

Initial state independence

While ETH normally applies to eigenstates, the dynamical version of thermalization and ETH can be understood by considering Fig. 2.2 again, where we expect that the gas would not only equilibrate but also thermalize. This means that the left top quarter will contain a quarter of the total number of atoms, as in a high-temperature thermal state in such a system. Further, this would hold true no matter what the starting conditions are. One could start with all the atoms in the right half and after long times, the top-left quarter would still contain a quarter of the total number of atoms. This is another defining feature of thermal systems: the final state does not depend on the initial conditions as all the memory of the initial conditions is lost during the dynamical evolution into highly non-local quantities, and becomes essentially irretrievable (except some extensive constraints like total energy, total particles etc [39, 84]). Hence, if one can find one observable that retains some memory of the initial conditions, this directly implies the failure of thermalization. Such a result would enable us to detect the MBL phase, which manifestly breaks many of such defining features of a thermal system. This is illustrated in Fig. 2.3. The total number of atoms in the top left quarter is monitored as a function of time starting from three different initial conditions. The black line shows the case when all the atoms were initially located in the top left quarter, the yellow line when half the atoms were in the top left and the other half in the top right quarter and the blue line when all the atoms are initially located in the bottom right quarter. In a thermal system, *all* of these starting initial states evolve into one homogeneous system at long times, and they all forget their memory of the initial conditions (or more precisely, convolve them into highly non-local, non-retrievable correlations).

Single Particle Dynamics and Anderson Localization

Short summary: The notion of single particle localization due to the addition of quenched disorder in lattice models is introduced. The similarities and differences between real-random and quasi-periodic potentials are highlighted.

3.1   Introduction

P. W. Anderson's work on "Absence of Diffusion in Certain Random Lattices" [24] suggested the possibility of absence of quantum transport in a disordered medium as a result of localization of eigenstates. Subsequently, such a localization was given the name of Anderson Localization (AL) and was recognized as a more general phenomenon associated with the wave-equation. In particular, it applies to many other systems, such as the propagation of electromagnetic and acoustic waves, and serves as the foundation of ergodicity breaking in interacting systems.

3.2   Conductors and insulators

To understand the absence of transport due to disorder, it is sufficient to consider the case of non-interacting fermions on a lattice. In this case, there is no notion of ergodicity or ETH but one can still have conductor-insulator transitions. Traditionally, we define a metal/conductor vs an insulator depending on the conductivity of the material at zero temperature:

$$\sigma(T = 0) = \begin{cases} 0, & \text{Insulator} \\ > 0, & \text{Conductor} \end{cases} \tag{3.1}$$

Fig. 3.1 compares the band structure of a metal, a band insulator, and an Anderson insulator. In a metal, Fig. 3.1 **A**, the Fermi level E_F lies inside the ground band. All eigenstates in the ground band are extended. Applying an infinitesimal DC electric field results in a current. Therefore, the system has a non-zero conductivity at zero temperature (and also at finite temperatures). Further, the excitations are *gapless* since the energy cost of
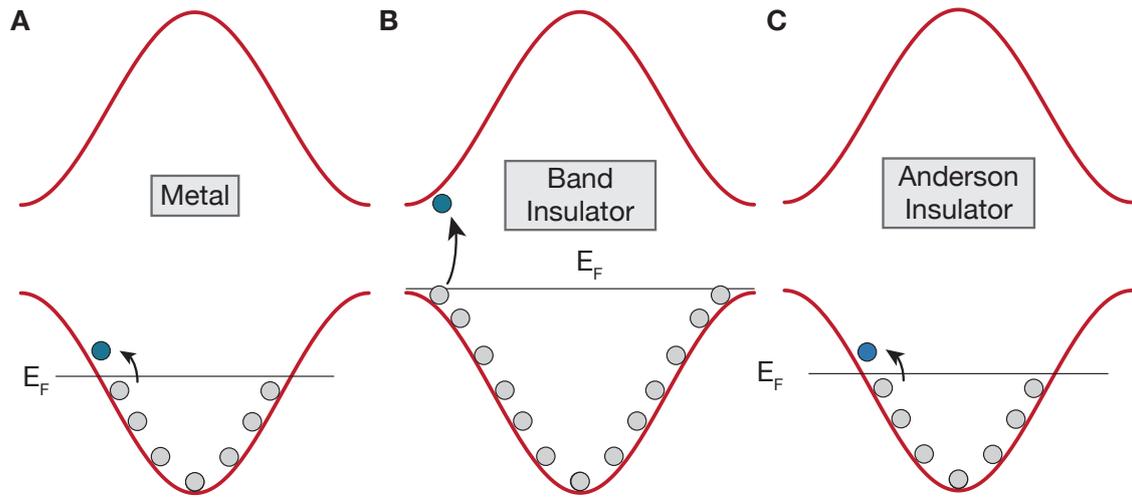
Figure 3.1: Metal, A: In a conventional metal, the ground band is partially filled with (e.g. spinless) fermions. At zero temperature, the lowest energy levels are occupied. It takes infinitesimal energy to cause an excitation (it has *gapless* excitations). Also, the conductivity of the system at zero temperature is strictly non-zero $\sigma(T=0)>0$. **band insulator, B:** In a conventional BI, all the available states in the ground band are filled, and it costs a finite energy to cause a current carrying excitation (*gapped*). Such a system has zero conductivity at zero temperature, $\sigma(T=0)=0$ and hence, it is an insulator. **Anderson insulator, C:** In such an insulator, the bands appear very similar to the metallic case, but still low energy excitations cannot carry current as the excited states are themselves localized. In such a case, the excitations can be gapless, but still the conductivity at zero temperature is zero, $\sigma(T=0)=0$, implying an insulator. However, unlike the BI, the conductivity in an AL can remain zero even in the excited states, implying a *finite temperature insulator*. Here, E_F is the Fermi energy at zero temperature, and blue symbols denote low-energy excitations.

making an excitation is infinitesimal. In a band insulator, Fig. 3.1 **B**, the ground band is fully filled with fermions and applying an infinitesimal DC electric field results in zero current. The lowest energy excitations are *gapped* since the smallest possible excitation has a finite energy cost as a particle has to be excited to the higher band. However, this is an insulator only at zero temperature with an exactly filled band. At finite temperatures, there are always a few mobile excitations, and hence, it does not have an exactly zero conductivity $\sigma \propto e^{-(E_2-E_1)/T}$ at non-zero temperatures.

While the band structure can explain the conducting/insulating behaviors for conventional metals and band insulators, one needs to investigate the conductivity of individual eigenstates in the case of Anderson insulators to understand why they do not conduct despite appearing similar to a metal in the band structure, Fig. 3.1 **C**. This happens because of a *mobility gap*, as each of the underlying eigenstates is localized itself, causing the conductivity to be zero in an infinite system. Hence, applying a small electric field does not result in a current, even though the excitations are gapless. In contrast to conventional insulators which have zero conductivity only at zero temperature, Anderson insulators have zero conductivity even at finite temperatures, as the low-energy excitations in the same band result in states being occupied, which themselves do not conduct.

3.3   Basic results on Anderson localization

In this section, after some known results on AL are presented, the main features of the dynamics of a single particle in disordered systems are illustrated with numerical calculations. This is done to illustrate the phenomenon and to show the dynamics in non-periodic systems in one dimension, which serve as a starting point to understand many of the results of the interacting system.

3.3.1   A simple tight-binding model

Many features of the quantum world can be understood via simple models. In order to understand the phenomena of quantum localization, we consider the following model in one dimension:

$$\hat{H}_{AL} = -J \sum_i (\hat{c}_{i+1}^\dagger \hat{c}_i + \hat{c}_i^\dagger \hat{c}_{i+1}) + \Delta \sum_i V_i \hat{n}_i \tag{3.2}$$

Here, i denotes the lattice site, J is the nearest-neighbor tunneling matrix element and $\hat{c}_i^\dagger(\hat{c}_i)$ is the creation(annhilation) operator of a single particle. The number operator is defined as $\hat{n}_i = \hat{c}_i^\dagger \hat{c}_i$ and its expectation value at a site gives the probability density of the particle on that site. $V_i \in [-1, +1]$ denotes the onsite potential and Δ is an overall strength of the *quenched* onsite potential. Some important special cases for the onsite potentials are as follows:

1. Real-random (RR): Since the system is in one dimension, for truly randomly distributed onsite potentials V_i in $[-1, 1]$, *all* eigenstates of the system are localized for $\Delta > 0$ and *all* eigenstates are delocalized for $\Delta = 0$. Hence, there is a quantum phase transition at $\Delta = \Delta_c = 0$. This is the kind of disorder studied in Ref. [24] that results in localization of eigenstates.

2. Aubry-André (AA): True disorder is not required for localization of eigenfunctions, which also occurs in quasi-periodic systems with $V_i = \cos(2\pi\beta i)$. Here, β is an irrational number, and *all* eigenstates of the system are localized for $\Delta > 2J$ and *all* eigenstates are extended for $\Delta < 2J$ [85–88]. This is the kind of onsite modulation which has been realized in our experiment.

3. It is expected that as long as V_i is such that for all $i \neq j$, $V_i \neq V_j$, and Δ is large, *all* eigenstates can be localized. Even other "random-enough" potentials such as $[V_i = (i\pi)^2 \bmod 2]$ with a large Δ can show localization. Here, mod is the modulus operator. While the necessary and sufficient requirement for single-particle localization is unclear, it appears that detuning the onsite energy of every lattice site with unity probability is enough to induce single-particle localization. Note that RR and AA satisfy this criterion.

All these kinds of localization phenomena, which pertains to the localization of eigenstates of the non-interacting Hamiltonian, are collectively referred as AL. When necessary, we would distinguish between them by referring to a specific type of potential as real-random or quasi-periodic.
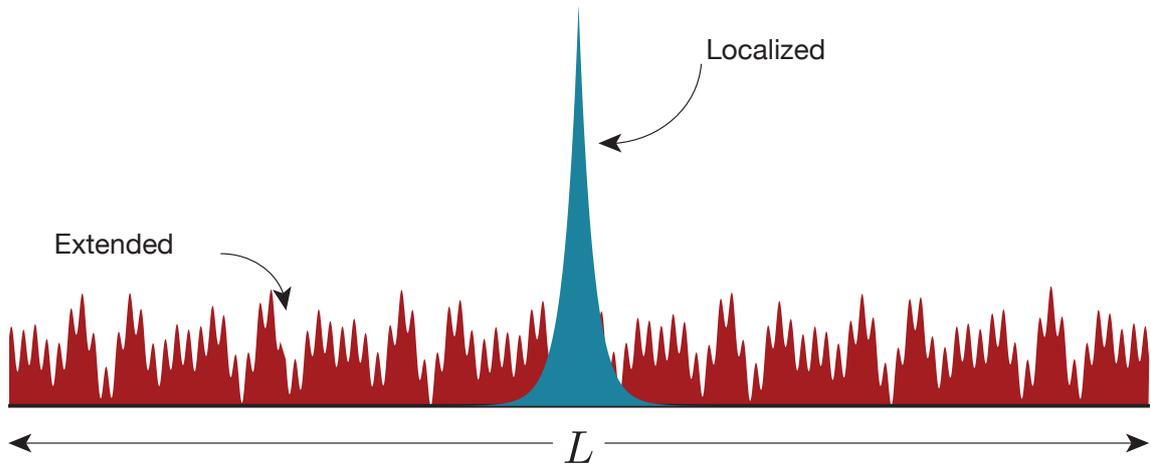
Figure 3.2: A localized and an extended state: Am illustration showing that a localized state (blue) has the bulk of its probability density localized in a small region in a large lattice of size L. On the contrary, an extended state (red) spans the entire lattice. Note that an extended state need not be periodic.

3.3.2 Localized eigenstate

A rough notion of a localized eigenstate is intuitively clear: something that is localized in a small region of the lattice. Therefore, we call a normalized eigenstate $|\phi\rangle$, expressed in the real space basis $|i\rangle$, as localized, if given any $c < 1$, there exists a site j and a length $l < \infty$, such that $\sum_{i=j-l}^{j+l} |\langle\phi|i\rangle|^2 > c$. Physically, this means that the bulk of the probability density of the eigenstate is localized in some region around some site. If the eigenstate does not satisfy this criterion, we call the eigenstate extended. Further, it turns out that the eigenstates of Eq. 3.2 in the case of both real-random and quasi-periodic potentials are *exponentially localized*. This means that the long distance envelope decays as an exponential with respect to some site j, i.e. $\phi \sim e^{-|x-j|/\xi}$, for $|x - j| \gg 1$. Here, ξ denotes the *localization length*.

3.3.3 Mobility edges

In both real-random and quasi-periodic disorders, *all* eigenstates are simultaneously localized above a critical value of the disorder strength. One can ask if this is always true or whether extended and localized states can simultaneously exist at different energy densities. If yes, one can have mobility edges, defined as the energy which separates localized states from delocalized states. Typically, one does not expect extended and localized states to coexist at the same energy density and survive small perturbations. As such, mobility edges must separate bands which are localized and extended. Further, we expect that near the band edges, it is easier to localize the eigenstates as compared to near the center and hence, one could have (two or more) mobility edges in a system with a bounded spectrum as depicted in Fig. 3.3 **B**. At least in the single-particle case, we explicitly know of models in one dimension with mobility edges, e.g. Refs. [89, 90].

A

B

C
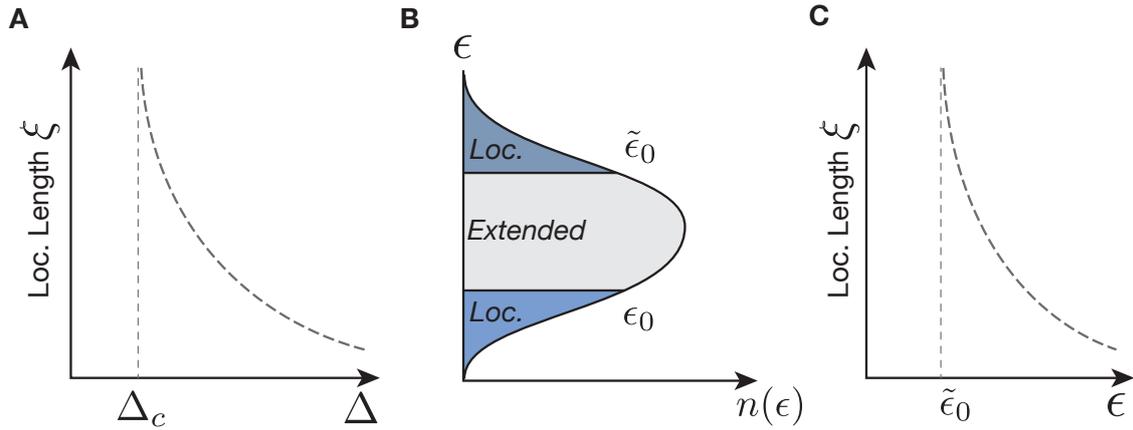
Figure 3.3: Localization length as a function of disorder strength, A: In general, a larger disorder strength Δ results in a lower localization length ξ. The *critical* properties, such as location of the critical point Δ_c, or how the localization length diverges near Δ_c, will depend on the type of disorder potential, dimensionality and energy density. **Mobility edges, B:** In the spectrum of the eigenstates a mobility edge might exist, i.e. a critical energy density which separates localized and delocalized eigenstates. In the diagram they are denoted at ϵ_0, $\tilde{\epsilon}_0$, separating localized and delocalized eigenstates. **Localization length divergence as a function of energy density, C:** Near the mobility edge, the localization length diverges, but as function of energy density. Note that in the one-dimensional non-interacting models with RR or AA type disorder, no mobility edge exists.

3.3.4 Higher dimensions, $d > 1$

The results mentioned above are all in one dimension, $d = 1$. The question about higher dimensions $d = 2, 3$ is interesting but also very challenging for both numerics and analytical results. In particular, many of the models introduced above are (at least partly) motivated to be able to get qualitatively similar features of higher dimensions in one-dimensional models, which are easier to study. Here, it is important to mention the results of Ref. [91, 92], about the "Scaling Theory of Localization" which predicts that for RR type of disorder, *all* eigenstates get localized for arbitrary small disorder strength in one and two dimensions, i.e. $\Delta_c^{d=1,2} = 0$. This would also imply the absence of mobility edges. On the other hand, in three dimensions $d = 3$, the critical value of the disorder strength is not zero, and mobility edges exist [91, 92]. Note that the non-zero value of the critical disorder strength does not imply the presence of mobility edges and hence, these are two different results (e.g. in the AA model, one has a non-zero value of the critical disorder strength but no mobility edges). These results are summarized in Table 3.1.

Finite size effects and effective mobility type effects

All real systems are finite. In this light, it is not only of academic interest but of fundamental importance to understand finite size effects in such synthetic systems. For the topics within this section, the important finite size effect is the following: effective mobility edges seem to exist even in models such as RR or AA, which do not have mobility edges. This is because typically the localization length ξ depends on the energy density and the system

d	Δ_c	Mobility Edge
1	0	No
2	0	No
3	> 0	Yes

Table 3.1: Critical disorder strengths and mobility edges in systems with real-random disorder: Following [91], the critical disorder strengths and the presence or absence of a mobility edge is given for the case of real-random disorder for different dimensionalities. In two dimensions, the system is critically localized for small disorders, and the localization lengths can be very large.

under consideration is of a finite linear size L. If $\xi \gg L$ a local observable will not be able to distinguish the system from a delocalized system.

3.4   Dynamics in Anderson localized systems

This section is devoted to showing (via simple numerics) the dynamics in an AL system and how crucially it differs from a clean non-disordered system. An important observable is introduced, namely the even-odd density imbalance, to understand many of the properties of the system. This is done for multiple reasons. First, this observable can capture the localization-delocalization transition and is easily measurable in the experiments. Moreover, the notion of the exponential decay of the wave-function will not remain useful in the presence of interactions. However, this even-odd imbalance will continue to be a measure of localization for both interacting and non-interacting cases, allowing us to make quantitative comparisons between single-particle and many-body localization.

3.4.1   The statics-dynamics duality and the expansion dynamics

Until now, we focused on *static* observables, such as the structure of the eigenstates, and classified the systems accordingly. However, experiments do not prepare single eigenstates but a superposition of eigenstates. Hence, we describe another method to characterize the system, by probing its *dynamics*. Intuitively, the duality and the illustration that follow can be understood by projecting the wave-function into the eigenstates and monitoring the expansion of the system. In an extended system, the particles are expected to expand indefinitely. On the other hand, in a localized system, the expansion would remain bounded. The case of a mobility edge is easy to understand as a superposition of the two cases as the corresponding expansion can be broken down as the sum of the extended case where the probability density escapes to infinite distance, and the localized case, the probability density of which remains bounded near the origin of the expansion.

In order to see this directly, consider a particle being released from a single site in the above Eq. 3.2 in one dimension. The sites are numbered from $i \in [1, L]$, where L is the system size and the site of release is the center of the system. This implies that the probability density of the particle, $d_i(t)$ at zero time is given by $d_i(t = 0) = \delta(i - L/2)$. We monitor the radius of expansion,
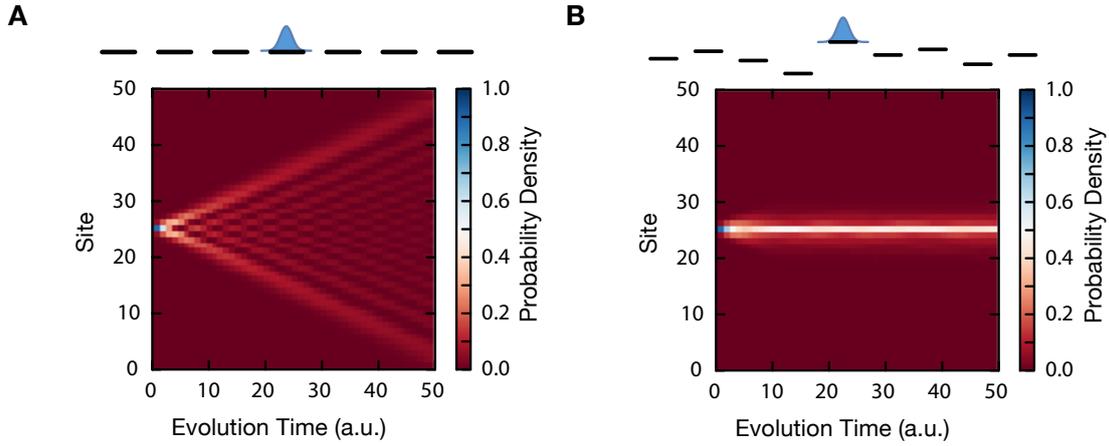
Figure 3.4: Expansion in a homogeneous lattice, A: For a system with all onsite energies the same, the plot shows the evolution of the probability density of the particle when it is released from the center of the lattice, exhibiting a ballistic spread. This kind of expansion would imply that the system has delocalized eigenstates. **Expansion in a disordered lattice, B:** If the onsite energies of the system are strongly disordered, the expansion completely stops, and the entire probability density remains localized near the origin. This dynamical signature is indicative of localized eigenstates. For these plots, we use Eq. 3.2 with the real-random disorder with an amplitude of $\Delta = 0$ for the homogeneous case and $\Delta = 5J$ for the disordered case. All times are given in terms of the hopping time $\tau = \hbar/J$.

$$R^2(t) = \sum_i (i - L/2)^2 d_i(t) \tag{3.3}$$

To be concrete, the model is fixed to Eq. 3.2. The following cases are of interest:

1. Free particle, $\Delta = 0$: For zero disorder, the particle expands in a ballistic fashion, i.e. $R \propto t$. A plot of the time evolution of the probability density of the particle is shown in Fig. 3.4 **A**, where one can observe a light cone like propagation. In this case, the eigenstates of the system are extended, resulting in an unbounded expansion.

2. Anderson localized particle, $\Delta \gg 1J$: If the disorder strength is much larger than the hopping strength, a particle can remain bounded in its expansion dynamics even at long times, $R(t \to \infty) \sim R_0$, where R_0 is some fixed distance. In this case, the time evolution of the particle is shown in Fig. 3.4 **B**, where the bulk of the probability distribution remains near the center of the system (the starting site). All the eigenstates of the system are localized, which results in bounded expansion. The final expansion radius increases with the localization length of the eigenstates, i.e. $R_0 \sim \xi$. For systems with true disorder, all eigenstates are localized for arbitrary small disorder strengths and hence, R_0 is finite for any finite Δ. For the quasi-periodic potential, all eigenstates are localized for $\Delta > 2J$ and hence, R_0 is finite only above this critical threshold strength.
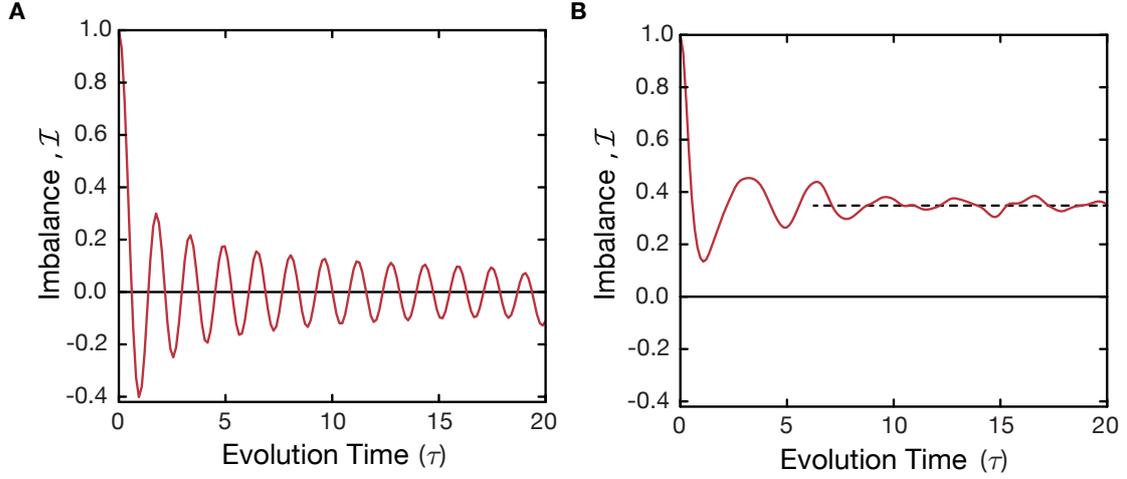
Figure 3.5: Imbalance evolution in a homogeneous lattice, A: The even-odd density imbalance, $\mathcal{I}$ is shown for a particle released in a clean lattice from an even site. The imbalance decays exponentially fast to zero, indicating that the system is delocalized. **Imbalance evolution in an AL system, B:** The imbalance equilibrates but does not relax to zero, implying that the system has localized eigenstates. For these plots, we use Eq. 3.2 with RR type disorder and amplitude of $\Delta = 0$ for the homogeneous case and $\Delta = 5J$ for the disordered case. All times are in inverse hopping $\tau = 1/J$.

3.4.2   Odd-even density imbalance

One can capture the extended-localized behavior with another observable, the density imbalance between the even and the odd sites:

$$\mathcal{I} = p_e - p_o \tag{3.4}$$

where $p_e(p_o)$ is the total probability density of the particle on even(odd) sites. While it can be related to the expansion and single-particle localization length, there are other significant advantages of it, the most important being that it is directly generalizable to the many-body case. In particular, starting from a density-wave and measuring the difference between the occupations of the even and the odd sites can provide signatures of many-body localization [93].

For the case of freely expanding fermions, the time evolution of the imbalance is shown in Fig. 3.5 **A**. The imbalance relaxes very quickly (exponentially fast [94–96]) to zero, indicating that the system is delocalized. Such a quick relaxation is important due to finite-time limitations in an experiment, see Chapter 7. In contrast, Fig. 3.5 **B** shows the imbalance time evolution for a system with localized eigenstates. While the imbalance equilibrates in this case also, it equilibrates to a non-zero value, as a result of localized eigenstates. Therefore, the transition from zero to a non-zero value of imbalance can serve as an order parameter for probing localization. One can summarize this as:

Delocalized Eigenstates	$\equiv$	Unbounded Expansion	$\equiv$	$\mathcal{I} = 0$
Localized Eigenstates	$\equiv$	Finite Expansion	$\equiv$	$\mathcal{I} > 0$
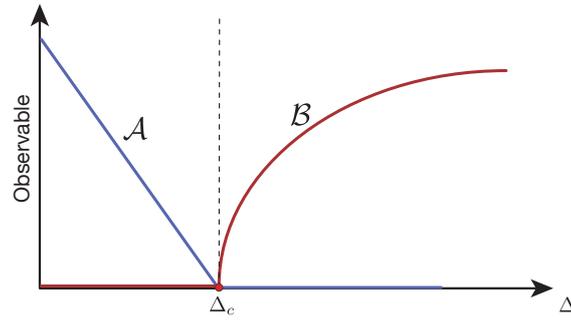
Figure 3.6: Observables for the delocalized and the localized phases: To quantify and characterize the delocalized phase for weak disorders and the localized phase for strong disorders, we use different observables. These observables can be grouped into two classes, $\mathcal{A}$ and $\mathcal{B}$, which quantify different phases. For example, expansion velocity at long times is a type $\mathcal{A}$ observable, as it characterizes the delocalized phase. On the other hand, if the expansion is finite and stops at a radius of R_0, then this R_0 is a class $\mathcal{B}$ observable, characterizing the localized phase. The expected behavior of a class $\mathcal{A}$ observable, such as the expansion velocity, is shown in purple. It continuously decreases upon increasing the disorder, until it vanishes at the critical point. In the localized phase, class $\mathcal{B}$ observables, such as the inverse of the expansion radius, $1/R_0$, can characterize the extent of localization (green curve). Note that a class $\mathcal{A}$ observable is not useful to characterize the localized phase and the vice versa.

3.4.3   The delocalized phase, the localized phase and the transition point

The kind and amount of disorder can result in very different phases and dynamics, and hence, we would like to characterize each of the phases with an appropriate order parameter. This is similar in spirit to the case of a non-interacting band insulator vs. a metal. In the metallic phase, the hopping determines the properties of the system, while in the band-insulating phase, it is the band-gap. In this sense, the hopping is not useful to characterize the band-insulating phase and the band-gap is not useful to characterize the metallic phase.

If we monitor the time evolution in the extended phase, then the radius of expansion will continue to increase. In general, the precise form of expansion can depend on the details of the disorder. At long times, the radius can increase as a function of time as $R = a(t)t^{b(t)}$. Here, $b = 1$ means ballistic expansion and $b = 0.5$ implies diffusive expansion. The long time limit of a can be used to characterize the extended phase, assuming that the expansion remains ballistic ($b = 1$). For the RR case, there is only one point $\Delta = 0$ which is extended and here, a particle has a constant expansion velocity, $R \propto t$. On the other hand, for the AA case, the velocity of expansion continuously decreases with increasing disorder up to the critical disorder of $\Delta = 2J$. Such measures which capture the rate of expansion can be used to characterize the delocalized phase. Similarly, the manner in which the even-odd imbalance $\mathcal{I}$ decreases to zero can characterize the delocalized phase. In the delocalized phase, one can observe the rate at which any memory of the initial condition vanishes $\frac{d}{dt}M_0$. We can use all such operators to classify the extended phase, and group them into type $\mathcal{A}$ observables, see Fig. 3.6.

On the other hand, in the localized phase, the expansion radius does not change at long times and saturates to R_0. We can use the inverse of R_0 as an order parameter that characterizes the localized phase. Similarly, the long time value of the imbalance can characterize the localized phase. We can also group such observables in class $\mathcal{B}$ and they will characterize the localized phase. Observables like imbalance can capture the effect of disorder and interactions. In general, observables which show the memory of the initial conditions would characterize the MBL phase and belong to class $\mathcal{B}$ observables. This is not meant as an exhaustive classification, but as an example to show the need for different parameters to probe and characterize different phases.

Breakdown of Thermodynamics in Isolated Quantum Systems via Many-Body Localization

Short summary: Many-body localization is introduced as a generalization of Anderson localization to interacting systems and argued as a generic Eigenstate Thermalization Hypothesis breaking phenomenon. The disordered XXZ Hamiltonian is introduced to elucidate its properties.

4.1   Introduction

Many phenomena in physics can be understood by considering non-interacting Hamiltonians, such as the integer quantum Hall insulator, a conductor and a band insulator. This does not mean that interactions are not present in an actual integer quantum Hall system or a band insulator. The physics of the system is just easier to understand and can be captured by the non-interacting limit. However, matter is indeed interacting and with the addition of interactions, comes a very large amount of complexity. Out of this complexity, fascinating quantum phenomena can arise near the ground states, such as the fractional quantum Hall effect [7] and (topological) Mott-insulators [97]. However, at finite energy densities, interactions in quantum systems are expected to generically result in thermalization [49], as was argued in Chapter 2. The only generic exception to this known so far, is the phenomenon of Many-Body Localization (MBL), an interacting generalization of Anderson localization.

4.1.1   Key-ingredients

Before introducing the XXZ Hamiltonian and MBL, a few terms are described because they are repeatedly used to understand the physics. These are:

1. Local short-range interactions: Throughout this thesis, only short-ranged and local interactions are considered. This implies that the interactions are local in space, e.g. on-site interactions and nearest-neighbor interactions. Longer-ranged interactions, such as Coulomb interactions, should also generate interesting dynamics, at least

at intermediate times, if not exhibit a true MBL phase. However, their adequate treatment is beyond the scope of this thesis [98].

2. Isolated quantum systems: The systems under consideration should be effectively isolated from any degree of freedom not explicitly mentioned in the Hamiltonian, and we will assume that the system undergoes unitary dynamics. The result of relaxing this assumption is explored in Chapter 7.

3. Finite-energy density: While localization can occur in all eigenstates (including ground states), we discuss it only in finite energy density states.

4. Many degrees of freedom: The discussions require many degrees of freedom, just like ETH would require many degrees of freedom interacting with each other. Finite-size effects are described in relevant subsections.

5. Disorder: The discussions rely on an explicit term of quenched disorder in the Hamiltonian, as described in Chapter 3. Whether MBL can exist in translationally invariant systems is currently an open question. This could happen for example via an effective disorder in the initial state itself [99, 100]. However, this is beyond the scope of this thesis.

6. Genericness: The results will be mostly about generic features under the above-mentioned conditions. This means that small, local perturbations are not expected to change the global features. For example, a small additional term like next-nearest-neighbor hopping should not change the global phase. This feature makes MBL dramatically robust compared to other non-thermal systems such as interacting integrable systems [49, 101]. Additionally, the notions are expected to be features of all similar systems at high energy densities, irrespective of the actual Hamiltonian, as long as the basic conditions described above are satisfied (i.e. it should also be visible in other Hamiltonians with an appropriate choice of parameters).

Under these conditions, two generic cases are currently believed to exist:

Thermalization or Many-Body Localization.

Out of these two, proving that a system is indeed *thermal* is hard – one would need to measure the density matrix of all possible subsystems and show that they approximate the thermal density matrix – a daunting task for systems with many degrees of freedom. Hence, throughout this thesis, we will not be able to show that the system thermalizes, but only be able to show that certain observables are consistent with the system being thermal or not, on the timescales of the experiment. Thermalization was argued as a generic phenomenon as described in Chapter 2 and in this chapter, we will describe its breakdown via MBL. A few other non-thermal cases, such as integrable systems and quantum-disentangled liquids [102] are expected to be fine tuned and are beyond the scope of this thesis.
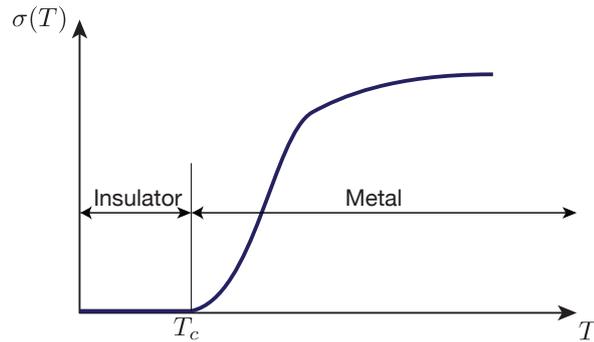
Figure 4.1: Finite temperature metal-insulator transition in an interacting isolated system: Summarizing Ref. [21], the figure shows the DC conductivity σ of a system remaining exactly zero up to a critical temperature $T_c > 0$ and the system undergoing a finite temperature metal-insulator transition. This scenario is argued to appear when there is no phonon bath and short-range electron-electron interactions are taken into account. Due to disorder, all the single-particle states are assumed to be well localized.

4.2 Phonons vs. Electrons

Disorder can localize all the single-particle eigenstates and lead to vanishing conductivity at zero temperature in a non-interacting system. However, experiments do not work at zero temperature, so the natural question to ask is, what are the relevant experimental signatures of this phenomenon. In real materials, there are typically some underlying phonon modes, which are activated at non-zero temperatures and interact with the electrons. In the absence of any electron-electron interactions, this leads to very small but *finite* conductivity at finite temperatures via the mechanism of hopping conductivity [43, 103]. Here, electrons can hop between the localized states via (virtual) energy exchange with the phonon bath. The conductivity generated by this mechanism at finite temperature T in d dimensions is given by:

$$\sigma(T) = \sigma_0 e^{-(T_0/T)^{1/(d+1)}} \tag{4.1}$$

where σ_0, T_0 are some energy scales dependent on the underlying disorder strength (and also weakly on temperature). This implies that the conductivity remains non-zero at non-zero temperatures for any disorder strength. A natural question to ask is if in the absence of any such phonon modes, can electron-electron interactions alone provide the necessary energy exchange and allow for delocalization? For example, electrons can re-instate hopping by causing correlated hops and hence, restore conductivity. This question was already addressed in the original paper by P. W. Anderson [24], arguing that in the presence of strong enough disorder, electron-electron interactions might be insufficient to restore conductivity. This was put on a much firmer footing by Refs. [21, 104], who showed that electron-electron interactions alone cannot cause the conductivity to become finite if the disorder is strong enough and as long as the temperature is below some critical temperature T_c, see Fig. 4.1. Roughly speaking, this is because in a system with strongly localized single-particle eigenstates, interactions effectively remain completely local and

hence, such interactions cannot couple the system fully and localization persists. Further, it is shown that if the temperature was high enough, the system always has finite conductivity. Together, these two statements imply that the system undergoes a finite temperature metal-insulator transition. This result was particularly intriguing, as we expect other interacting insulators (such as the Mott-insulator) to have finite conductivity at finite temperatures.

4.3 The disordered XXZ Hamiltonian

To numerically explore the features mentioned above, we describe the model used by Oganesyan and Huse in Ref. [105], wherein a random field (disorder) was added to an otherwise delocalized, one-dimensional XXZ Hamiltonian. The resulting Hamiltonian offers exciting possibilities to study many interesting cases of high-temperature dynamics. Each of them is briefly discussed below, as they serve as starting cases for understanding the dynamics in the experiment.

Almost all of the numerical results on MBL in one dimension are performed on the disordered XXZ Hamiltonian. In this sense, it becomes quite instructive to understand many generic properties of MBL systems with this Hamiltonian. This is *not* the model which is realized in the experiments but nevertheless, this model should still be useful for understanding many properties of excited states of all local Hamiltonians with not too fine-tuned parameters. We refer to reviews [22, 23, 40] for a in-depth reviews.

The Hamiltonian

The one-dimensional XXZ Hamiltonian is a spin model, written as:

$$\hat{H}_{\text{XXZ}} = J_\perp \sum_{i=1}^{N-1} (\hat{X}_i \hat{X}_{i+1} + \hat{Y}_i \hat{Y}_{i+1}) + J_z \sum_{i=1}^{N-1} \hat{Z}_i \hat{Z}_{i+1} + \sum_{i=1}^{N} h_i \hat{Z}_i \qquad (4.2)$$

where, M_i with $M \in \{\hat{X}, \hat{Y}, \hat{Z}\}$ are the Pauli matrices for a spin-half particle on site $i \in \{1, N\}$ and the reduced Plank's constant is set to unity. There are no motional degrees of freedom, only spin degrees of freedom. The Jordan-Wigner transformation [106] shows that this Hamiltonian is exactly equivalent to spinless fermions with nearest-neighbor interactions in one-dimension. The physical interpretation of each of the microscopic parameters is described as follows:

1. $J_\perp$ is a fixed number and can be set to unity. It represents a *hopping* term and merely rescales the overall energy scale (and with it, the hopping time). If the Hamiltonian only had this term, it would be a free-fermion Hamiltonian.

2. J_z represents an *interaction* term. In $d > 1$, this would introduce interactions between particles and the system is expected to be ergodic. However, in one dimension it represents a fine tuned case, and the system represents an integrable model. The addition of any small term, e.g. three body interactions, is expected to break such fine-tuned integrable behavior.
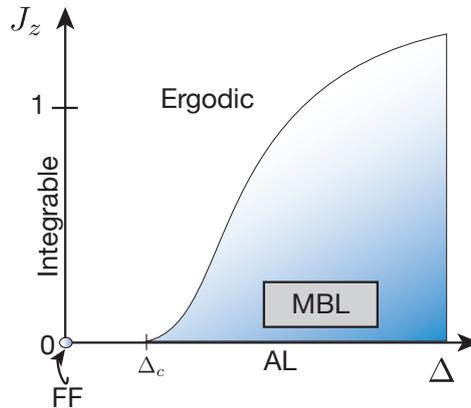
Figure 4.2: Phases of the one-dimensional disordered XXZ Hamiltonian: Keeping the hopping term $J_\perp = 1$ fixed, one can obtain many different phases of the disordered XXZ Hamiltonian. For zero interactions, $J_z = 0$, and zero disorder, $\Delta = 0$, one obtains a free fermion (FF) model, denoted by a dot. Along the x-axis, there are no interactions but the disorder term is finite, and one obtains a localized system beyond a critical disorder Δ_c. Along the y-axis, there is no disorder, and the model reduces to an integrable model. For weak interactions and strong disorders, the system shows MBL (blue area), while for weak disorders and strong interactions, the system shows ergodic behavior (white area).

3. h_i is a random number chosen between $[-\Delta, \Delta]$ and represents the amount of *disorder* in the system. Here, $\Delta \geq 0$ is the strength of the disorder in the system. For $0 < \Delta \ll 1$, we expect the system to be ergodic (as it also acts as an integrability breaking term), while for $\Delta \gg 1$, the system can show MBL (current estimate of critical disorder strength is about $\Delta_c \approx 3.7 \pm 1$ [22]). The bulk of the results below will focus on tuning this term, i.e. the strength of the disorder, keeping the hopping and the interaction fixed to $J_\perp = 1$ and $J_z = 1$, respectively.

4.3.1 High-temperature regimes

What is remarkable about this Hamiltonian is that by merely changing two parameters (Δ and J_z) one can obtain many distinctive high-temperature regimes and study their dynamics. As illustrated in Fig. 4.2, this Hamiltonian can show five distinct types of high-temperature regimes: an ergodic phase, an Anderson localized state, a free fermion system, an interacting integrable model, and the MBL phase. The ergodic phase is described in Chapter 2 and the AL/free-fermion cases are described in Chapter 3. After a brief comment on the interacting integrable model, the properties of the MBL phase are described in some detail.

4.3.2 Interacting integrable systems

Interacting integrable systems are non-disordered systems, which do not thermalize even though they are interacting. Such systems are restricted in their dynamics due to an ex-

tensive number of conserved quantities. They are believed to be fine tuned cases, whereby interactions are unable to cause thermalization. As far as I know, interacting integrable models are only known in one-dimension. Eq. 4.2 remains integrable for all interactions $J_z \geq 0$ as long as the disorder is zero, $\Delta = 0$. This Hamiltonian exhibits a very rich dynamical spectrum. For vanishing interactions, the system shows ballistic transport. Usually, one could expect the transport to become diffusive as soon as interactions are turned on. However, this model is special and upon turning on interactions, for $J_z < 2$, the system remains ballistic [107]. For larger interactions though, $J_z > 2$, the system becomes diffusive [108]. Other interesting examples of integrable systems include the one-dimensional Bose-Hubbard model in the hard-core limit, which shows ballistic transport (with no doublons, and it essentially behaves the same as non-interacting particles) [109–111] and the one-dimensional Fermi-Hubbard model for all interactions [112].

4.4 Many-body localized systems

The addition of strong disorder can make generic interacting systems non-ergodic [21, 104, 113], including the XXZ Hamiltonian. In this setting, MBL would imply that Anderson localization due to disorder would survive interactions. The notion of eigenstates being localized in some region is no longer valid because, in a many-body system, eigenstates span the whole system. However, as described below, localization would be preserved in the sense that, the memory of initial conditions remains preserved *locally*. This result is surprising because, in principle, the entire spectrum gets coupled upon turning the interactions on and yet, localization survives. The many-body eigenstates span the entire space, and hence the system should naively conduct (if one just considers at eigenstates, which appear extended). However, the system still does not conduct. Additionally, to observe the phenomenon, one has probe the non-equilibrium dynamics of the system [114, 115].

To understand this notion of localization, the time evolution of a product-state in the disordered XXZ Hamiltonian is shown. Interactions are turned on, i.e. $J_z > 0$ and an odd-even spin imbalance is monitored. If this imbalance remains non-zero, it directly shows a breakdown of ergodicity and a persistent memory of the initial state. This is because the expectation value of energy on even and odd sites is the same (zero) and hence, according to micro-canonical prediction the spin density must have equal value in these two subspaces and hence, the imbalance must relax to zero. If it does not relax to zero, this implies that the system breaks ETH.

4.4.1 Non-ergodic time evolution

To understand the relaxation dynamics in such a system, the initial state is fixed to be an infinite temperature state with classical Néel order, i.e. an alternating spin up, spin down configuration, $|\psi\rangle_{\text{initial}} = |... \uparrow\downarrow\uparrow\downarrow ...\rangle$. The total spin imbalance, which is the amount of total spin on even sites minus the total spin on odd sites is calculated from the wave-
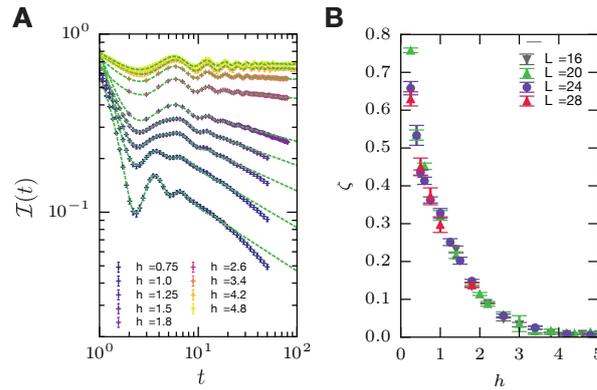
Figure 4.3: Time evolution of spin-imbalance in the XXZ Hamiltonian, A: The figure shows the evolution of spin imbalance as a function of time and for various disorder strengths. The relaxation of the spin-imbalance continuously slows down with increasing disorder strength, and for large enough disorder strengths, there seems to be no relaxation, and the spin-imbalance saturates to a non-zero value. This shows the breakdown of ergodicity, a hallmark of MBL. **Relaxation exponents ζ, B:** The relaxation can be captured with a power-law, with an exponent ζ, which captures trend and almost vanishes around $h \approx 4$. L denotes the length of the spin chain and $h = |\Delta|$ is the magnitude of disorder amplitude. Figure adapted from Ref. [116] with permission. Copyrighted by the American Physical Society.

function $|\psi(t)\rangle$ at time t as $\mathcal{I}(t) = \sum_i \langle \psi | (-1)^i \hat{Z}_i | \psi \rangle$. Here, $\hat{Z}_i$ is the z-Pauli matrix on site i. The result of such a calculation is shown in Fig. 4.3 A, adapted from [116].

The plot shows that for weak disorders $h < 4$, the system relaxes slowly and the imbalance decreases in time. This rate of relaxation is captured by the relaxation exponent ζ, which is shown in Fig. 4.3 B, with $\mathcal{I} \propto t^{-\zeta}$ (see Chapter 9 for further details on this). We see that the system relaxes progressively slowly until a critical disorder strength of roughly $h_c \approx 4$ is reached, beyond which the imbalance is non-zero, and the relaxation vanishes. This indicates the beginning of an MBL phase, which would be consistent with other studies which have probed this using other parameters [28, 117, 118]. Beyond this critical value of the disorder, the system is MBL and the systems show persistent memory of the initial conditions, demonstrating a breakdown of ergodicity via MBL.

4.4.2 Entanglement

Many important distinctions can be made between different systems from the entanglement properties of the eigenstates of the system and the growth of spatial entanglement after a quantum quench of a spatially non-entangled product state. It is believed that typical eigenstates of many-body systems follow a "volume-law" for entanglement. This is to be distinguished from their ground states, which can support an "area-law" of entanglement [120]. These notions can be calculated for the *Von Neumann* entanglement entropy:

$$S(t) = -\mathbf{Tr}(\rho \log(\rho)) \tag{4.3}$$

A

B
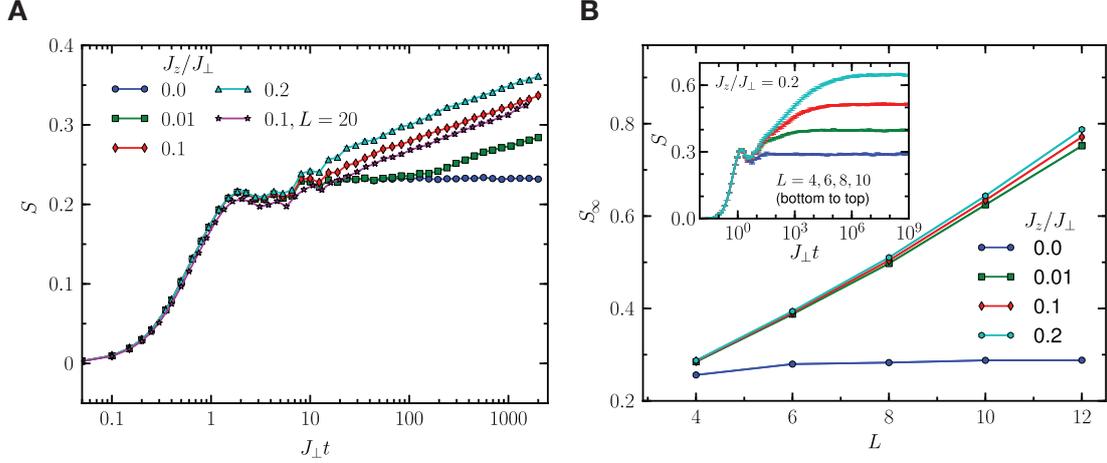
Figure 4.4: Entanglement growth in AL vs. MBL systems, A: The growth of entanglement entropy $S(t)$ is shown as a function of the interaction strength. In the AL case ($J_z = 0$), the entanglement entropy saturates after a small increase. In contrast, in the MBL phase $J_z > 0$, the entanglement entropy grows slowly, increasing logarithmically with time. This is quite different to non-disordered systems, where entanglement is expected to grow linearly with time. L denotes the size of the spin chain. **The unbounded growth of the entanglement entropy in the MBL phase, B:** The growth of the entanglement is unbounded in the MBL phase, and the saturation S_∞ follows a volume law (i.e. proportional to L in one dimension). The inset shows the time dependence for various system sizes. In contrast, the AL system has a bounded entanglement growth. The surprising feature of the MBL phase is the growth of entanglement without any particle transport. Figure adapted from Ref. [119] with permission. Copyrighted by the American Physical Society.

where **Tr** is the trace operator and ρ is the density matrix of a sub-system. Naturally, there is no entropy in the entire system, as it is assumed to be in a pure state. Instead, typically one can consider a small subsystem A of the entire system, which is entangled with the rest of the system. Importantly, such a sub-system A is chosen in real space (as we are discussing localization in real space).

For states which follow an "area-law", the entanglement of the subsystem A, with a density matrix ρ_A, scales as the periphery of the system (a pictorial depiction is shown in as the cover illustration of the thesis):

$$S_A = -\mathbf{Tr}(\rho_A \log(\rho_A)) \propto L^{d-1} \tag{4.4}$$

where L is the linear size of the sub-system A and d is the number of dimensions of the system. This implies that if the system indeed follows an "area-law", then the sub-system has very little influence on far away parts of the system. In one dimension, *ground-states* of all local and gapped Hamiltonians follow such an area law, e.g. band insulators and Mott-insulators [120, 121]. Higher dimensions and longer-range interactions are fundamentally harder to understand, and it is not so clear if area laws also hold true in those systems [120]. Further, *finite-energy-density* states are different and are expected to follow a "volume-law" of entanglement for subsystems, i.e. $S_A \propto L^d$. We expect such a volume-law to hold for delocalized systems at finite energy density. The systems mentioned above

which satisfy the area law, such as the Mott-insulator and the band insulator, possess *localized* states. However, the excited states of those Hamiltonians, away from those exact filling, have no localization property and hence, should follow volume-law entanglement. On the other hand, localization persists in AL and MBL cases for all energy densities, and hence, one expects them to follow an area-law [40].

Probing the dynamics in such systems can also reveal interesting features. For a simple illustration of the dynamics of entanglement entropy, we consider the above mentioned XXZ Hamiltonian, and probe the growth of entanglement entropy $S(t) = \mathbf{Tr}(\rho_A(t) \log(\rho_A(t)))$ after starting with an initial state as the classical Néel state which has zero entanglement and taking the subsystem to be one-half of the system. We remark that in this initial state, there is no entanglement in the *real-space* basis. For this system, the growth of the entanglement after a quantum quench *without disorder* was studied in Refs. [122–124] and shows a ballistic entanglement growth, $S(t) \propto t$. This was found to be true for both integrable and non-integrable systems. The key property of these systems was their delocalized nature, and the spatial entanglement grew in a ballistic fashion [38]. Furthermore, in the non-integrable model which is expected to follow ETH, as studied in Ref. [124], the entanglement saturated $\propto L$, i.e. volume law. This is also the expectation from a thermal state. Note that this is not precisely $S_\infty = L/2$, as shown in Ref. [125], but in the thermodynamic limit, the relative error is small. This implies that the dynamics are consistent with a fully mixed and thermal system.

On the other hand, it was found that in MBL systems, the entanglement entropy grew proportional to the logarithm of time, i.e. $S(t) \propto \log(t)$, as reported in Ref. [126] in 2008 (the year after the XXZ model was introduced in Ref. [105]), highlighting the localized nature of the eigenstates in the MBL phase. Moreover, it was found that the growth of entanglement entropy was unbounded, and the saturation only happened after an exponentially long time in the system size $t \sim e^L$ and followed a volume-law $S(t \to \infty) \propto L$ [119]. Naively, this would imply that the system eventually always thermalizes just slower than normal systems. However, the saturation value of the entanglement entropy per site was found to be smaller than the infinite temperature thermal value (which would be associated roughly with two states per site, for the randomness associated with two spins) [40, 127, 128]. This can heuristically be understood as a result of dephasing due to interactions, which fully mix the quantum phases, but do not delocalize the system.

The results of Ref. [119] are shown in Fig. 4.4. After a quench in the MBL or AL phase, the spin density imbalance saturated to a non-zero value, supporting the absence of transport. In the AL phase, the entanglement entropy growth halts at a finite value and also shows the same behavior as the spin imbalance. However, in the MBL phase, the entanglement continues to grow indefinitely, showing volume law saturation. We note that entanglement entropy can grow even without interactions in the delocalized phase due to particle transport. The surprising feature is the continuous increase of the entanglement even in the absence of any particle transport. Additionally, the results show that the saturation follows volume law, but it is still *sub-thermal*, showing that MBL systems do not fully thermalize (unlike the ergodic case).

Behavior	XXZ Parameter	Transport	Entanglement	Expt. Examples
FF	$J_z = 0, \Delta = 0$	Ballistic	$S \propto t, S_\infty \sim V$	$U = 0$ FHM [129] $U = 0$ BHM [111]
AL	$J_z = 0, \Delta > 0$	0	$S \propto c, S_\infty \sim c$	RR/AA [63, 64]
II	$J_z = 1, \Delta = 0$	Ballistic	$S \propto t, S_\infty \sim V$	1D-FHM [72] 1D HC-BHM [111]
Thermal	$J_z = 1, \Delta = 1$	Diffusive	$S \propto t, S_\infty \sim V$	2D-FHM [129] 1D-BHM [79, 111]
MBL	$J_z = 1, \Delta = 10$	0	$S \propto \log(t), S_\infty \sim \alpha V$	1D MBL [72]

Table 4.1: Summary and important characteristics of the five high-temperature regimes: The table shows a summary of the five high-temperature behaviors and their central properties. These properties are written for the known case of XXZ parameters. While entanglement growth is hard to measure in an experiment, one can consider coupled systems to probe many properties of the systems to distinguish the interacting vs. non-interacting cases, see Chapter 7. c is a constant and α is some constant less than unity which describes the non-thermalness of the MBL phase. The abbreviations used stand for: FF = Free fermions, AL = Anderson localized, II = Interacting integrable, MBL = Many-body localized, BHM = Bose-Hubbard Model, FHM = Fermi-Hubbard Model, HC = Hard core interactions, $U = \infty$, RR = real-random disorder, AA = Aubry-André. S denotes the spatial entanglement growth after quench from a product state. S_∞ is the spatial entanglement after infinite evolution times, and V denotes "volume law".

In summary, the MBL phase shows a logarithmic entanglement growth without particle transport which saturates to a volume but the sub-thermal value at infinite times (or more precisely at exponentially long times in the system size). Further, this growth begins roughly around inverse local interaction timescales $\propto 1/J_z$. Having discussed these two results, one can also ask about the results at the MBL critical point and the behavior of entanglement *at* the critical point [41, 42]. Unfortunately, while being extremely interesting, this is currently far away from understood, like most other questions about relaxation near the critical point.

Overview of the Experimental Setup and the Measurement Techniques

Short summary: The experimental setup is briefly overviewed. In particular, two important processes are described: the construction of discrete lattice models from continuous optical fields and the band-mapping sequence used to extract the even-odd imbalance.

5.1 A degenerate gas of fermionic Potassium-40 atoms

All experiments in this thesis are performed with an ultracold fermionic gas of Potassium-40 (^{40}K) atoms, produced via sympathetic cooling with bosonic Rubidium-87 (^{87}Rb) atoms. These two gases are captured together in a dual-species Magneto-Optical trap and then cooled evaporatively. The entire production procedure and the evaporative cooling sequence is fairly involved and can be found in earlier Ph.D. theses from our group [130–132]. Only the essential characteristics of the resulting ultracold gas are briefly overviewed.

The reduced temperature of the ultracold Fermi gas in the dipole trap is $T/T_F \approx 0.15$, where T_F if the Fermi temperature, with about $5\% - 10\%$ fluctuations between different experimental realizations. The total atom number is about 10^5, with similar relative fluctuations as in the temperature. The total atom number can be varied up to a factor of 2-3, without changing the temperature. However, this does not change the effective system size much, especially in lower dimensions d, as the effective system size scales more weakly ($\propto N^{d/3}$) than atom numbers. Hence, within the current status of our experiment, we can assume the system size to be approximately fixed. Such a filling results in about 200 atoms in the central tube along the x-direction and a similar number of atoms along the y-direction. Due to a much stronger confinement along the z-direction, the size of the ultracold gas along the z-direction is about five times smaller. All experiments in this thesis are restricted to a maximum of two dimensions and for almost all times, the z-direction would be effectively uncoupled (i.e. the probed timescales are such that there is negligible hopping along the z-direction).

The experiments utilize a mixture of the two lowest-hyperfine levels of ^{40}K atoms, which are denoted as the up-spin $|F, m_F\rangle = |\frac{9}{2}, -\frac{9}{2}\rangle \equiv |\uparrow\rangle$ and down-spin $|F, m_F\rangle = |\frac{9}{2}, -\frac{7}{2}\rangle \equiv |\downarrow\rangle$, with a purity such that we cannot detect any other hyperfine levels in the dipole trap (hence, estimated to be above 99%, given the current imaging calibration). The relative

atom numbers between the two spins can be tailored. For most of the experiments, it was chosen to be 50 % in each spin state and we call this as the "spin-balanced" case. Note that due to the fermionic nature of the atoms and point-like interactions, the balanced mixture produces the "most" amount of interaction, as the same spin states effectively do not interact. The other case we sometimes use, which we call the "spin-polarized" case, has over 95 % of the atoms in the up-spin state. This allows us to switch the interactions off and use it to probe the properties of the non-interacting gas. We utilize this to set benchmarks via comparisons with explicit calculations of the corresponding non-interacting quantum models (which are much easier to simulate as compared to interacting models).

5.2   From running optical fields to discrete lattice models

While the lattice models which we want to simulate are discrete, the optical light fields we use are continuous. This dichotomy can be understood via a combination of the geometry of the problem and a separation of energy (and time) scales of the problem.

After obtaining a cold gas of fermionic atoms, we switch on the "lattice" lasers. These lasers are aligned so that they are reflected back on their incoming path from a mirror, as shown in Fig. 5.1. This forms a standing wave caused by the interference of the "forward" and the "backward" propagating optical fields, creating a periodic modulation of the light intensity in space, where the period is given by the lattice constant, $l_d = \lambda/2$, where λ is the wavelength of the laser. Depending on the detuning of the laser with respect to the transition wavelength, the atoms can be located at the intensity minimum or maximum, as the potential can be attractive or repulsive [133]. For the lattices which we have employed in the experiments, the wavelength of the lattice light and the atomic transition wavelength are well separated. If the wavelength of the light is more than the wavelength of the atomic transition, the potential is red-detuned. In this case, the minimum of the potential is found near the positions with maximum intensity, and hence, ultracold atoms are located near the *maximum* of the intensity. On the other hand, if the wavelength of the lattice laser light is less than the wavelength of the atomic transition, the potential is blue-detuned. In this case, ultracold atoms are located near in the *minimum* of the intensity of the light [133].

These periodic potentials generate many energy bands [134], which the atoms can populate. For carefully picked lattice parameters, only the ground band can be chosen to be predominantly populated. For such a case, the size of the laser beam forming the lattice should be large enough compared to the size of the atomic cloud and the intensity should be strong enough to separate the ground band from the higher bands. Additionally, the lattices have to be turned on slowly, so as to remain as adiabatic as possible. Even though the optical fields are still continuous, with almost unity probability, the atoms can now be located only at discrete points, corresponding to the potential minima, forming a discrete lattice. The "size" of a lattice site is normally much smaller than the distance between two consecutive minima. There is an appreciable probability of an atom tunneling between nearest sites, which depends on the lattice spacing l_d between them and the height of the potential barrier, controlled by the lattice laser intensity.
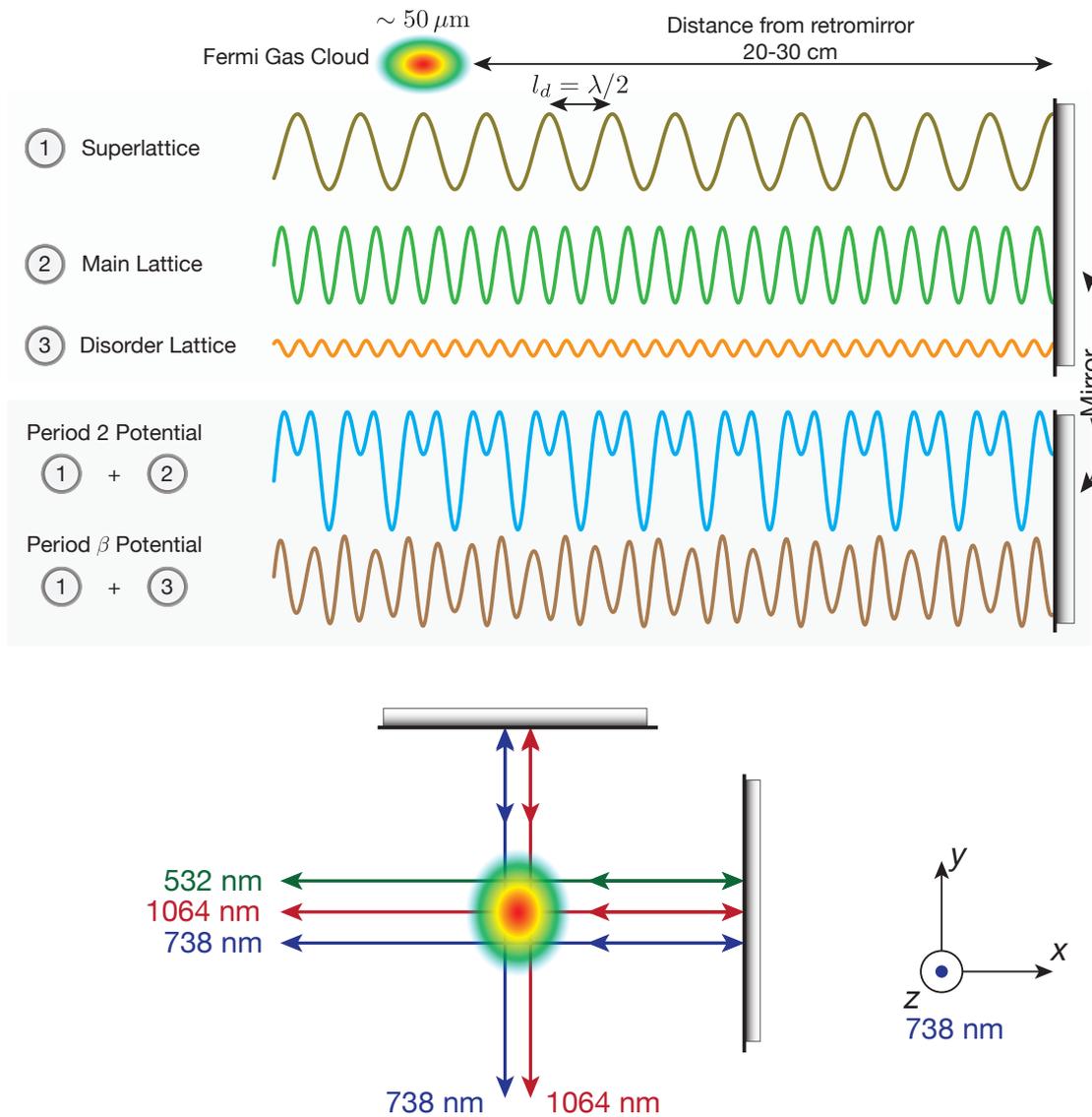
Figure 5.1: Lattice formation and experimental parameters: All lattices in this thesis are formed via retro-reflecting optical laser fields from a mirror. Upon adding a main laser to the superlattice laser (of twice the wavelength), one can obtain period-two potentials, used to create the period-two density-wave. These lasers are typically used with comparable power. The distance between the retro-mirror, and the atoms is about $20 - 30$ cm. This is much bigger than the size of the atomic cloud (FWHM of $\sim 50\,\mu$m). The size of the cloud encompasses many lattice periods, each of which is separated by half of the wavelength of the lattice light, $l_d = \lambda/2 \sim 0.5\,\mu$m. Quasi-periodic potentials are created by superposing two lasers with an irrational wavelength ratio β. The disorder laser utilizes much lower intensity as compared to the main laser, creating only a small perturbation at the minima of the potential. The picture is not to scale and is only for depiction. Additional elements, which are required to maintain the Gaussian shape of the laser beam and correct for a finite Rayleigh range, are omitted for clarity. Individual lattice wavelengths along all the directions are shown in the second picture. See Table 5.1 for more details.

Direction	Main-Lattice	Disorder-Lattice	Super-Lattice
x	532 nm	738 nm	1064 nm
y	738 nm	1064 nm	
z	738 nm		

Table 5.1: The table shows the lattices and their wavelengths which have been used in the experiment along the three directions. The z-direction points against gravity and the $x - y$ plane is orthogonal to it.

While the lattice spacing is not controllable in our experiment, the height of the potential can be tuned and hence, the tunneling can be controlled at will. Since the interactions are point-like, they are effective only if two atoms occupy the same site. Hopping to the next-nearest-neighboring sites is typically negligible, as it is multiple orders of magnitude smaller [135]. Hopping between nearest-neighbors is typically tunable between $100\,\mu s$–$1 s$, corresponding to an energy scale of $h \times 1$ Hz-10 kHz. The energy scale of the interactions is about $h \times 0$ Hz-10 kHz and the energy scale of the on-site energies is about $h \times 0$-5 kHz. The higher bands are effectively detuned away, with a minimum band-gap of about $h \times 50$ kHz (when the energy scales of the lowest band is about $h \times 1$ kHz). Here, h is Plank's constant. Further, the atom number lifetime in the dipole trap is more than 30 s and remains more than 1 s for most lattice configurations which are used. A full derivation for our setup for these parameters of the lattices is described in further detail in the following theses [132, 136]. Since the time evolution is typically restricted to 50 ms, the only relevant scales are the hopping in the ground band, the interactions between different spins on the same site and the on-site potentials. These parameters can be calculated from the intensities of each lattice laser and the magnetic field (which controls the scattering length) [132, 136], see also Appendix.A.

5.3   Optical lattices and the initial state preparation

The experiments utilize a total of six optical beams for the lattice lasers. They are obtained by distributing power from three lasers and hence, are of total three distinct wavelengths, as summarized in Table 5.1. The source of the 532 nm light is a Coherent 18 W Verdi, the source of the 738 nm light is a Coherent titanium-sapphire laser pumped with another Coherent 18 W Verdi and the source of the 1064 nm light is a Nufern amplifier 50 W pumped with about 100 mW of Rock laser. Here, W denotes the power in Watts.

The turning on of the optical lattice potentials is done slowly so as to minimize heating and be as adiabatic as possible. The crucial factor here is to load as many atoms as possible into the *ground* band of the resulting optical lattice. The full sequence to load into a deep lattice to freeze the system is shown in Fig. 5.2. All optical powers are expressed in terms of their respective recoil depth energy, $E_r^\lambda = h^2/(2m\lambda^2)$. Here, h is Plank's constant, m is the atomic mass of ^{40}K atoms and λ is the wavelength of the laser light.

By controlling the wavelength of each of the lasers, the phase of the lattice at a given point in space can be controlled. This can be understood as follows: the zero of the phase
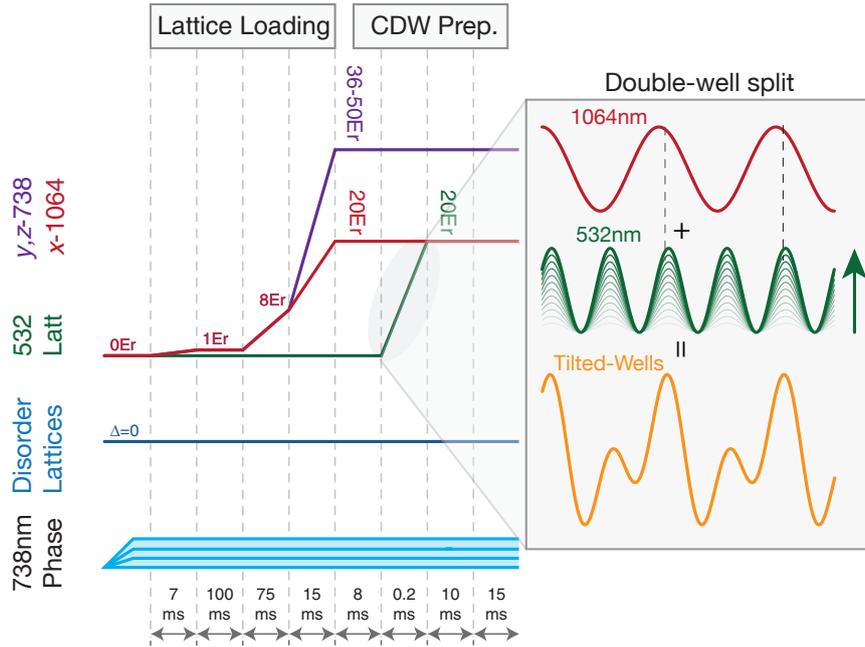
Figure 5.2: Creation of the one-dimensional charge-density wave (CDW): The atoms are transferred from the optical dipole into an optical lattice by slowly turning on the intensity of the lattice lasers. Along the x-direction, we additionally use a super-lattice potential composed of 532 nm and 1064 nm lasers to create tilted wells, by first switching on the 1064 nm laser and following by switching on the 532 nm laser with a phase difference. At the end of this sequence, the atoms predominantly occupy one side of the well, which has lower on-site potential. The 738 nm lattices along the y-direction and the z-direction are kept deep during this time.

is set by the retro-mirror but the atoms are located at some distance from the mirror. The effective phase at a point in space, say at a distance L away from the mirror, is given by $2L/\lambda \mod 2\pi$. Here, mod is the modulo operation. Since the atomic cloud is about 20 cm away from the retro-mirror, tuning about 1 GHz results in about 2π or one lattice site of phase change. While this frequency change is negligible concerning the modification of the lattice parameters, such as hopping or on-site interactions, it allows the control over the lattice phase. This phase control is crucial for the preparation of the density wave, as the *relative* phase between two super-lattice lasers allows us to create the density modulation.

Along the x-direction, we first switch on the 1064 nm lattice laser slowly to a depth of $1\,E_{\mathrm{r}}^{1064\,\mathrm{nm}}$, so that the atomic distribution can adjust to the lattice potential. Next, we slowly increase the intensity of the lattice potential to a depth of $8\,E_{\mathrm{r}}^{1064\,\mathrm{nm}}$, where the dynamics are relatively frozen. We then increase the lattice depth to about $20\,E_{\mathrm{r}}^{1064\,\mathrm{nm}}$. Next, we increase the intensity of the 532 nm lattice laser to a depth of $20\,E_{\mathrm{r}}^{532\,\mathrm{nm}}$, with a phase of about $\pi/3$, such that the individual double well it forms with the 1064 nm lattice is highly tilted, resulting in primarily loading all atoms on one-side of the well, which has lower on-site energy. This is because, in the reduced basis of a double well, the ground band is almost completely localized on the deeper side.

The main lattices along the y-direction and the z-direction are similarly first ramped to shallow and then to higher values. The final values of their intensity depend on the

experiment since we redistribute the available laser power according to the requirement of the experiment. However, typically they were chosen to be between $36 - 50\, E_\mathrm{r}^{738\,\mathrm{nm}}$, creating a deep enough lattice, so that the hopping was strongly suppressed during the loading sequence.

5.3.1   Super-lattice setup

The super-lattice is a combination of two lattices - the 532 nm lattice and the 1064 nm lattice. The 1064 nm laser output can be as large as 50 W, but typically only about 10 W of laser power is used. It is locked to an external cavity which is thermally stabilized and acoustically isolated to provide a short-term stability of about 100 kHz. Since about 1 GHz of change in the frequency of the laser implies a phase change of π; and this stability is sufficient for the experiment. The 532 nm laser is locked to the 1064 nm laser, by frequency doubling the 1064 nm light and then locking them together via an offset beat lock, which provides feedback to the 532 nm laser. The short term stability is approximately 1 MHz. This is covered in more detail in Ref. [132].

5.3.2   The main-perpendicular lattices

The main perpendicular lattices are the 738 nm lattices which run along the y-direction and the z-direction (and the same laser also provides the power for the disorder lattice along the x-direction). By controlling the source frequency, their phase can be controlled. This also means that independent control over the phase along each of the directions is not possible. However, this is not expected to be important for the measured observable. The laser generates about 4.2 W of power, out of which roughly about 2 W is put along the y-direction and 1.5 W along the z-direction and the rest along the x-direction. The short term stability of the laser is measured to be about 1 MHz.

5.3.3   Disorder lattices

The disorder lattice along the x-direction is the 738 nm lattice laser, which forms a quasi-periodic potential upon superposing it with the main lattice laser of a wavelength of 532 nm. Along the y-direction, power from the 1064 nm laser serves as the source of quasi-periodic potential for the main lattice laser of wavelength of 738 nm. Although the disorder lattices are designed to be like any other lattice, they primarily use little power as they essentially act as a perturbation to the main lattice.

5.4   Even-odd atom number readout via band-mapping

Measuring the number of atoms on the even and the odd sites allows us to extract the imbalance of the system. This is performed by utilizing the same period two superlattice which was used to create the density-wave [138, 139]. After various evolution times, the distribution of atoms is frozen by suddenly increasing the depth of the 532 nm lattice
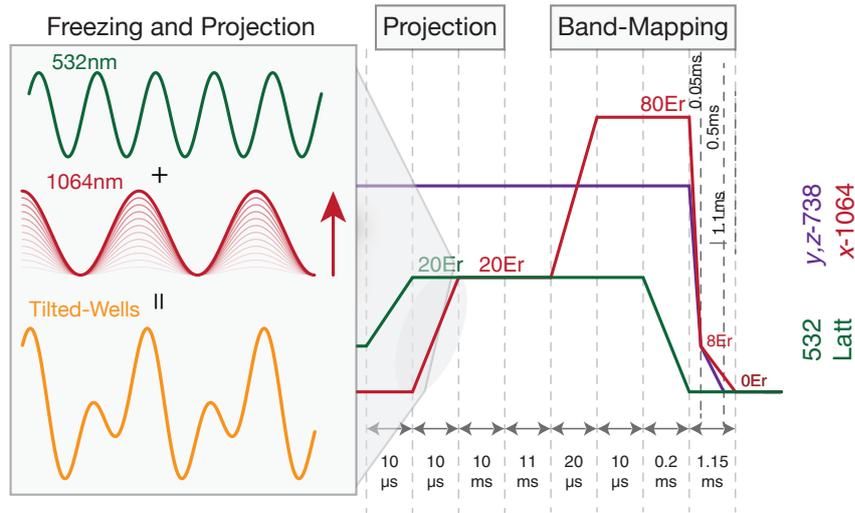
Figure 5.3: Side-projection and band-mapping: Brief schematic of the lattice ramps that lead to the creation of double wells. The band-mapping sequence follows, in which the atomic distribution is mapped to the bands of a very deep 1064 nm lattice. Finally, the 1064 nm lattice is band-mapped [137], where the atoms in the first band correspond to the atoms in the left side of the well (even sites of the 532 nm lattice) and the atoms in the third band correspond to the right side of the well (odd-sites of the 532 nm lattice).

to $20\,E_\mathrm{r}^{532\,\mathrm{nm}}$, as shown in Fig. 5.4 **A**. Simultaneously, $20\,E_\mathrm{r}^{1064\,\mathrm{nm}}$ of the 1064 nm lattice is added along this direction, with a phase difference of about $\pi/3$ to the 532 nm lattice. Since the total depth of the two lattices is large and there is a phase difference between the two lattices, it creates an array of effectively isolated double wells.

Fig. 5.4 **B** shows an individual double well, where the left side of the well contains the atoms from the even sites, and the right side contains the atoms from the odd sites of the main lattice. We now increase the depth of the 1064 nm lattice quickly, so that there is a level crossing between the second band and third band [136]. This transfers the atoms which were originally on the right side of the double well to the third band. The 532 nm lattice is then switched off so that the atoms occupy the first (=ground) band and the third band (=second excited band) of the resulting wells. The 1064 nm lattice is now turned off slowly compared to the band gaps, to not cause any excitation to the higher bands but fast compared the hopping in the lattice. This maps the quasi-momentum occupation in the lattice onto the real-space momentum. All confining potentials are then switched off simultaneously. After 8 ms of time-of-flight, we illuminate resonant light on the atoms to image them. By counting the number of atoms in the different bands, the atom numbers on the even and the odd sites at the end of the time-evolution can be extracted.

Finally, Fig. 5.4 **C** shows three exemplary band-mapped images. Since the initial state contains almost all the atoms on the even sites, this implies that the band-mapped image should contain a very high population of atoms in the ground band. This is indeed the case as shown in the first image. On the other hand, if the atoms are equally distributed between the even and odd sites, then the first and the third bands should be equally populated. This is the case shown in the second image. Finally, the third image shows
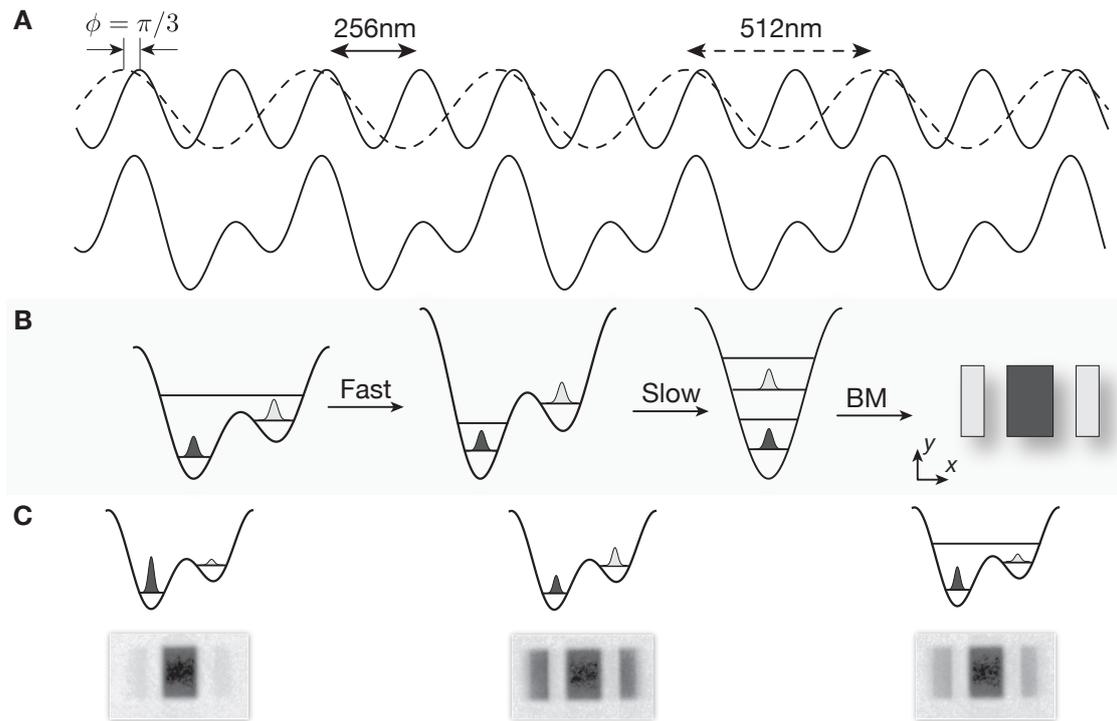
Figure 5.4: Freezing of the dynamics and creation of isolated double wells, A: After the dynamical time evolution is complete, we increase the depth of the main lattice (solid line) quickly and superpose it with a long lattice of double the wavelength (dashed line) with a phase difference of about $\pi/3$. This creates an array of isolated and tilted double wells (bottom). **Band mapping sequence, B:** In the individual double wells, the left well has the atoms from the even sites, and the right well has the atoms from the odd sites. We now ramp the long lattice quickly to even deeper values, to make the second and third band of the double well cross their energies. Next, we switch the main lattice off. This projects the atoms on the even sites on the ground band and on the odd sites on to the second excited band. Upon switching off the long lattice, the quasi-momenta of these bands projects onto real-space momenta. **Example band-mapped time-of-flight images, C:** Upon switching off all the potentials, the atoms are released in free-fall for about 8 ms. Subsequently, we shine resonant light and perform absorption imaging. Three exemplary resulting cases are shown. The first one has a strong imbalance between the left and the right side, and hence, almost all of the atoms are measured in the ground band. This is what the initial state in the experiment maps to. The second one has an equal number of atoms on the even and the odd sites and results in zero imbalance between the even and the odd sites. This is how a thermal state would appear. Finally, an intermediate case is shown with a visible imbalance between the left and the right sides. This is typical when the system is well localized.

an interesting case, where the system is not the same as the initial state but also does not show full redistribution between the even and odd sites, indicating partial memory of the initial atom distribution.

5.5   Doublon fraction and energy density

Usually, the energy density of a state is associated with its temperature – the higher the temperature, the higher is the energy density. For systems which obey ETH, this makes sense, as the temperature is the single parameter which essentially characterizes the observables at a given energy density. However, since MBL systems do not thermalize, they do not have a well-defined temperature. Hence, we use the energy density to characterize different observables and not the temperature.

To vary the energy density of the system in the lattice Hamiltonian, one could change the temperature of the ultracold gas in the dipole trap. However, these two cases are not the same. This is because, by increasing the temperature of the ultracold gas, one would also necessarily increase the size of the cloud, resulting in a more dilute gas of atoms. Therefore the size of the system dramatically changes in the lattice, as well as increases the average distance between the atoms (by introducing more holes in the state), effectively reducing the interaction strength of the system. It creates additional complications by populating higher bands during the loading process and therefore, changes the density of the ground band which we are interested in probing. Finally, this creates a counter-intuitive situation: one would expect a high energy-density state of a repulsive Hubbard model to have a lot of doublons (sites with double occupations), but a high-temperature state in the dipole trap translates to having almost no doublons in the lattice.

An alternative way to change the energy density of the state is via the number of doublons in the initial state. This can be achieved by controlling the interspecies scattering length during the lattice switch on. Subsequently, the interactions can be independently chosen during the time evolution. To characterize this, before the lattices are switched on, we slowly change the interspecies interactions strength to different values using a Feshbach resonance at 202.1 G [140] and then switch the lattices along the y-direction and the z-direction to a depth of $36E_r^{738\,nm}$. Simultaneously, we also increase the depth of the 1064 nm lattice along the x-direction to $20E_r^{1064\,nm}$ and then quickly ramp it further deep to $40E_r^{1064\,nm}$. This freezes the atomic distribution during the time of measurement of the doublon fraction. The Feshbach field is then tuned in about 3 ms to either 206.3 G, which is above the resonance or to 198.3 G, which crosses the resonance. Upon crossing the resonance, doublons on a single site are converted to Feshbach molecules with very high fidelity [141]. The bound molecules have a slightly different resonance wavelength as compared to the unbound single atoms. Hence, the normal imaging sequence can be used to detect the number of atoms which were on singly occupied sites, and this provides an estimate of the number of doublons.

Fig. 5.5 **A** shows this measured doublons fraction as a function of the scattering length during the lattice switch on. By making the scattering length strongly repulsive, one suppresses almost all doublon formation, while if we make the interaction strength attractive, then we can obtain close to 50 % doublon fraction. The resulting number of doublons in the lattice depends on the temperature of the ultracold gas in the dipole trap and on the adiabatic-ness of the loading procedure [142]. For all the experiments in this thesis, this remains limited to a maximum of 50 % in the initial state. Fig. 5.5 **B** shows the measured doublon fraction as a function of the temperature of the ultracold gas in the dipole trap
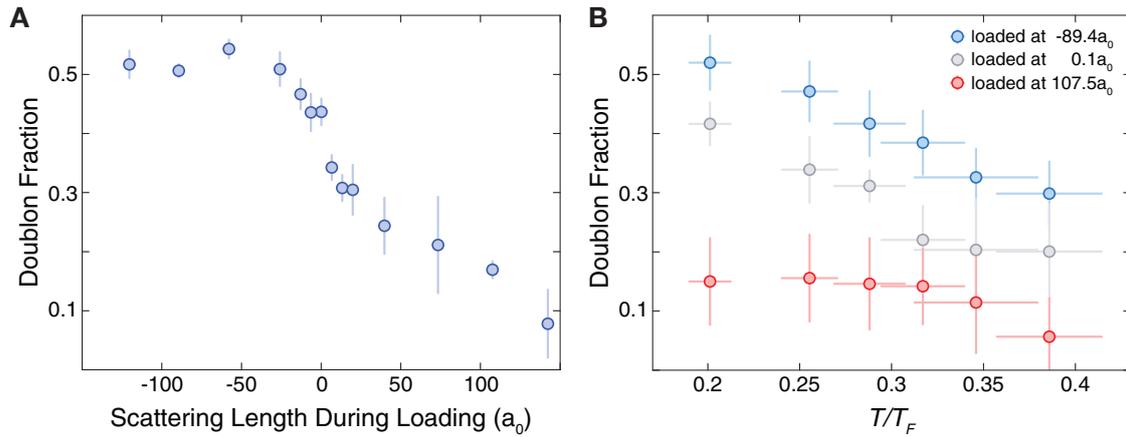
Figure 5.5: Doublon fraction as a function of the scattering length, A: The doublon fraction can be varied by choosing different interspecies interaction lengths before the optical lattice potentials are turned on. This shown for a reduced temperature of $T/T_F = 0.2$. Attractive interactions result in a higher doublon fraction as compared to repulsive interactions. **Doublon fraction as a function of temperature, B:** For three difference interspecies scattering lengths, we show the measured doublon fraction as a function of the reduced temperature. We observe that colder temperatures result in higher doublons. Error bars show the standard deviation.

for three different scattering lengths. First, we consider the non-interacting case which is easier to understand. We measure significantly more doublons at lower temperatures compared to higher ones. This can be understood by thinking about the extreme cases first. At zero temperature, the system has no entropy. This would correspond to a state in which each site occupies one doublon, and hence have zero spin and zero hole entropy. On the other hand, at high temperatures, the ultracold gas becomes both big in size as well as dilute. This would result in a very low doublon fraction. For a flat box, it is easy to estimate the doublon fraction from this argument. Consider a L site system and $N/2$ particles of each spin state and $\alpha = N/L \leq 1$ characterize this. One can, therefore, estimate the probability of the doublon fraction as $\alpha/(2-\alpha)$. As α increases with decreasing temperature, the doublons fraction increases with decreasing temperature. This increasing doublon fraction with decreasing temperature is shown in Fig. 5.5 **B**. This is because it is harder to create a doublon starting from a large cloud of atoms with low density. Tuning the scattering length to repulsive (red symbols) suppresses doublon formation. Qualitatively, this can be understood as a result of different energy scales. If the repulsion is stronger than all other energy scales, a low-temperature state contains almost no doublons. Therefore, changing the temperature has a negligible effect on the doublon fraction. Similarly, attractive interactions (blue symbols) favor doublon formation.

# Many-Body Localization in a One-Dimensional Optical Lattice

Short summary: We observe the breakdown of ergodicity, indicating many-body localization of interacting fermions in a one-dimensional quasi-periodic optical lattice potential. This is achieved by monitoring the relaxation of a period-two density-wave, prepared as the initial state. The experimental results show a highlighted difference between the dynamics in the MBL phase and the ergodic phase.

6.1 Introduction

The ergodic hypothesis forms the backbone of statistical mechanics and allows us to gain a quantitative description of many-body systems and their long-time dynamical response. In an ergodic time evolution, local degrees of freedom get fully entangled with the rest of the system, leading effectively to a classical description at long times [39]. Ergodicity is thus responsible for the demise of quantum correlations in the dynamics of many-body systems. It is therefore of fundamental interest to investigate regimes where ergodicity breaks down and understand the alternative, genuinely quantum paradigms for the dynamics that would ensue in its absence. Recent theoretical works have pointed to many-body localization in a disordered quantum system as a robust, generic alternative to ergodic behavior [21, 104, 143]. In such an MBL phase, the relaxation of local observables does not follow the conventional paradigm of thermalization and is expected to show ergodicity breaking explicitly.

While the non-interacting case of Anderson localization has seen several experimental realizations, including light scattering from semiconductor powders [144], photonic lattices [145], and in ultracold atoms [63, 64, 146], the interacting generalization of MBL has been harder to unambiguously detect. In traditional condensed matter systems, the underlying phonon bath is expected to mask the signatures of MBL [147]. On the other hand, it is aa challenging task to introduce interactions in optical light fields which mimic quantum models.

Ultracold atoms provide a unique opportunity to explore this phase because of control over both interaction as well as disorder and can be approximated very well as isolated systems. One important distinction between our experiment and most theoretical studies is that the onsite energies in our experiment are not distributed in a real-random way,
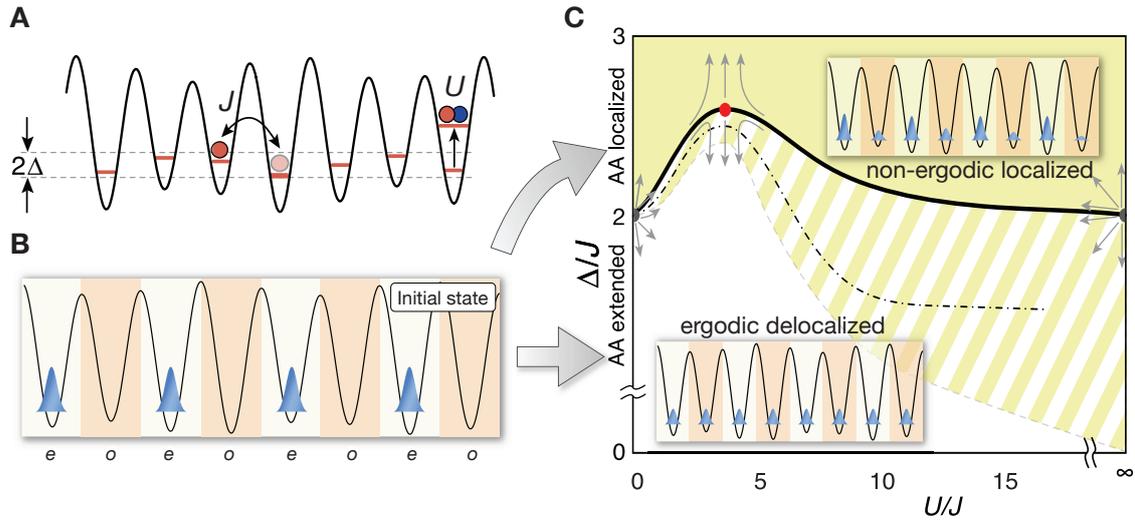
Figure 6.1: One-dimensional interacting Aubry-André model, A: The Hamiltonian of the system is composed of three terms: the hopping between neighboring sites J, the onsite interaction energy U and the quasi-periodic disorder potential with the strength Δ. **Initial state density-wave, B**: The atoms are prepared in a high energy-density state, such that only the even sites are predominantly occupied with atoms, while the odd sites are unoccupied. This is a far-from-equilibrium state whose relaxation is monitored. **The ergodic phase and the non-ergodic phase, C**: The resulting phase diagram is shown as a function of the disorder strength Δ and the interaction strength U. In the ergodic phase, the density-wave quickly smears out. In the non-ergodic localized phase, the system retains partial memory of the initial state and a part of the density-wave order persists. For zero-interactions, the system has a (de)localization transition at $\Delta = 2J$. Upon introducing interactions, the system can undergo the (de)localization transition depending on the strength of the disorder. For sufficiently large disorder strengths, interactions are unable to cause delocalization. The exact boundary of the transition further depends on the energy density of the initial state, and is expected to lie in the shaded area. The solid black line denotes the expected phase boundary in the absence of doublons, where the critical disorder strength for hard-core interaction is the same as the non-interacting case.

but in a quasi-periodic fashion. However, this does *not* a priori preclude the existence of an MBL phase and several theoretical studies find evidence for the existence of localization with interactions even in quasi-periodic potentials [148–151]. In fact, there is some evidence that the MBL phase might even be more stable in quasi-periodic systems as compared to systems with real-random disorder [152]. Note that, in Ref. [72], we had called this kind of disorder as "quasi-random" and "quasi-periodic" more or less interchangeably. However, with growing semantics and the possibility of different critical properties in systems with deterministic versus non-deterministic disorders [152], it seems appropriate to call this kind of onsite disorder term quasi-periodic potential.

6.2   Model

Our system can be described as the one-dimensional Fermi-Hubbard model with quasi-periodic onsite energies. This is equivalent to the one-dimensional Aubry-André model [85] with onsite interactions between the two-spin species. The Hamiltonian of the system can be written as:

$$\hat{H} = -J \sum_{i,\sigma} (\hat{c}_{i,\sigma}^{\dagger} \hat{c}_{i+1,\sigma} + \hat{c}_{i+1,\sigma}^{\dagger} \hat{c}_{i,\sigma}) + \Delta \sum_{i,\sigma} \cos(2\pi\beta i + \phi) \hat{n}_{i,\sigma} + U \sum_{i} \hat{n}_{i,\uparrow} \hat{n}_{i,\downarrow} \qquad (6.1)$$

The terms of the Hamiltonian are illustrated in Fig. 6.1 **A** and their physical meaning is explained below:

1. $J \approx h \times 550\,\text{Hz}$ is the nearest-neighbor tunneling matrix element, and controls the hopping time between neighboring sites, $\tau = h/(2\pi J) \approx 0.290\,\text{ms}$. It is set by the main lattice with a lattice spacing $l_d = \lambda/2 = 256\,\text{nm}$ and the depth of the lattice $8\,E_r^{532\,\text{nm}}$. All evolution times are given in terms of this hopping rate. Throughout the experiment, this serves as the energy scale.

   $\hat{c}_{i,\sigma}(\hat{c}_{i,\sigma}^{\dagger})$ are the destruction (creation) operators and as the particles are fermions, they obey anti-commutation relations. The spin of the particle is given by $\sigma \in [\uparrow, \downarrow]$, i denotes the lattice site and the number operator is defined as $\hat{n}_{i,\sigma} = \hat{c}_{i,\sigma}^{\dagger} \hat{c}_{i,\sigma}$.

2. U is the interaction term, which is the energy cost of putting two atoms on the same site. As the atoms are fermionic, they must have opposite spins. The magnitude of the interaction can be controlled by tuning the scattering length via a Feshbach resonance [140]. Using the repulsive side of the resonance, the maximum accessible U/J is approximately 20. Using the attractive side, we can access much larger $|U/J|$, but it is less stable as compared to the repulsive side.

3. Δ sets the strength of the quasi-periodic potential. For $\Delta = 0$, the Hamiltonian reduces to the one-dimensional Fermi-Hubbard model, which is integrable for all interaction strengths [112]. For any small but finite value of the disorder $\Delta > 0$ and the interaction $U > 0$, the system is expected to be away from the integrable limit.

   The quasi-periodic potential is parametrized by the incommensurable number $\beta \approx 532\,\text{nm}/738\,\text{nm} \approx 0.721$ and the phase of the disorder realization ϕ.

It is widely believed that for almost every irrational β, all single-particle eigenstates are localized for disorder strengths $\Delta > 2J$, all single-particle eigenstates are delocalized for $\Delta < 2J$ and there is a *single* metal-insulator transition at $\Delta = 2J$ at all energy densities [85–88]. This is in contrast to real-random disorder, wherein localization occurs for arbitrarily small disorders. This model was experimentally realized with ultracold atoms in the group of M. Inguscio in Italy [63] by superposing two lasers with incommensurate wavelengths. The non-interacting system with a real-random disorder was realized using ultracold atoms in the group of A. Aspect in France [64] using speckle potentials. In

many ways, the expansion dynamics studied in these experiments forms the basis of our experiment, extended to the realm of individual particles and sites.

6.3   Observable

The initial state in the experiment is prepared using the superlattice setup, such that only every second site is occupied, as depicted in Fig. 6.1 **B**. This density-wave is the starting point of the experiment. The relaxation of this density-wave is monitored and character-ized by our main observable, the imbalance, defined as the difference in the fraction of atoms on the even and the odd sites,

$$\mathcal{I} = \frac{N_e - N_o}{N_e + N_o} \tag{6.2}$$

where, $N_e(N_o)$ is the total number of atoms on the even (odd) sites. Such an observable has several key advantages. In the absence of disorder, the particles will quickly tunnel to nearby sites and the imbalance will vanish in a few tunneling times [93, 95, 96] (see Fig. 3.5). This allows us to clearly separate a longer, disorder induced timescale. The im-balance serves as our dynamical order parameter and characterizes the system as localized or delocalized by its value at long times,

$$\lim_{t \to \infty} \mathcal{I}(t) = \begin{cases} 0 & \text{Delocalized} \\ > 0 & \text{Localized} \end{cases} \tag{6.3}$$

Since no experiment works at truly infinite times, our measure will be to look at times which are much bigger than the hopping time, i.e. $t/\tau \gg 1$, to infer the localization properties of the system.

6.4   Results

6.4.1   Observation of Anderson localization with non-interacting fermions

Since the non-interacting system is easy to both simulate and understand, the experiment is first benchmarked against this case. To this goal, the interaction strength is set to zero by tuning the magnetic field to approximately 209 G [140] and the imbalance is monitored for various evolution times for different disorder strengths. This is shown in Fig. 6.2.

In part **A**, the imbalance is shown as a function of the evolution time for three important cases. The imbalance is close to unity at zero evolution times since only the even sites are occupied in the initial state. In the absence of disorder, $\Delta/J = 0$, the system is expected to be delocalized and hence, the imbalance should quickly vanish. This is indeed observed to be the case, and the imbalance vanishes within a couple of tunneling times. This supports that the system is delocalized.

On the other hand, upon tuning the disorder to higher values, and in particular, beyond the localization transition at $\Delta/J = 2$, the time evolution is expected to result in a non-zero value of the imbalance at long times. This is indeed observed in the time traces of
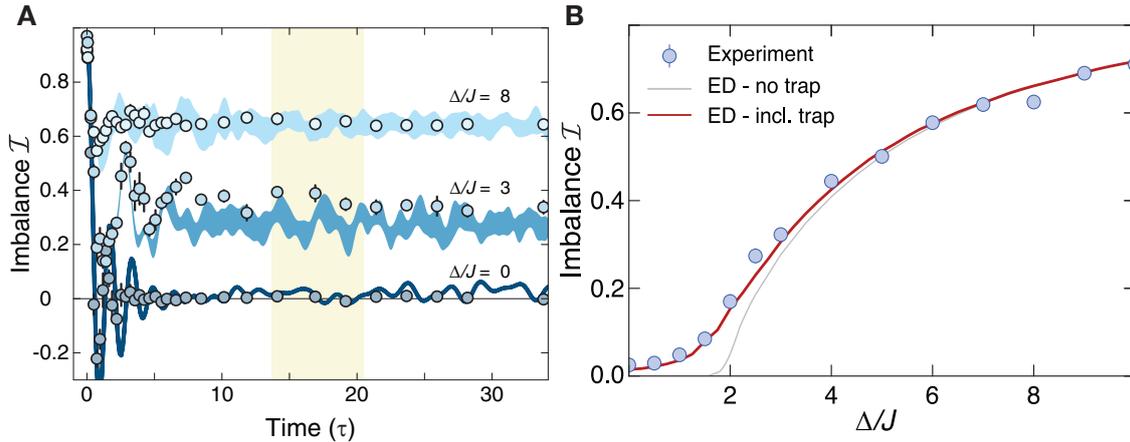
Figure 6.2: Non-interacting time evolution, A: For three different disorder strengths and zero interacting strength, we show the imbalance as a function of time. In all cases, the imbalance at zero evolution time is close to unity, since almost all the atoms are located on the even sites in the initial state. However, the relaxation dynamics of the imbalance is strongly governed by the disorder strength: for no disorder $\Delta/J = 0$, the system is delocalized and the imbalance relaxes quickly to zero. On the other hand, at $\Delta/J = 3$ and 8, the imbalance remains non-zero to very long times, signaling localization. The yellow shaded area indicates the time window used to extract the quasi-stationary imbalance. Solid lines denote Exact Diagonalization (ED) calculations, and their width denotes the standard deviation calculated from several phase realizations of the disorder. Each point is an average over six individual experimental realizations. Error bars denote the error of the mean. **Disorder dependence of the quasi-stationary imbalance, B**: The average value of the imbalance in the yellow shaded area is shown as a function of the disorder strength. We observe that the imbalance increases continuously with increasing disorder strength. ED calculations taking into account the harmonic trap are shown as the red line. The gray line shows the same calculation in the absence of a harmonic trap. The harmonic trap effectively sets a cut-off for the maximum length scale in the non-interacting system. The non-interacting transition occurs at $\Delta/J = 2$. To be sure that the system is non-interacting, a spin-polarized gas was employed and additionally, the interaction strength was set to zero.

the imbalance for $\Delta/J = 3$ and 8. The imbalance decreases from unity but stays non-zero, indicating localization. Moreover, the saturation value of the imbalance is observed to be larger for $\Delta/J = 8$ as compared to $\Delta/J = 3$. This shows that the system is localized more strongly for larger disorder strengths. The experimental data (symbols) are well supported with ED calculations (solid lines). To capture the behavior of the system with disorder systematically, the imbalance is measured after an evolution time of $12 - 20\,\tau$, once the initial dynamics have subsided and the system has attained a quasi-stationary value. This is shown in Fig. 6.2 **B**. The imbalance increases continuously with increasing disorder strength (symbols – experimental data, red solid line – ED calculations). A sharp change at $\Delta/J = 2$ is not observed in the experiment since an effective cut-off length-scale is imposed by the finite size of the system due to the harmonic confinement of the dipole trap and due to finite times of measurement [72, 132]. In the ED calculations, the effect of the absence of the harmonic confinement is simulated and a sharper feature can be seen near $\Delta/J = 2$ (gray line).
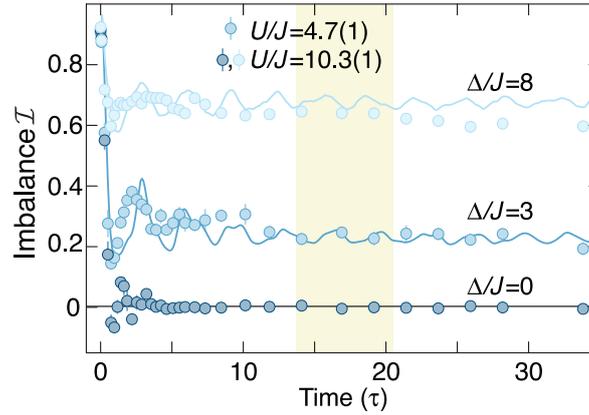
Figure 6.3: Time evolution in the interacting system: The imbalance is plotted as a function of the evolution time for several interacting cases. For larger disorder strengths, the imbalance remains non-zero even for long times. This signals localization in the presence of interactions. Each data point is averaged over six individual experimental realizations and solid lines show the result of DMRG simulations. Error bars denote the error of the mean. The yellow shaded region is used to extract the quasi-stationary imbalance.

6.4.2 Survival of localization in presence of interactions

The existence of many-body localization can be cast in terms of the stability of the imbalance plots when the system turns interacting i.e. the imbalance remains non-zero in the presence of interactions. We implement this by using a spin-mixture and the Feshbach resonance [140] to obtain the interacting system. The resulting evolution of the imbalance is shown in Fig. 6.3. We observe that the imbalance can indeed remain non-zero in several interacting cases. This supports the existence of MBL for larger disorder strengths. Note that the interactions are non-zero in all these cases. It might even appear quite similar to non-interacting time traces, supporting the result of Ref. [21], that once the single-particle eigenstates are well localized, interactions only have a marginal effect.

Fig. 6.4 shows the quasi-stationary imbalance as a function of interactions for multiple disorder strengths. Tuning the interactions from zero to intermediate values ($U/J \leq 5$) results in a reduction of the quasi-stationary imbalance. However, increasing the interactions to even larger values, *increases* the value of the quasi-stationary imbalance; a feature related to the energy density and the dimensionality of the system, explained in the next section. Experimental data points (symbols) are well supported by numerical simulations (solid lines) employing Density matrix renormalization group (DMRG) techniques. Fig. 6.4 **B** shows the phase diagram as a function of the disorder and the interaction strength, extracted by measuring the quasi-stationary imbalance. The white line denotes the equi-imbalance line passing from the known non-interacting transition point of $\Delta/J = 2$, providing an estimate for the phase boundary between the delocalized and the localized regions in interacting cases. This estimate turns out to be a lower bound of the transition, due to additional slowing down emerging from Griffiths-type effects near the MBL transition which are absent in the non-interacting model, see Chapter 9 for fur-
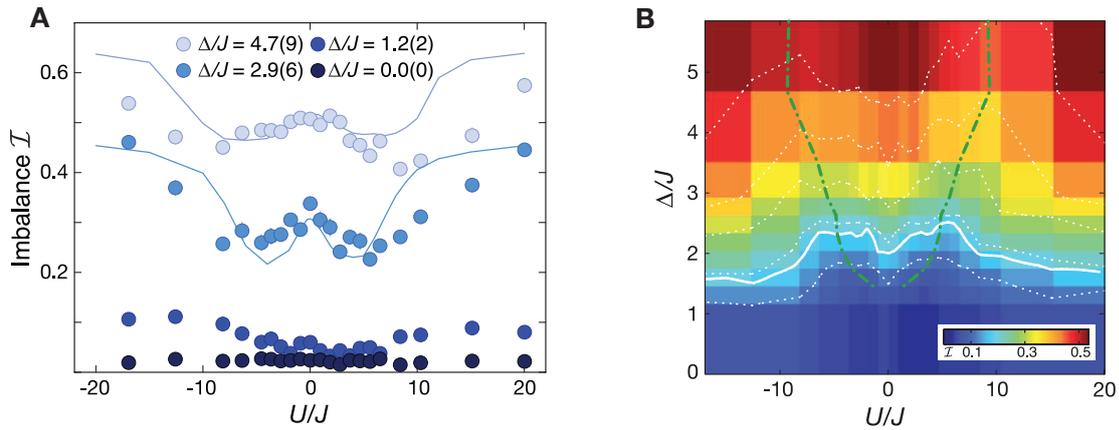
Figure 6.4: Interaction effects on the quasi-stationary imbalance, A: To illustrate the delocalizing effect of interactions, the quasi-stationary imbalance (yellow shaded region in Fig. 6.3) is shown as a function of the interactions for several disorder strengths. The quasi-stationary imbalance decreases upon tuning the interactions from zero to small values. The increase in imbalance at larger disorders is related to the presence of doublons in the initial state, due to their reduced mobility for strong interactions. Each data point is an average of twelve individual experimental realizations and error bars denote the error of the mean. Solid lines denote the results from DMRG calculations. **Expected phase diagram, B:** We plot the quasi-stationary imbalance as a function of the interaction and disorder strength. The white line is an equi-imbalance line, originating from the known non-interacting transition point at $\Delta/J = 2$, giving an estimate for the transition in interacting cases.

ther details. Furthermore, the data is observed to be symmetric under the transformation $U \rightarrow -U$, arising from a dynamical symmetry of the Hubbard model [72, 129].

6.4.3 Energy density and doublons

Small to moderate interaction strengths exhibit a lower quasi-stationary imbalance as compared to the non-interacting case. For a fixed disorder strength, the imbalance decreases from $U \sim 0$ till $U \sim 2\Delta$, after which it increases again. For very strong interaction strengths, the quasi-stationary imbalance was observed to be even larger than in the non-interacting case. Qualitatively this can be understood as follows: the initial state is prepared with a vanishing scattering length between the two spins, and hence, some of the sites (about 30% in this particular case) contained two particles. For sufficiently strong interactions, $U > 8J$, these two particles can get bound into a heavier quasi-particle (called a doublon), which has a much smaller hopping strength, $J_D \sim J^2/U \ll J$. This strongly enhances the effective disorder strength for a doublon $\Delta_D/J \propto \Delta/J_D \gg \Delta/J$, resulting in stronger localization.

To probe the effect of the energy density on the dynamics, we measure the quasi-stationary imbalance for $\Delta/J = 3$ with three different doublon fractions in the initial state, shown in Fig. 6.5. By controlling the scattering length between the two spins during the preparation of the initial state, we can tune the fraction of doublons in the initial
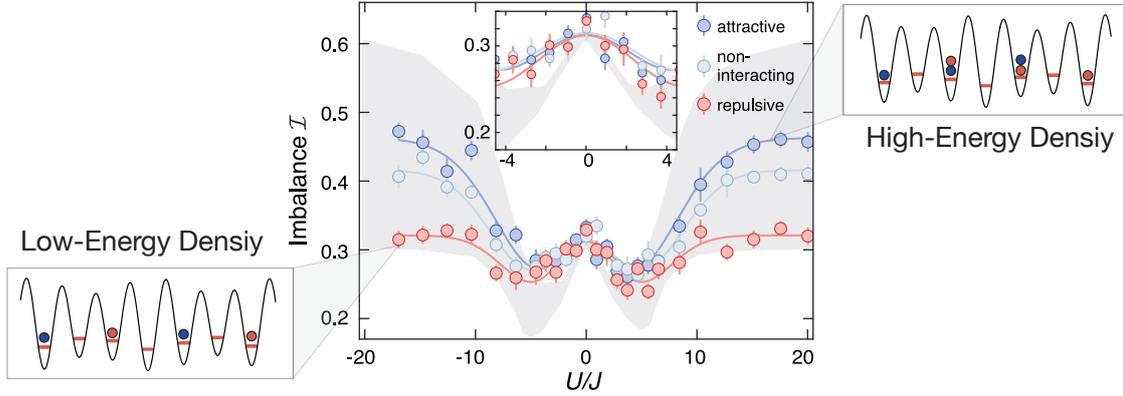
Figure 6.5: Effect of the energy-density on the dynamics in one dimension: By controlling the fraction of doublons in the initial state, we can vary its energy density and observe its effect on the dynamics. In this specific case, we test three initial states with different energy densities, varying from almost no doublons (red symbols) to about 40% doublons (dark blue symbols). We observe that more doublons result in a higher quasi-stationary imbalance at large interaction strengths. Each point is an average of twelve individual experimental realizations and error bars denote the error of the mean. Solid lines are guides to the eye. The gray shaded area represents results for the same parameters using DMRG simulations with the doublon fraction varying from 0% to 50%.

state. Attractive interactions result in many doublons and repulsive ones result in very few doublons in the initial state. In Fig. 6.5, the red symbols denote the quasi-stationary imbalance for the initial state with almost no doublon fraction, resulting from repulsive loading, the light blue points denote the case of about 30% doublon fraction, resulting from non-interacting loading and lastly, the dark blue points denote the case of about 40% doublon fraction, resulting from attractive loading. These observations can be understood by categorizing them into three effective regimes:

1. **Small interactions,** $U < 5J$: In this regime, we observe no difference in the three cases and the quasi-stationary imbalance generically reduces upon increasing the interaction strength, showing that interactions favor delocalization. Naively, this would imply the absence of a mobility edge in this regime, since there is no dependence of imbalance on the energy density. However, this might be inaccurate because the energy density varies very little in this regime. Consider the case with the interaction strength of $U = 3J$ and disorder strength of $\Delta = 3J$. The expectation value of the energy density in the initial state is zero in the absence of doublons. With about 30% doublons, it can be estimated to be roughly $0.3 \times U/2 = 0.45J$.

   The minimum possible energy density is expected to be $-2J$ (we can assume in this case that the low potentials ($\Delta_i \approx -2J$) and lower quasi-momentum states are occupied (contributing another $-1J$)). The maximum possible energy density would arise when all particles are paired to form doublons. This would total to an energy density of about $5J$. This implies that both states, with and without doublons, are essentially in the middle of the spectrum and the *relative* change in the energy density of the two states is small. Hence, the relative change in the
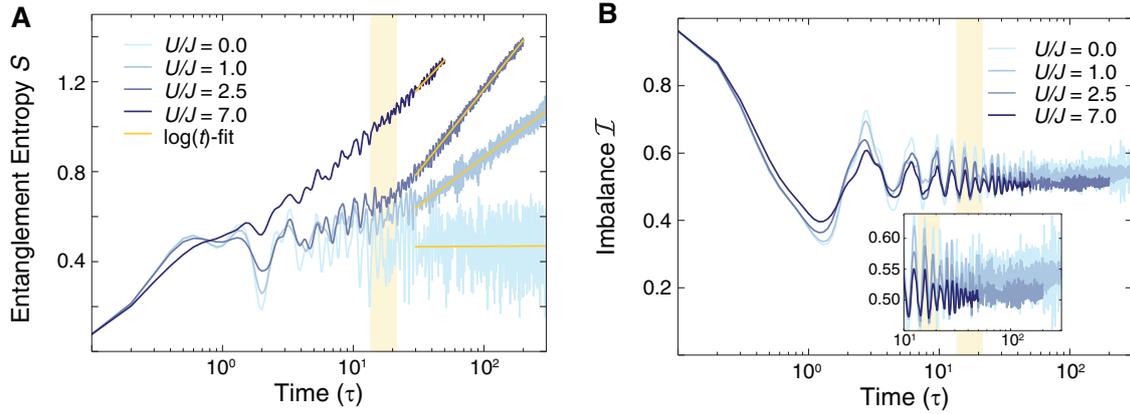
Figure 6.6: Entanglement entropy growth, S **and long term imbalance dynamics**: The DMRG simulations are shown (no experimental data) in the the plots. In **A**, the growth of the entanglement entropy as a function of evolution time is presented, showing a slow growth consistent with a logarithmic increase (At this point, it is actually unclear the exact form of the growth, see [153]). In part **B**, the imbalance is visibly non-zero and stationary, showing the stability of the MBL phase.

resulting imbalance would be negligible. For this reason, we would not be able to observe it. Hence, it is unclear whether or not a mobility edge exists (for larger changes in the energy density).

2. **Intermediate interactions (**$5J < U < 10J$**):** Upon increasing the interaction strength, we see an increase in the quasi-stationary imbalance. This increase depends mildly on the energy density and could be either a finite time effect (since doublons take longer to dissociate) or it could be due to the presence of a mobility edge.

3. **Strong interactions** $U > 10J$: At even stronger interactions, there is a marked difference between the quasi-stationary imbalance of the three cases. In the absence of doublons (red symbols), the infinitely strong interactions are known to map to non-interacting particles. Hence, the imbalance is expected to be the same for both cases, as measured in the experiment. Upon increasing the doublon fraction, we observe an increase in the quasi-stationary imbalance. In this regime, the doublons form quasi-particles and are very hard to dissociate as that requires higher-order processes. This introduces a new timescale in the dynamics, namely the hopping of the doublons, which is much slower. While the data might not be truly indicative of the infinite time answer, it shows that the dynamics are drastically slowed down. This data would also be consistent with the presence of a mobility edge.

6.4.4   Growth of the entanglement entropy

Entanglement growth has been argued to capture quantum dynamics which particle transport cannot. While in extended integrable and non-integrable systems, the entanglement grows ballistically after a quantum quench [122, 124], it was shown to increase in a log-

arithmic fashion in MBL systems [126]. While it is prohibitively hard to measure entanglement entropy in large quantum systems, it can be calculated using DMRG simulations. The long time growth of the entanglement entropy for our system is presented in Fig. 6.6. Part **A** shows the growth of the entanglement entropy as a function of evolution time, and part **B** shows the imbalance. Even without any particle transport (i.e. a stationary and non-zero imbalance), the entanglement entropy continues to increase slowly, and in a logarithmic manner (yellow lines). It remains an important challenge for experiments to measure such quantum dynamics, especially in the absence of particle transport. Such results further support and demonstrate the stability of the MBL phase, since the imbalance does not relax to zero, even at very long times.

6.4.5 Conclusion

Our experiment provides a first experimental exploration of dynamics of interacting particles in quasi-periodic potentials, showing a breakdown of thermalization to very long times, even for moderate disorder strengths which are well within the two-particle energy bandwidth. Excellent agreement with high-performance numerical calculations demonstrates the viability of such an experimental platform to probe such regimes. Moreover, the experiment clearly shows the role of the interaction, the energy density and the possibility of localization in the entire spectrum of a many-body Hamiltonian.

6.5   Discussions

Several pertinent topics are discussed in this section, including supporting material for the main results.

6.5.1   Imbalance of an exponentially localized wave-function

A natural question to ask is the connection between the non-interacting localization length and the imbalance. We can estimate this by calculating explicitly the imbalance of a perfect exponential, and infer the connection between the critical exponents of the transition and the divergence of the inverse imbalance.

We assume that the density of a single particle has relaxed to a steady state after the quench and that the time-averaged wave-function of the particle can be described by the following form (written in real space basis, with i denoting the lattice site index):

$$\psi_i = \frac{1}{A} e^{-\frac{|i|}{2\xi}} \tag{6.4}$$

where, $1/A$ is the normalization of the wave-function with the relaxation length $\infty > \xi > 0$. Using,

$$\sum_{i=-\infty}^{\infty} |\psi_i|^2 = 1 \tag{6.5}$$

we can obtain a closed form expression for the normalization:

$$1/A = \frac{e^{1/\xi} - 1}{e^{1/\xi} + 1} \tag{6.6}$$

as well as the imbalance $\mathcal{I}$,

$$\mathcal{I} = \sum_{i=-\infty}^{\infty} (-1)^i |\psi_i|^2 = (1/A)^2 \tag{6.7}$$

Note that the infinite disorder limit $\xi \to 0$ gives imbalance of $\mathcal{I} = 1$ as expected and the vanishing disorder limit $\xi \to \infty$ gives $\mathcal{I} = 0$ as expected. Further, as $\xi \to \infty$, we can obtain

$$\mathcal{I} \sim 1/\xi^2 \tag{6.8}$$

An important feature of the imbalance is that it can continue to serve as an order parameter in the MBL phase, where ξ is ill-defined. These relations can also be connected to the disorder strength, and will, in general, depend, on the nature of the disorder. For example, it is known that in quasi-periodic potentials, the localization length of the single-particle eigenstates, ξ_0 is independent of the eigenenergy and is given by [85]:

$$\xi_0 = \frac{1}{\log(\frac{\Delta}{2J})} \tag{6.9}$$

We distinguish this from the relaxation length ξ, resulting from a stable wave-function after the time evolution. In general, the two could be connected via an exponent μ (and possibly a scaling), both of which can depend on the energy density. In this case, the imbalance will vanish as $\lim_{\delta \to 0} \mathcal{I} \sim (\delta/J)^{2\mu}$, where we have approximated the logarithm near the critical point of $\Delta = 2J$, such that $\delta = \Delta - 2J$. Hence, to probe the critical properties, one could measure the divergence of inverse of the imbalance at long times, both for the MBL and AL cases and possibly for different kinds of disorders (e.g. real-random or quasi-periodic), and compare the resulting critical exponents ν,

$$1/\mathcal{I} \sim 1/(\Delta - \Delta_c)^\nu \tag{6.10}$$

Note that the above calculation is just to illustrate how a larger localization length can be connected to a smaller imbalance and not show how one can exactly solve the expansion dynamics analytically.

6.5.2 Deviations from the ideal Aubry-André model

This subsection briefly overviews the main deviations from the exact quasi-periodic model that has been presented. The emphasis is to present the physical effects of the underlying mechanisms in an isolated fashion, and not to perform a full simulation with all the experimental details.

A

B
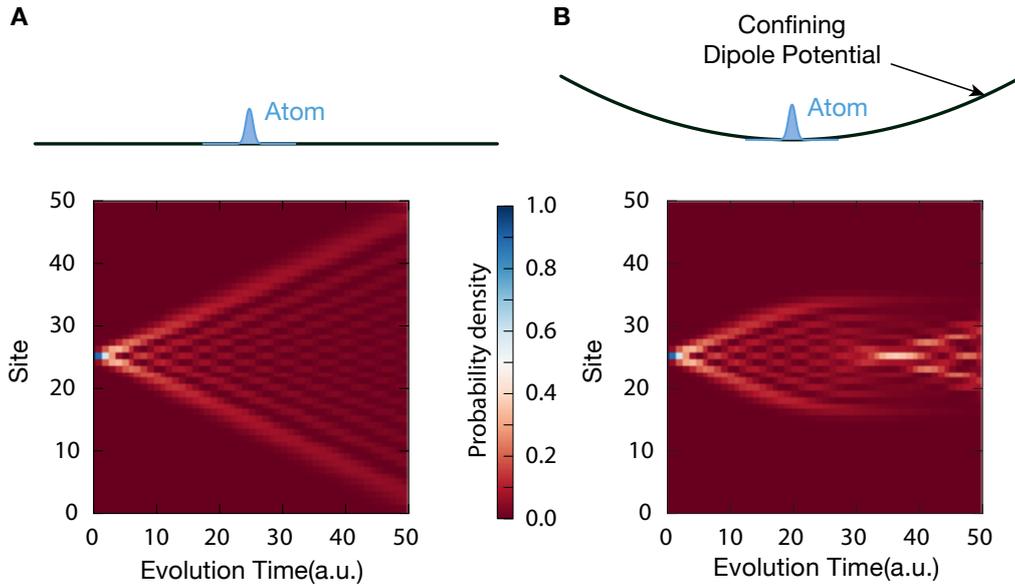
Figure 6.7: Expansion dynamics of a single particle in a homogeneous lattice, A: An atom released in a flat potential expands indefinitely in a light cone fashion, as shown in the plot. The y-axis denotes the lattice site number and the particle is released in the center of it. The particle expands exploring the entire space. **Expansion dynamics of a single particle in a global confining potential, B:** The dipole trap effectively provides a confining potential, which for the deep depths we work at, acts like a $\sim r^2 \times \omega^2$ confining potential, with r being the distance from a center and ω the dipole frequency. The particle is released from the center of such a trap (blue area), under a strong confinement. The particle *rebounds* back after reaching a distance where the dipole potential roughly equals the kinetic energy. The particle then shows damped oscillations near the center. Such effects, which arise from a *finite dipole length*, are even more severe away from the center. We expect them to be less important in case of an interacting system.

Effect of the dipole trap

The dipole trap is a far-detuned laser beam of Gaussian shape employed to hold the atoms in a conservative potential. This Gaussian profile can be approximated as a harmonic potential near its center, resulting in a confining potential of the form $V(r) \propto r^2 \times \omega^2$, where r is the distance to the center of the trap and ω is the dipole frequency. This sets the limit to the particle expansion. This is because the energy of the particle has to be conserved during the time evolution and hence, it cannot tunnel to arbitrarily large distances. The cut-off distance can be estimated roughly to be the distance where the potential energy of the dipole trap equals the kinetic energy of the particle. We note that this puts a cut-off length-scale in the experiment, and smears out the transition point. To show the dynamics in a confining potential, we show the expansion of a single particle with and without a strong dipole trap in Fig. 6.7. The confining effect of the dipole trap limits how far the particle can spread. Note, this is just an illustration of the main effect, see Ref. [72] for complete details.
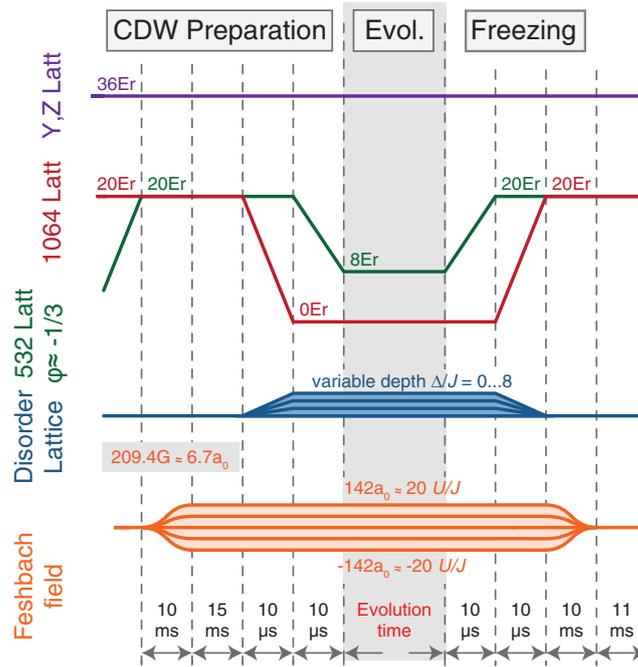
Figure 6.8: Experimental sequence: The plot shows the lattice and magnetic field ramps, phase settings, and the charge-density-wave (CDW) preparation. At the end of the sequence, we initiate the band-mapping sequence to measure the number of atoms on the even and the odd sites.

Dephasing contributions to the non-interacting imbalance

In addition to the dephasing caused by the dipole trap (since different atoms experience different dipole potentials), there are modulations of the hopping J, in the presence of the disorder lattice. This is because the addition of an incommensurate potential alters the position of the minimum of the individual wells of the lattice as well as the barrier height by a small amount and hence, the hopping is modulated slightly. This effect is less than 10 % for most of the disorder strengths we have used. Furthermore, we expect the slightly lower and the slightly higher hopping to cancel out their contribution to the average imbalance to first order and hence, the effect of hopping modulation on the imbalance is negligible. However, the inhomogeneous hopping masks the oscillations of the imbalance.

Additionally, the finite size of the lattice beams also changes the value of Δ/J between different individual tubes. The lattice beams have a $1/e^2$ waist of roughly $\sim 150\,\mu$m at the position of the atoms. The size of the atomic cloud corresponds to a full width at half maximum of approximately $\sim 50\mu$m in the horizontal plane and about $15\,\mu$m in the vertical direction. From this, we estimate that about 90 % of the atoms see less than 20% of the change in the tunneling J. Along the direction of the beams, the Rayleigh range is sufficiently large such that there is no appreciable change in the beam shape along this direction. These differences in the tunneling make different tubes dephase differently and while it does not change the mean value of the imbalance appreciably, the oscillations of the imbalance are damped faster than what is expected from a single tube.

Coupling Identical Many-Body Localized Quantum Systems

Short summary: MBL systems can reach local thermal equilibrium when they are coupled to an external bath. Further, coupling identically disordered MBL systems with each other can be enough to destabilize *all* of them as they can serve as a bath for each other and result in delocalizing all of them. This coupling can be used as a *tool* to distinguish interacting vs. non-interacting localized systems.

7.1   Introduction

Hamiltonians describe the physics of closed and isolated quantum systems and the underlying system is assumed to be describable with a wavefunction. Naturally, a question of direct significance arises: How can the knowledge about perfectly isolated systems be connected to real experimental systems, which are never perfectly isolated and importantly, the reverse? Typically, there exists a timescale (or alternatively a frequency/length scale) which sets a *cut-off* for the observable physics. This cut-off will depend inversely on the effective coupling Γ between the non-perfectly isolated system and the coupled environment. The following section describes these ideas more specifically in the context of ultracold atoms and many-body localization.

While an MBL phase describes a stable non-thermal phase at high energy densities, this phase is not robust to coupling to an external bath or bath-like structure [22, 73, 76, 103, 154–160]. Any such coupling will eventually always result in a thermal system, see Fig. 7.1. Intuitively, it can be understood by observing that the system can now exchange heat with the bath freely with some coupling Γ. This coupling allows the system to freely explore otherwise restricted areas of the system by energy exchange with the bath and explore the full phase space. This thermalizes the system. Since all experiments are inevitably coupled to some external environment, it is crucial to understand the effects of such a coupling quantitatively. This also lets us understand the limits of the experimental results. Note that, it is not just the MBL phase, but all other coherent quantum many-body phases are susceptible to such couplings to a generic external environment at a high temperature. A strong enough stochastic environment should always destroy the coherence of a quantum state and hence, erase the interesting quantum features.
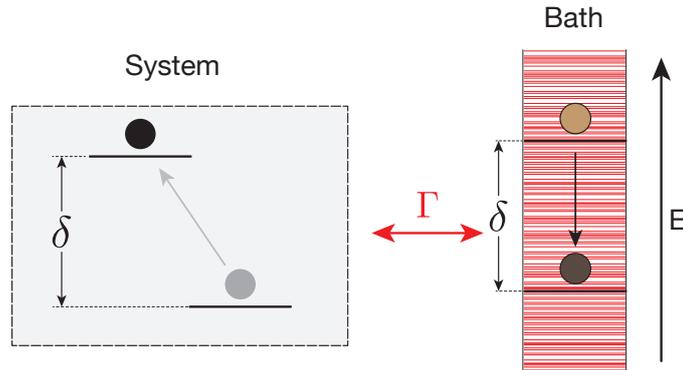
Figure 7.1: Bath-induced hopping: The cartoon depicts how coupling a system to an external bath can restore hopping of a single particle. The left part shows a system with just two lattice sites detuned in energy by a large amount δ, and hence, in a closed system evolution, a particle cannot be transferred from the lower to the higher energy level. On the other hand, upon coupling this system to a high-temperature external bath with which it can freely interact, the particle can absorb energy of exactly an amount δ and hop on the higher energy site. Such processes also restore hopping on a more general lattice system and destroy localization, both when the system is Anderson localized or when it is many-body localized.

The transition between the ergodic phase and the MBL phase becomes a crossover at a non-zero coupling to the environment. Qualitatively, this can be understood by first looking at the Mott insulator-superfluid transition [20]. As shown in Fig. 7.2 A, at zero temperature the excitation gap changes as the interactions are tuned, **(a)**. Up to some critical interaction strength $(U/J)_c$, the system is gap-less. However, beyond this critical interaction strength, a gap in the excitation spectrum opens. On the other hand, the coherence of the system, (for e.g. in the time-of-flight experiments), **(b)**, vanishes beyond the critical interaction strength $(U/J)_c$. The two ensuing phases at zero temperature are the superfluid phase at weak interactions and the Mott-insulator phase at strong interactions. The finite but low-temperature properties of this Hamiltonian are shown in the $T > 0$ graph, where one observes a "fan" up to a critical temperature till where one can see signatures of the ground state either in the coherence (corresponding to the superfluid regime) or of the gap (corresponding to a Mott-insulator regime). In between, one can observe a crossover region which behaves quantum critical. In a perfectly isolated quantum system, one can observe similar features across the MBL transition, Fig. 7.2 B. All observables in class $\mathcal{B}$, (as defined in Chapter 3) e.g. measurement of imbalance and its change at a critical disorder strength Δ_c from zero to non-zero and provide a measure of the transition. Using class $\mathcal{A}$ operators, such as measuring *how* the imbalance relaxes, can shed light on the critically slowly relaxing phase below the transition [77]. This time dependence can be captured using a relaxation exponent. For a finite value of the bath-coupling, there is a crossover between the two regimes. However, these two observables can still be used to diagnose the transition point with a finite bath-coupling at times much smaller than the inverse coupling, as shown in the graphs with $\Gamma > 0$.
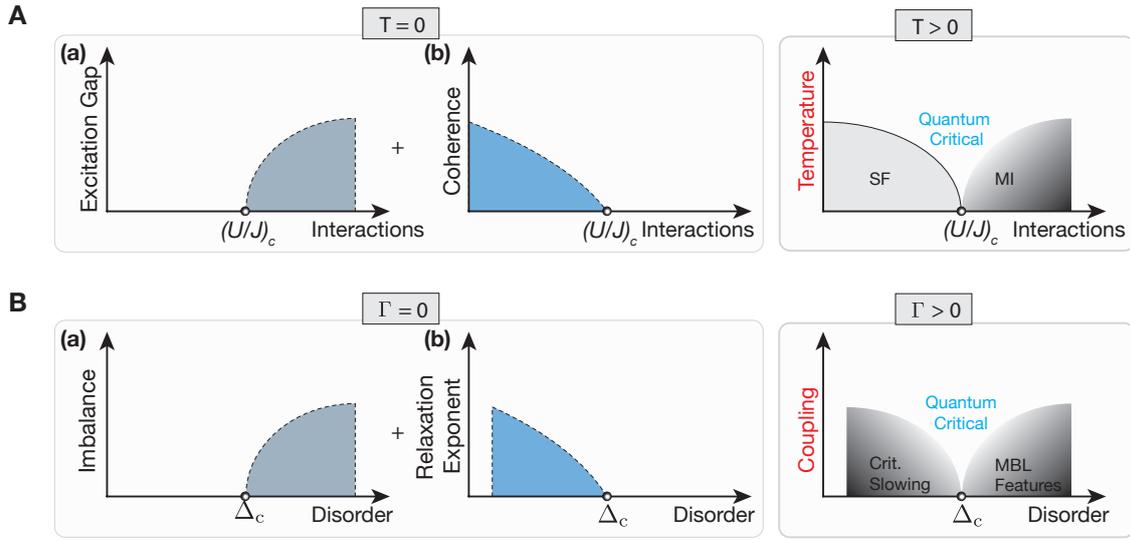
Figure 7.2: Finite temperature/coupling effects: The figures compare and contrast two different experimental observables at zero and finite temperatures, for the case of **A**: Mott insulator to superfluid transition and **B**: Many-Body Localization-Delocalization transition. The variables with a visible "fan" at finite temperatures ($T > 0$) for the MI-SF transition can be for e.g. excitation gap/coherence. Similarly, one can observe something similar for the MBL transition with imbalance and the relaxation exponents, which result in a crossover region at finite coupling to an external environment ($\Gamma > 0$). While the superfluid state extends to arbitrarily small interaction strengths, it is unclear if the critical slowing can be observed to arbitrarily small disorder strengths.

7.2 Model

Our system consists of an array of one-dimensional tubes along the x-direction. These tubes have quasi-periodic disorder and can be described by the AA model with onsite interactions between atoms of two different spins. A finite coupling between the different 1D lattices is present and is controlled the hopping rate $J_\perp$ between the tubes. The system can be effectively described by the following Hamiltonian:

$$\hat{H} = -J \sum_{i,j,\sigma} (\hat{c}^\dagger_{i+1,j,\sigma} \hat{c}_{i,j,\sigma} + \text{h.c.}) - J_\perp \sum_{i,j,\sigma} (\hat{c}^\dagger_{i,j+1,\sigma} \hat{c}_{i,j,\sigma} + \text{h.c.})$$
$$+ \Delta \sum_{i,j,\sigma} \cos(2\pi\beta i) \hat{n}_{i,j,\sigma} + U \sum_{i,j} \hat{n}_{i,j,\uparrow} \hat{n}_{i,j,\downarrow}, \tag{7.1}$$

Here, $J \approx h \times 550\,\text{Hz}$ is the tunneling matrix element along the x-direction. The creation (annihilation) operator for a fermion on a site i in a tube j in the spin state $\sigma \in \{\uparrow, \downarrow\}$ is defined as $\hat{c}^\dagger_{i,j,\sigma}$ ($\hat{c}_{i,j,\sigma}$) and the local number operator is defined by $\hat{n}_{i,j,\sigma} = \hat{c}^\dagger_{i,j,\sigma} \hat{c}_{i,j,\sigma}$. The quasi-periodic on-site disorder is characterized by the disorder amplitude Δ and the incommensurate wavelength ratio $\beta = \lambda_s/\lambda_d \approx 0.721$. The on-site interaction energy between two different spin states is given by U. The different 1D tubes are coupled via the tunnel matrix element between the adjacent tubes along the y-direction, $J_\perp$. A schematic of the setup is shown in Fig. 7.3.
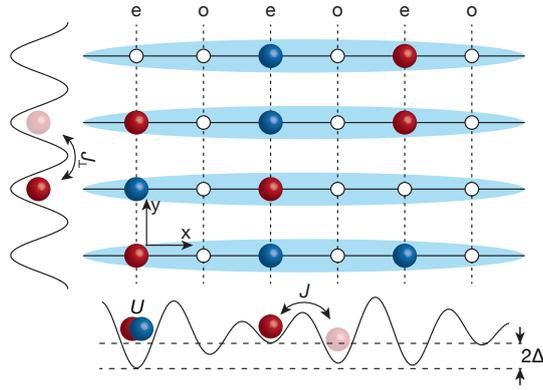
Figure 7.3: Schematic of the experiment: The relaxation of an initially prepared density-wave is monitored. The disorder Δ, hopping J and interaction U are identical in all the tubes. Red and blue spheres denotes the two-spins of the fermionic atoms. The redistribution of atoms between the even (e) and the odd (o) columns is studied for different tunnel matrix elements $J_\perp$ along the y-direction, which couples the different 1D tubes (blue shading). The case of $J_\perp/J = 10^{-3}$ is referred as the 1D$^+$ case and the case of $J_\perp/J = 1$ is called the 2D case.

Experimental control of the microscopic parameters in the Hamiltonian

The experiment allows almost complete control over the different parameters described above. The tunnel matrix element along the x-direction J is controlled by the lattice depth of the main lattice along the x-direction. For the current experiment, this was kept constant at $8\,E_r^{532\,\text{nm}}$ and sets the energy scale of the system. The disorder strength Δ is controlled by the depth of the disorder lattice along the x-direction. The onsite interaction strength U can be tuned by the magnetic field using a Feshbach resonance at 202.1G [140]. The tunneling matrix element along the y-direction, $J_\perp$, is controlled by the lattice depth of the main lattice along the y-direction.

For the current experiment, the variation of the hopping rates along the x-direction and y-direction is in the range $J_\perp/J \in [1, 10^{-3}]$. The two extreme limits of almost zero coupling, $J_\perp/J = 10^{-3}$ and equal coupling, $J_\perp/J = 1$ are termed as the 1D$^+$ and 2D cases, respectively. It is important to stress here, that even the lowest achievable coupling in the case of 1D$^+$, is not the same as the theoretical limit of an exact 1D system. The small but finite coupling is exactly what will set the limit to experimentally relevant timescales. It is also this coupling that acts like a bath and sets the cut-off timescale of the experiment.

7.3 Results

7.3.1 Single-particle localized vs many-body localized

The disorder strength is fixed to $\Delta = 5\,J$. For this disorder strength, a perfectly isolated 1D system should be localized at all interaction strengths [72]. In the experiment, however, we cannot realize a perfectly isolated 1D system and instead study the weakly coupled 1D$^+$ and strongly coupled 2D system. We monitor the time evolution of the imbalance
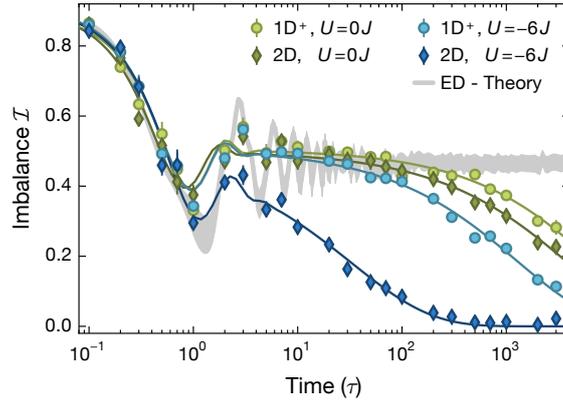
Figure 7.4: Instability of MBL under coupling: The plot shows the temporal evolution of imbalance $\mathcal{I}$ for a fixed disorder strength of $\Delta = 5J$ in the non-interacting $U = 0J$ (green points) and interacting $U = -6J$ (blue points) cases for the $1D^+$ (circles) and the 2D (diamonds) system. The imbalance is almost identical for the non-interacting case. In contrast, there is a large difference in the time evolution of the measured imbalance in the interacting case. The gray shaded area denotes exact diagonalization calculations for the non-interacting system. Each experimental point is an average of six individual experimental realizations. All times are given in units of the hopping time, $\tau = h/(2\pi J)$.

for two different interaction strengths (i) the non-interacting system $U = 0$ and for (ii) a strongly interacting system $U = -6J$. This is shown in Fig. 7.4. The time evolution can be understood by partitioning it into three different regimes, which continuously crossover from one to another:

1. $t \ll 10^0 \tau$: For times shorter than the single particle hopping time, we find that all the four traces lie on top of each other. This just represents single particle dynamics where the system is suddenly allowed to relax, and there is an initial relaxation between the even and odd sites, resulting in the reduction of imbalance from almost unity to a finite value (in Fig. 7.4, it drops to roughly 0.4). One does not need interactions, or coupling effects, to understand this relaxation, which is just a single particle expansion to the nearest neighbor sites.

2. $t \in [10^0, 10^2] \tau$: After just a couple of tunneling times, the above description fails. Particles have explored their neighborhood and interacted with their neighboring particles. As such, in the interacting case of $U = -6J$, we see the strong difference between the two time-traces. On the other hand, the non-interacting traces are still almost on top of each other and exhibit a time window where they are almost flat. Further, the imbalance closely matches the exact diagonalization calculation (gray shaded area) in the background.

This qualitative difference in behavior in the interacting vs. non-interacting cases can be understood as follows. Along the y-direction, each particle sees no change in the onsite potential (since the disorder is identical in all tubes). Hence, it can freely move in that direction. In the interacting case, this means that the particles are free
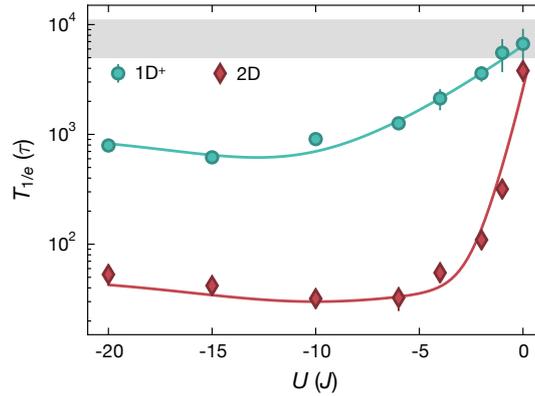
Figure 7.5: Interaction effects: The plot shows the extracted imbalance lifetime as a function of interactions for the 1D$^+$ and 2D cases for a fixed disorder strength of $\Delta = 5J$. In the 2D case, away from $U = 0$, the lifetime sharply drops signaling delocalization in the interacting case. Note that the 1D$^+$ case differs crucially from the ideal isolated 1D system. Error bars denote the fit errors. Light gray shading near the top of the graph represents the measured atom number lifetime, denoting experimental limits of the measured lifetime.

to interact with other particles in that direction. Note that this is not the same as saying that they can freely exchange energy with them. In principle, the y-direction represents a one-dimensional Fermi-Hubbard model and that is integrable for all interacting strengths U. As such, particles cannot thermalize.

However, this integrability is broken as many MBL tubes are coupled to each other. Hence, the aforementioned integrability along the y-direction is broken by the disordered tubes along the x-direction, and the localization along the x-direction is broken by energy relaxation along the otherwise integrable system along the y-direction. This coupling is only present when the system has non-zero interactions. In the case of the non-interacting case of Anderson Localization, there are no interactions and hence, the x-direction and y-direction remain uncoupled (in other words, the Hamiltonian becomes separable along the two directions). Hence, while AL is protected against such a coupling, MBL breaks down.

3. $t \gg 10^2\tau$: For even longer times, even the non-interacting cases of Anderson localization start to deviate from the exact diagonalization calculation. Here, other sources of noise in the experiment, such as lattice noise, photon scattering, etc. become dominant, and the system cannot be taken as a reliable quantum simulator [76].

We find that the decay of the plateau can be well captured by a stretched exponential of the form $e^{-(\Gamma t)^\beta}$. Here, Γ denotes the decay rate and β is the stretching exponential. The inverse of the relaxation rate is then defined as the imbalance lifetime $T_{1/e} = 1/\Gamma$. The physical origin of a stretched exponential (instead of a normal exponential) can be connected to the inhomogeneity of the underlying potential which gives rise to a distribution of local relaxation times [160].
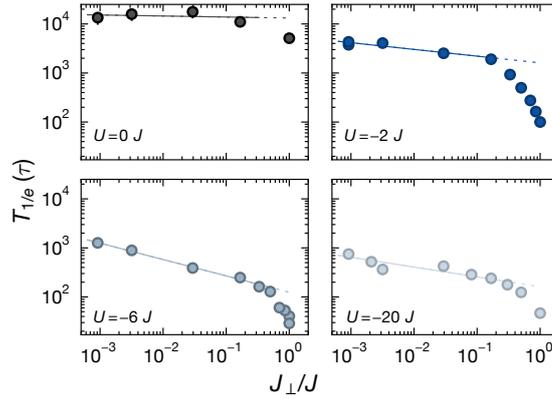
Figure 7.6: Weak coupling - strong coupling crossover: The figure shows the measured imbalance lifetimes for a fixed disorder strength of $\Delta = 5J$ as we continuously tune from weak coupling regime with $J_\perp/J = 10^{-3}$ to strong coupling regime with $J_\perp/J = 1$. For all interacting cases, we find that the lifetime continuously decreases as the coupling is increased. The form of the decrease of the lifetime, however, appears to change its nature from a power law for weak coupling case to something much faster for the strongly coupling case. This might happen as the leading order process changes as we tune the coupling. Error bars denote the fit errors and are mostly smaller than the individual points.

7.3.2   Interaction dependence

We directly study the interaction dependence of the imbalance lifetime quantitatively for the 1D$^+$ and the 2D cases by measuring it as a function of the interaction at a fixed disorder strength of $\Delta = 5J$. This is shown in Fig. 7.5.

Firstly, we see similar lifetimes in the case of different non-interacting systems, which lie in the atom number lifetime range (gray shaded band). In the 2D case, going away from the non-interacting case strongly reduces the lifetime, signaling delocalization. Further, one also sees a slight increase in the lifetime for very large interactions. This could happen due to the reduced rate of thermalization at hard-core interactions as compared to intermediate ones. We have separately checked that this is not due to a small number of residual doublons, by also measuring the lifetime after removing the small number of the leftover doublons using near-resonant light pulse [111]. Nevertheless, the same qualitative trend can also be observed in the 1D$^+$ case. This could mean that even in the 1D$^+$ case, the small but finite coupling (since $J_\perp/J = 10^{-3}$ is not exactly zero) could still be the limiting factor. To directly check this, we measure the imbalance lifetimes as a function of $J_\perp/J$, i.e. go from the weak coupling case of 1D$^+$ to the strong coupling case of 2D.

7.3.3   Weak coupling - strong coupling crossover

We measure the imbalance lifetime for a fixed disorder strength of $\Delta = 5J$ as we directly tune the inter-tube coupling strength. This is shown in Fig. 7.6. We do this for different regimes of interactions, varying from the non-interacting limit to the strongly interacting limit. Each of the limits is described in detail as follows:
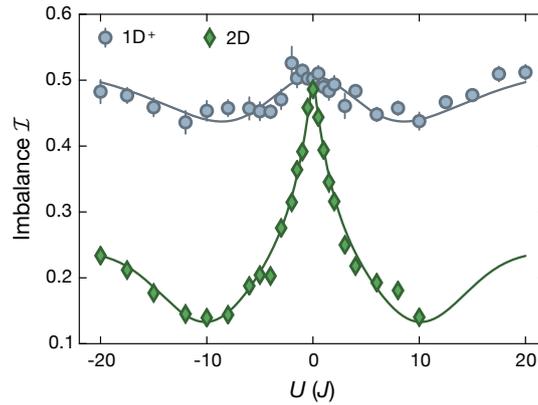
Figure 7.7: Intermediate time imbalance: The plot shows the imbalance measured after an evolution time of $40\,\tau$ for the weakly coupled $1D^+$ case and the strongly coupled 2D case. The strong disparity between the two cases of coupling for any interactions is already visible at these times, where we can neglect the effects of external noise sources with good confidence. In the $1D^+$ case, the data represents the value if the system was perfectly isolated, while in the 2D case it is indicative of a decay lifetime. Each point is an average of twelve individual experimental realizations, and solid lines are guides to the eye. The 2D data is limited to $U = 10\,J$ due to details of the used Feshbach resonance.

1. $U = 0$: As described earlier, in the non-interacting case, the system is separable in the two orthogonal directions. This holds irrespective of the coupling strength $J_\perp/J$. Hence, we expect the lifetime to be largely independent of the coupling strength and to be limited by other factors, such as noise in the stability of the optical fields, off-resonant photon scattering, etc. This is also visible in the non-interacting case of Fig. 7.6, where we obtain lifetimes of about $\approx 10000\,\tau$, consistent with our atom number lifetime and almost independent of the coupling strength. We attribute the small decrease in the lifetime for the 2D case ($J_\perp/J = 1$) to the system not being exactly separable (due to finite lattice widths for example) and due to experimental uncertainties in maintaining absolute zero scattering length throughout the measurement. Nevertheless, we find long lifetimes which are largely independent of the coupling strength and provide strong experimental support for a stable AL phase.

2. $|U| > 0$: In the interacting cases ($|U| = 2, 6, 20\,J$), the qualitative behavior it quite different. For the weakest coupling that was realized in the experiment, called the $1D^+$ case, we still see large lifetimes of about a thousand tunneling times. However, upon increasing the coupling strength such that weak coupling still holds $J_\perp/J \ll 1$, we find that the lifetimes decrease in a power law fashion. However, upon reaching the strong coupling behavior of the 2D case, we find that there is a crossover to a much faster rate of relaxation with lifetime of a few tens of tunneling times (for these values, even our assumption of fitting a plateau breaks down as we observe a quick relaxation). Further, we see a strong contrast in the strong coupling lifetime between the non-interacting and the interacting cases, with almost two orders of magnitude of lifetime difference. This would indicate that MBL breaks down under any such coupling.
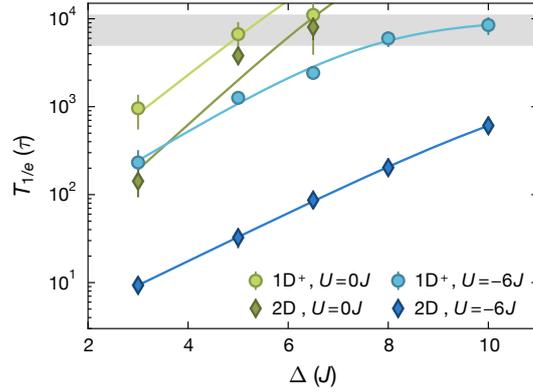
Figure 7.8: Effect of disorder strength on the imbalance lifetimes: The lifetimes are extracted from fits with data measured up to evolution times of $3000\,\tau$ and hence, can only be trusted up to this limit. We find that the imbalance lifetime increases strongly with disorder strength in all cases. The gray shaded area denotes the atom number lifetime. Error bars denote the fit uncertainty, and solid lines are guides to the eye.

Intermediate time imbalance

This strong contrast between the imbalance lifetimes in one and two dimensions in the interacting cases can also be seen directly in the value of imbalance after an evolution time of $40\,\tau$, as shown in Fig. 7.7. In the $1D^+$ case (blue circles), we find that the imbalance is always high and displays the characteristic "W"-shape behavior. The data can be well described with matrix product state simulations for a perfectly isolated 1D system for all interactions at these times, giving us strong confidence on the unitary dynamics assumption. In comparison, the imbalance for the strongly coupled 2D case at the same evolution time is also shown (green diamonds). We observe that that non-interacting case agrees with the imbalance in the non-interacting case of $1D^+$ system because the system is separable. In all other cases, we see a strong reduction in the value of imbalance, signaling delocalization. This data can also serve as a benchmark for theoretical simulations in higher dimensions, where perhaps the behavior discovered in the experiments could be captured with a few one-dimensional tubes coupled to each other.

Disorder dependence of the rate of relaxation

Until now, all measurements were performed at a fixed disorder strength of $\Delta = 5J$. Even though we expect that MBL systems will ultimately always delocalize due to such a coupling, the *timescale* of such a process can be strongly dependent on the disorder strength. To quantitatively see this, we measure the lifetime of the weakly coupled ($1D^+$) and strongly coupled (2D) systems for different disorder strengths, as shown in Fig. 7.8. We observe that the imbalance lifetime increases strongly with the disorder strength. Even in the strongly coupled case (2D), the imbalance lifetime of the interacting system can increase strongly with increasing disorders. This could be understood qualitatively by first looking at the underlying non-interacting case. Due to the decreasing localization lengths
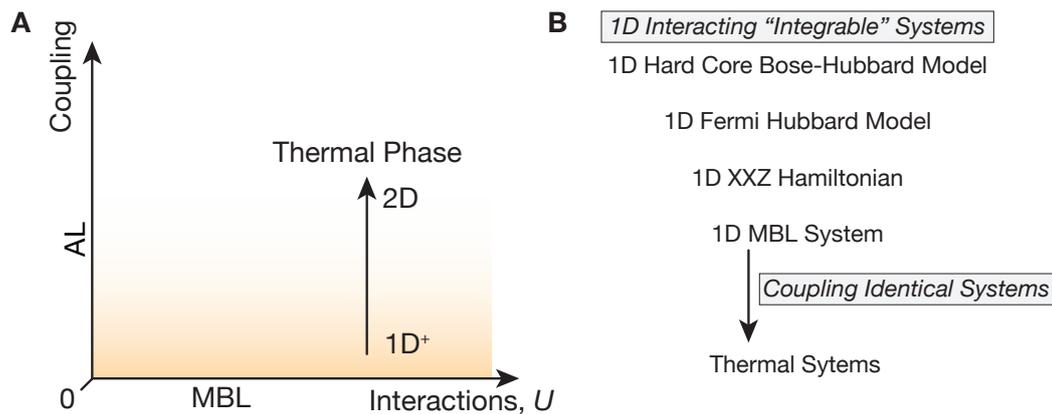
Figure 7.9: Coupling identical MBL systems, A: The diagram summarizes the effect of coupling identical MBL systems with each other. While AL is protected against such a coupling, any other case will eventually always thermalize. However, there exists a crossover timescale (shaded region) between the three regimes. The crossover timescale will depend on the microscopic details such as the coupling, interactions, and the underlying disorder strength. **Generalization and other examples, B**: The second part shows that this phenomenon also occurs in other integrable systems, wherein coupling identical systems in one dimension result in thermalization of each of them. For example, coupling the integrable one-dimensional hard-core Bose-Hubbard model results in the thermal two-dimensional hard-core Bose-Hubbard model [111]. Note that interactions are necessary for such a conclusion, the non-interacting system remains non-thermal.

with increasing disorder strength, the matrix overlap between neighboring sites strongly reduces and hence, the *rate* of hopping decreases. This results in strongly increasing lifetimes with increasing disorder. In the case of experiments, this is then cut off by other sources of noise, giving an upper bound on the lifetime and the atom numbers (the gray shaded region).

7.3.4 Conclusion

In conclusion, we have seen that coupling identically disorder tubes could delocalize all of them if they are interacting. On the other hand, Anderson localization would be protected in the presence of any such coupling. This can be summarized in Fig. 7.9 which shows that MBL would only survive if the coupling between such tubes is identically zero, as denoted on the x-axis. On the other hand, if the interactions are zero, as on the y-axis, then coupling would not destroy localization. In the experiment, there are some finite residual interactions and finite residual coupling. This renders the experiment very close to x-axis in the case of the $1D^+$ system. This is denoted by the shaded region showing that one can still study the properties of the MBL phase up to some timescale. Other the other hand, upon increasing the coupling (along the direction of the arrow), one can completely thermalize an otherwise MBL phase. The only case stable to such a coupling is the non-interacting case.
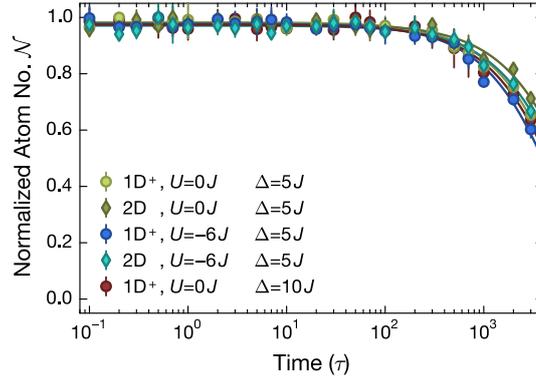
Figure 7.10: Lifetime of atom numbers: The figure shows normalized atom numbers as a function of evolution time for many different cases. We fit exponentials to them and find that the lifetimes are typically more than $5000\,\tau$. Each point is an average of six individual experimental realizations and error bars represent the error of the mean.

7.4 Discussions

7.4.1 Coupling "non-identically" disordered tubes

For the cases explored till now, the particles were free to move along the y-direction as the underlying potential landscape was not disordered along the y-direction. In the non-interacting case, this gave rise to delocalized modes along the y-direction and localized modes along the x-direction. Upon introduction of interactions, these modes were coupled and the delocalized modes destroyed the localized ones.

An immediate question that arises is the fate of the system if the disorder is not identical in all tubes? This is not clear, as the problem reduces to the question of the existence of MBL in two dimensions, which is discussed in Chapter 9. This is because if the disorder is not identical in all the tubes, then along the y-direction the particles cannot move freely. The result, in this case, cannot be inferred from the above analysis, and it might or might not delocalize depending on the disorder type. It might even be possible to destroy AL if the disorder is not identical.

7.4.2 Coupling effects in higher dimensions

The bath-like properties that coupled systems with identical disorder exhibit should hold true also in higher dimensions. We have observed this effect in two dimensions, by measuring accelerated relaxation of coupled identically disordered two-dimensional planes, see Chapter 9.

7.4.3 Atom number and imbalance lifetime extraction

The time dependence of the imbalance is captured using the following fit:
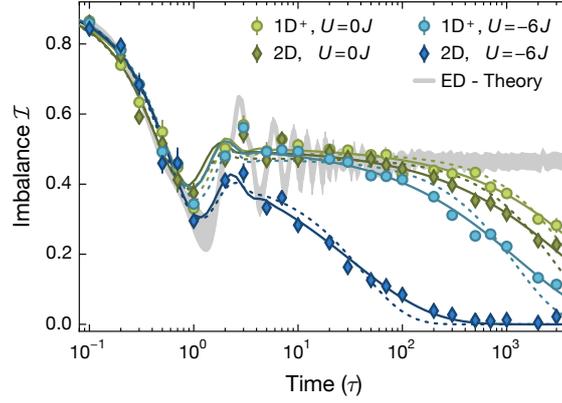
Figure 7.11: Stretched vs normal exponential fit comparison: We show Fig. 7.4 along with normal exponential fits where we find significant improvement in the fit quality using stretched exponential fits (solids lines) as compared to the normal exponential fits (dashed lines).

$$\mathcal{I} = (A e^{-t/t_1} \cos(\nu t) + I_{\mathrm{st}}) e^{-(\Gamma t)^{\beta}} \qquad (7.2)$$

Here, A is the amplitude of a damped sinusoidal function, with $t_1 \sim 1\,\tau$ and frequency $\nu \sim 1/\tau$. It then saturates to a plateau value of I_{st}. This imbalance plateau value then decays slowly with a long lifetime, $T_{1/e} = 1/\Gamma$, which depends on the coupling between the tubes, where Γ is the decay rate and β is the stretching exponent.

We fit an exponential decay to the measured atom numbers as a function of evolution time to obtain the atom number lifetime. Five curves for this are shown in Fig. 7.10. The lifetimes are similar across all the presented parameter ranges, and we do not observe any strong dependence on interactions, disorder strength or the dimension. The extracted lifetime ranges from $0.5 - 1.1 \times 10^4\,\tau$, with systematic errors occurring possibly due to the limited measurement times of $3000\,\tau$.

7.4.4   Normal vs stretched exponentials

We find that the quality of the fit is significantly better if we use stretched exponentials $\sim e^{-(\Gamma t)^{\beta}})$ as compared to a normal exponential function $\sim e^{-\Gamma t}$. However, none of the quantitative numbers or the conclusions of the paper change due to this. Further, a stretched exponential might be naturally expected because of different regions having different local disorder strength. This gives rise to a variety of relaxation timescales, which result in a stretched exponential function as compared to a normal exponential. We show this difference between normal and stretched exponential fits in Fig. 7.11.

7.4.5   Stretching exponents

The value of the stretching exponents β might contain additional information on the nature of the dynamics. For example, one can expect that a homogeneous thermal system will decay with a stretching exponent of one (i.e. like a normal exponential), which could
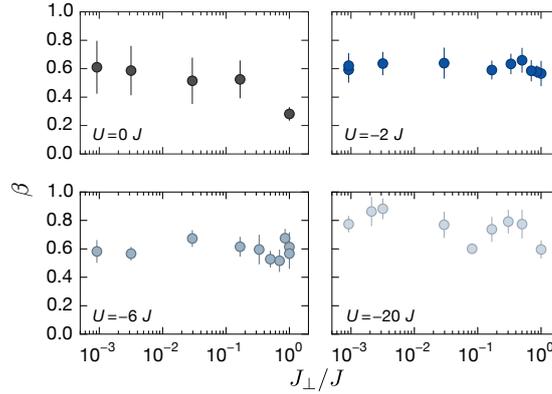
Figure 7.12: Stretching exponents across the weak coupling-strong coupling crossover: We find that the stretching exponents to the imbalance time evolution in Fig. 7.6 do not change within error bar with a mean of 0.6. The data is measured at a fixed disorder strength $\Delta = 5\,J$. Error bars denote the fit error. Weak coupling denotes $J_\perp/J \ll 1$ and strong coupling denotes $J_\perp/J \sim 1$.

be expected in the case when the bath completely dominates the relaxation. We show the extracted stretching exponents in Fig. 7.12. Within the experimental uncertainty, we do not observe a systematic change in β, but mostly find it to scatter around 0.6.

7.4.6 The phase of the quasi-periodic disorder

The relative phase, ϕ, between the disorder lattice and the main lattice along the x-direction is not discussed until now. This term is present in the quasi-periodic potential, $\cos(2\pi i \beta + \phi)$. However, such a term is not expected to change the imbalance of a large system and hence, is not emphasized. We have checked this in the experiment by comparing the mean from six individual experimental realizations with a constant phase with the imbalance measurements averaged over six different phases and found them to be identical. This can be understood by thinking that in a thermodynamic system, different phases are automatically averaged in different regions of the system and hence, no phase averaging is necessary. We expect the experimental system sizes to be large enough to be close to this limit.

7.4.7 A dynamical symmetry for the Hubbard models

There exists a dynamical symmetry, i.e. in the time evolution in the Fermi-Hubbard Model, as was revealed in the experiments studying expansion dynamics of the Fermi-Hubbard model [129]. Here, it was realized that the expansion velocity of a two-component fermionic gas in two dimensions is independent of the sign of interactions U, i.e., the expansion velocity was the same for both $+U$ and $-U$, as long as the starting state was the same. A similar behavior was also observed in the expansion of a homogeneous Bose gas in one and two dimensions in Ref. [111] and also for the one-dimensional MBL phase [72]. In our work, we found that such behavior can still be observed with the disorder only
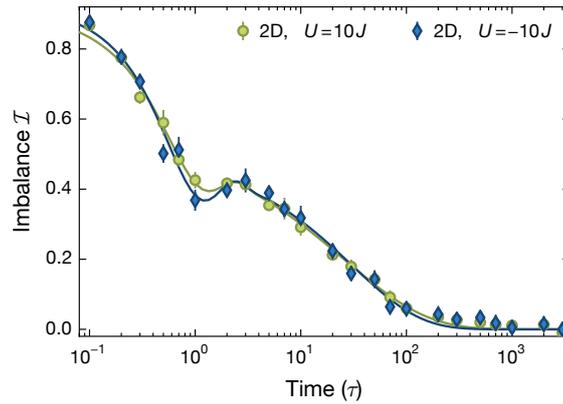
Figure 7.13: Dynamical symmetry between the positive and the negative interactions: We fix the disorder to be $\Delta = 5J$ and measure the imbalance after different evolution times for positive and negative interactions with a strength of $10J$. We find that the imbalance is identical for both cases, revealing the presence of a dynamical symmetry between $+U \leftrightarrow -U$. Each point is an average of six individual experimental realizations and the error bars denote the error of the mean. Solid lines are guides to the eye.
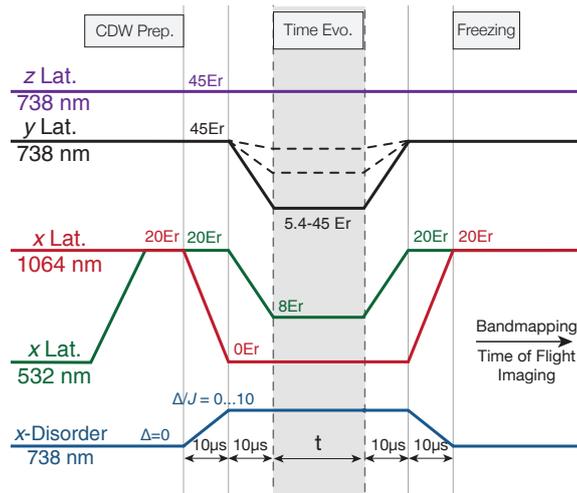
Figure 7.14: Experimental lattice sequence: The schematic shows the various lattice ramps for the experiment. Importantly, the y-lattice is ramped to various values to obtain the configurations which range from 1D$^+$ to 2D.

present along the x-direction. To check this directly, we also measured the time evolution of the imbalance for interactions $U = \pm 10\,U$ and we find this symmetry to hold to very long times, as shown in Fig. 7.13.

7.4.8   Experimental sequence

The experimental sequence till the production of ultracold fermions and loading it into a lattice with the even sites occupied is the same as described in Chapter 5. The lattice ramps after that are shown in Fig. 7.14, where the lattice depths are denoted in the units

of their respective recoil energies $E_r^\lambda = h^2/2m\lambda^2$. Here, h is Plank's constant, m is the mass of the Potassium-40 atom and λ is the wavelength of the lattice. Along the x-direction, the 1064 nm x-lattice is switched off quickly in 10 μs to $0\,E_r^{1064\,\text{nm}}$. Simultaneously, the 532 nm lattice is ramped down from $20\,E_r^{532\,\text{nm}}$ to $8\,E_r^{532\,\text{nm}}$ and the 738 nm main lattice along the y-direction is ramped down from $45\,E_r^{738\,\text{nm}}$ to various lattice depths to obtain different perpendicular hoppings, $J_\perp$. For example, for the case of the weakest coupling of the 1D$^+$ case, $J_\perp/J = 10^{-3}$, the final depth stays at $45\,E_r^{738\,\text{nm}}$ and for the case of the strongest coupling used in the paper, $J_\perp/J = 1$, we decrease the y-lattice depth to $5.4\,E_r^{738\,\text{nm}}$. See Appendix. A for additional values of the parameters. The magnetic field is appropriately adjusted to change the scattering length to compensate for the reduction of the Wannier overlap so that we obtain the same value of the onsite interaction strength U as the perpendicular hopping is changed. After variable evolution times, the dynamics are frozen by increasing the depth of all lattices to large values and performing the band-mapping procedure to extract the imbalance as described in Chapter 5.

Periodically Driving a Many-Body Localized Quantum System

Short summary: Periodically driven disordered systems can avoid the heat-death that other ergodic systems are expected to suffer. Such regimes of extreme stability in a periodically driven system are observed.

8.1 Introduction

The time dependent Schrödinger equation can be written as:

$$i\hbar\frac{\partial}{\partial t}\,|\Psi\rangle = \hat{H}(t)\,|\Psi\rangle \tag{8.1}$$

It governs the unitary time evolution of an isolated system in a state $|\Psi\rangle$ evolving with a time-dependent Hamiltonian $\hat{H}(t)$. In full generality, this is a very hard problem to study, with its solutions possibly containing the design of insects and trees, amongst others. For a much simpler case, one can consider a closed-system Hamiltonian which is *independent* of time, by solving just the eigenstates of the *static* matrix $\hat{H}$. This is also impossible to solve in full generality. However, we know of many interesting quantum phenomena which are present in this class of static quantum systems such as superconductivity and the quantum-Hall effects.

One of the tractable ways to study time-dependent systems is to consider a subclass which possesses *periodicity* in time. Such systems, called *Floquet* systems, are such that the Hamiltonian can be described by $\hat{H}(t+T) = \hat{H}(t)$, with a period of repetition T. Here, one can construct the time-independent *Floquet* Hamiltonian $\hat{H}_F$ from the effect of a single period of the drive:

$$e^{-\frac{i}{\hbar}\hat{H}_F T} = \mathcal{T}e^{-\frac{i}{\hbar}\int_0^T \hat{H}(t)dt} \tag{8.2}$$

Here, $\mathcal{T}$ is the time-ordering operator. This is recasting the problem so that we focus on one period and subsequently, generate the dynamics by applying the Floquet unitary multiple times. This Floquet unitary governs the stroboscopic dynamics (i.e. dynamics observed after integral multiples of the period T) of the system.

One would expect to find new phases of matter and interesting dynamics in these new class of systems. However, in such systems, local correlations do not persist, and most
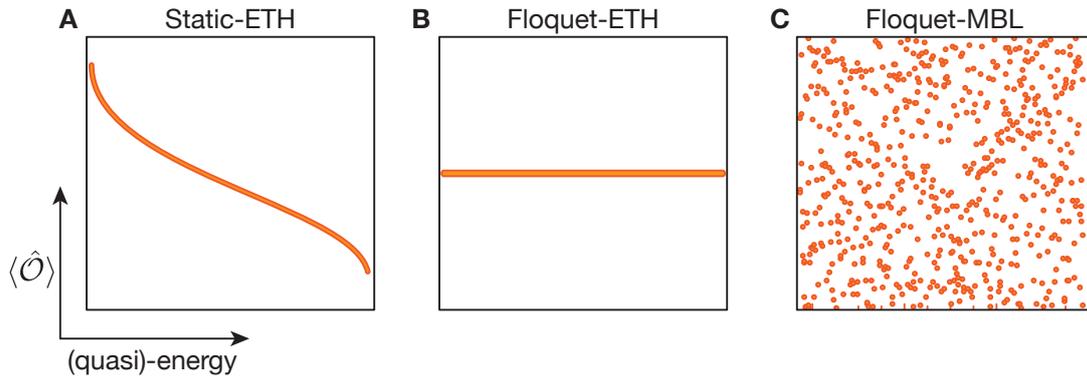
Figure 8.1: Static-ETH, Floquet-ETH, Floquet-MBL: The diagram shows the result of calculating the expectation value of a simple operator in different eigenstates. In static-ETH systems, **A**, this gives rise to a purely energy dependent and smooth behavior (ETH-preserving). Here, quasi-energy is the same as the eigenenergy. In contrast, in Floquet-ETH systems, **B**, one only finds an infinite temperature behavior, and all states show *infinite-T* behavior. Finally, in MBL systems (Floquet or otherwise), **C**, the expectation value can wildly oscillate from eigenstate to eigenstates, violating ETH very strongly.

Floquet-systems inevitably heat up to featureless infinite temperature states. This provides a generalization to ETH in periodically driven systems, with an important distinction: the system thermalizes but to an *infinite-temperature* state. However, this eventual result is not the only possible fate, and a counter-example is presented in strongly MBL systems [161–167]. It must also be noted here that, such results are for infinitely long time, and interesting dynamics should be present even in non-MBL systems (at least in lower dimensions) to very long times [168]. Since, transients are all that exist in the real world and have been demonstrated in many relevant cases [169–175], these works establish Floquet-engineering as a tool to engineer quasi-stable phases. However, recent theoretical works have demonstrated that one can instead have an exact notion of sharply delineated phases in driven systems [176–182] if they are MBL and show a stability to heating due to the drive. Such systems will be the focus of this chapter. ac

To understand these cases, it is illuminating to look at Fig. 8.1. Here, we consider the expectation value of a simple operator as a function of the eigenstates, ordered according to their increasing eigenenergy. Then, if the system obeys ETH, nearby eigenstates have the same expectation value of the operator, and hence, the overall change is smooth in the energy of the system, as shown in Fig. 8.1 **A** [162]. On the other hand, generic periodically driven systems without disorder become fully mixed. Further, one can only define *quasi-energy*, instead of eigenenergy, defined as energies modulo 2π, Fig. 8.1 **B** [183]. In such systems, energy is not conserved, and one finds no structure in the observables. Finally, in **C**, one can see the same for Floquet-MBL states showing strong fluctuations in the expectation value of the operator. Here, the system is driven and interacting, but still, fails to thermalize and shows drastic deviations from ETH of either form.

This chapter describes our experiment in which we have realized the cases of **B** and **C** in a periodically modulated one-dimensional lattice. We measure imbalance, which does
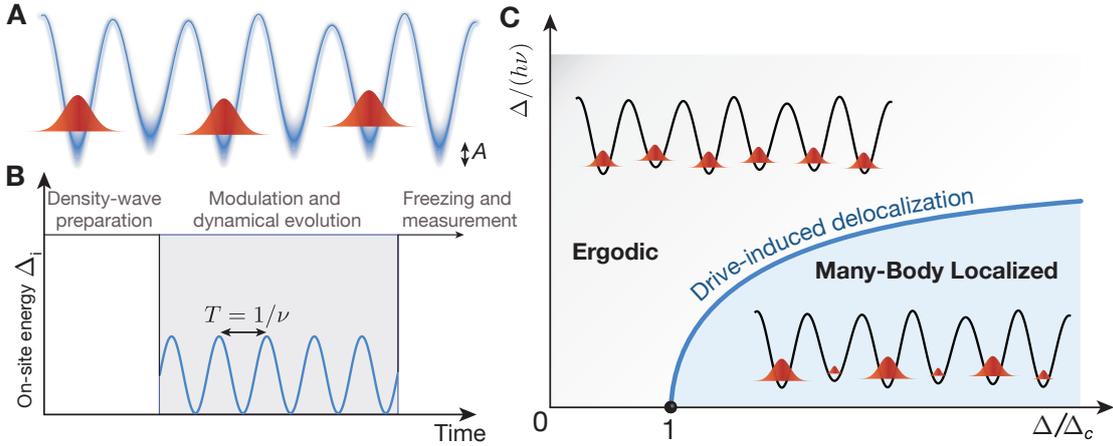
Figure 8.2: Initial state, A: A density wave of spinful atoms is loaded on only the even sites of a one-dimensional lattice. **Time dependent modulation, B:** The lattice potential is given by a time-periodic disorder which varies with a frequency ν. **Phase diagram, C:** The resulting phase diagram for a large amplitude of the drive $A \sim \Delta$ shows a localized phase at large disorders and high frequencies and an ergodic phase otherwise. They are separated by a delocalization-localization transition, induced due to the drive.

not relax to the value predicted from Floquet-ETH, due to the addition of disorder, and present an estimate of the phase transition between the Floquet-ETH and the Floquet-MBL phases.

8.2 Model

As in the previous experiments, the tunneling along the y-direction and z-direction is strongly suppressed as compared to x-direction. This effectively decouples the tubes which run along the x-direction which form one-dimensional systems. An individual tube along the x-direction can be theoretically described by the one-dimensional Aubry-André model with on-site interactions [148] and a time periodic quasi-random disorder potential:

$$\hat{H} = -J \sum_{i,\sigma} (\hat{c}^{\dagger}_{i+1,\sigma} \hat{c}_{i,\sigma} + \text{h.c.}) + U \sum_{i} \hat{n}_{i,\uparrow} \hat{n}_{i,\downarrow}$$
$$+ [\Delta + A\sin(2\pi\nu t)] \sum_{i,\sigma} \cos(2\pi\beta i + \phi) \hat{n}_{i,\sigma}. \tag{8.3}$$

Here, $J \approx h \times 550\,\text{Hz}$ is the tunneling matrix element between neighboring sites and h is Planck's constant. The fermion creation (annihilation) operator in the spin state $\sigma \in \{\uparrow, \downarrow\}$ on site i are denoted by $\hat{c}^{\dagger}_{i,\sigma}$ ($\hat{c}_{i,\sigma}$) and the particle number operator is $\hat{n}_{i,\sigma} = \hat{c}^{\dagger}_{i,\sigma}\hat{c}_{i,\sigma}$. The on-site interaction strength between the two spins is given by U.

The disorder is parametrized by its strength Δ, the incommensurate wavelength ratio $\beta = \lambda_s/\lambda_d$, and the relative phase ϕ. The disorder strength Δ is modulated periodically in time, with the amplitude A effectively reducing or increasing the instantaneous disorder

strength. In the experiment, this is implemented by periodically modulating the intensity of the disorder lattice such that the amplitude of the drive A is restricted to $\in [0, \Delta]$. This modulation happens in a sinusoidal fashion with a frequency $\nu = 1/T$, where T is the period of one cycle of modulation. This makes the Hamiltonian periodic in time $H(t) = H(t + T)$. In the case of zero amplitude of drive $A = 0$, the model is the same as the one studied earlier as the time-independent MBL case in Chapter 6 and shows a many-body localization transition around $\Delta = 4J$ for $U = 4J$.

Periodically modulated optical fields

In principle, modulating any of the terms in the Hamiltonian J, U or Δ periodically would make the system Hamiltonian periodic in time. However, there are certain practical restrictions on each of them. Due to the fast timescales involved, the magnetic field usually cannot be easily periodically modulated in the high-frequency limit. Hence, we choose to modulate the optical fields rather than magnetic fields. One could modulate the hopping J or the disorder Δ term. However, the hopping J is not modulated proportional to the power of the optical field, since the hopping has exponential dependence. Hence, the disorder potential is used as the modulation parameter, by merely modulating the intensity of the disorder laser. While this also perturbs the hopping, this perturbation is small, and it is not expected to change the global relaxation dynamics. A possibility in the future would be to use the drives mentioned in many theoretical proposals. These drives could be gradient drives such as modulation of the dipole trap, a magnetic field gradient or staggered drive, which can be implemented by using the super-lattice laser, allowing us to experimental realize several novel regimes [161–167].

8.3   Results

8.3.1   Stroboscopic time-evolution

We first set the interactions to $U = 4J$. We also fix the disorder strength to $\Delta = 7.5J$ such that the undriven system is strongly localized. We then monitor the time evolution of the imbalance $\mathcal{I}$ for the case of very strong driving $A = \Delta$. Two exemplary traces are shown in Fig. 8.3 for a high drive frequency $\nu = 2.0\,\Delta/h$ and a low drive frequency $\nu = 0.4\,\Delta/h$. The reason for calling them high and low will be explained in the coming sections. The normalization of imbalance is performed with the asymptotic imbalance of the undriven system $\mathcal{I}_0 \approx 0.6$. This is because we would like to understand the *additional* effect of the drive as compared to the dynamics of the undriven system. In any case, this merely scales the y-axis. This is also the reason why the normalized imbalance, $\mathcal{I}/\mathcal{I}_0$ is higher than unity at zero time of evolution (cut-off from the graph). This will not be important, as we will focus on the long time value. We have plotted all times in terms of the tunneling time $\tau = h/(2\pi J)$.
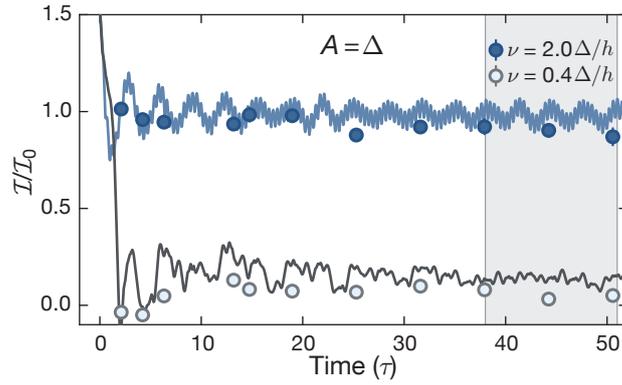
Figure 8.3: Time evolution of imbalance for low and high drive frequency: We fix the disorder strength to $\Delta = 7.5\,J$, interactions to $U = 4J$ and work with a strong drive $A = \Delta$ and show the resulting evolution of the normalized imbalance $\mathcal{I}/\mathcal{I}_0$ as a function of time for one high frequency $\nu = 2.0\,\Delta$ and one low frequency $\nu = 0.4\,\Delta$. Here, $\mathcal{I}_0 \approx 0.6$ is the asymptotic imbalance in the undriven case. All times are given in units of the hopping time $\tau = h/(2\pi J)$. We observe a large imbalance for the case of high frequency but a vanishingly small imbalance for the case of driving with low frequency. Each point is an average of six individual experimental realizations, and the error of the mean is smaller than the point size. Theoretical data obtained from matrix product simulations is shown as lines, and gray shaded region denotes the time window considered for obtaining the asymptotic imbalance.

Time evolution

We observe that at high frequency $\nu = 2.0\,\Delta/h$ the normalized imbalance is almost unity ($\mathcal{I}/\mathcal{I}_0 \sim 1$, blue points). This supports that the system is essentially transparent to the drive in this regime and the resulting imbalance is the same as the case with no drive. On the other hand, we find that the imbalance is qualitatively different and almost vanishes for low drive frequency, $\nu = 0.4\,\Delta/h$. Here, the dynamics in the periodically modulated Hamiltonian permits the redistribution of atoms between even and odd sites, leading to a vanishingly small imbalance ($\mathcal{I}/\mathcal{I}_0 \sim 0$, gray points). Theoretical simulations using matrix product states on a fairly large system (L=32) are shown in solid lines and strongly support our conclusions. Furthermore, the good agreement indicates that one can consider the system to be fairly well isolated from the rest of the environment at these times scales.

On the instantaneous Hamiltonian

We note the following two points about the drive amplitude and frequency from the mathematical structure of the drive:

1. Consider two arbitrary frequencies ν_1 and ν_2 (one low and one high). Additionally, we fix the total time of evolution t of the Hamiltonian, such that $t = m/(\nu_1 \nu_2)$, where m is some integer, ensuring stroboscopic measurements. This also guarantees that the total time spent by the instantaneous Hamiltonians such that the instantaneous disorder amplitude is less than the critical value in the undriven case is *independent* of the drive frequency and only depends on the amplitude of the drive. This is in

contrast to keeping the number of cycles fixed, in which the systems spends different amount of total time in the low disorder phase. Hence, the response in Fig. 8.3 cannot be explained by the reduction of time in the delocalized phase.

2. For a strong drive amplitude $A \sim \Delta$, the system continuously crosses the critical disorder strength of the undriven system. In a conventional phase transition, one could expect the system to *strongly* heat up, as it crosses a quantum critical point continuously. This idea appears to break down in the case of a high-frequency drive in disordered systems.

To understand the experimental observations, a small digression is presented. This digression would focus on the non-interacting case since it is easier to understand qualitatively. The experimental results after this section show the results for the interacting case, which share many of the qualitative features.

Failure of a simple freeze-expand model

Consider the following model in which the disorder is periodically switched between a very large value $\Delta \gg \Delta_c$ (strongly localized, localization length $\xi \ll 1$) and zero $\Delta = 0$(delocalized). We monitor the expansion of a particle, starting from a single site. Naively, one would expect that the expansion (and hence. imbalance) would be independent of the drive frequency but only depends on the total evolution time. This follows directly if one assumes that during the time of large disorder, the particle completely freezes and during the time of low disorder, the particle expands. Then, the total expansion would only depend on the time spend in the delocalized phase. Since this is independent of the frequency, one would conclude that the expansion is independent of the drive frequency.

This is not what one observes because the time evolution is highly *coherent* and the backscattering during the time of high disorder strongly suppresses the expansion during the low disorder. This implies that even in the phase without the disorder, there is a *memory* of the phase with the disorder, reflected in the destruction of the coherence, required for expansion (result in the absence of expansion even in the low disorder phase). At high enough frequencies, the expansion can even be completely suppressed, even though the system has arbitrarily long amounts of time at zero disorder. The central realization is that it is the total amount of time in the delocalized phase in *one period* that is relevant, and not the total time in the delocalize phase.

8.3.2   Phase diagram and the drive-induced delocalization

To understand what is a low frequency and what is a high frequency, one can systematically examine the value of imbalance after a time evolution of $50\,\tau$ as a function of frequency. This time is chosen so as to be long compared to few local interaction timescales (which normally should lead to thermalization of simple operators) but not too long so that the imbalance gets affected by the background bath coupling. Further, we expect this timescale to be capturing the asymptotic imbalance as long as the system is sufficiently far
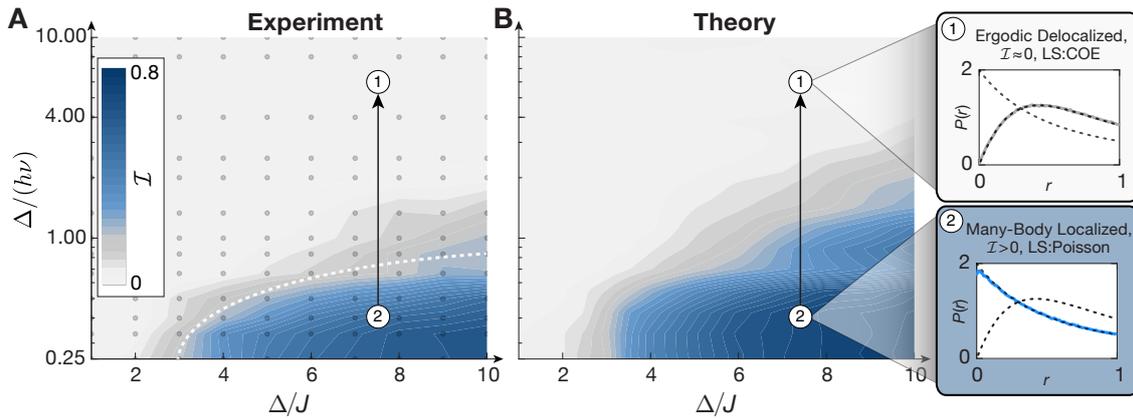
Figure 8.4: Phase diagram for large amplitude drive: We extract a phase diagram of the strong amplitude drive with $A = \Delta$ as we vary the disorder potential and the drive frequency. The interactions are fixed to $U = 4J$. Experimental results are shown in **A** and theoretical results are shown in **B** and show the imbalance measured after a time evolution of $\sim 50\,\tau$. In both the theory and the experiment, we find that the system remains localized at high frequencies for strong disorders but gets delocalized at low disorders or low enough frequencies. Further, in the insets, we show the theoretical calculation of the level statistics parameter $P(r)$ of the effective Floquet Hamiltonian, which shows COE statistics (gray line) in the delocalized phase signaling ergodic behavior and shows Poisson level statistics (blue line) signaling MBL. Dashed lines show their functional forms as a guide to the eye. Hence, they affirm our expectations based on the resulting asymptotic imbalance.

away from any critical point. We comment below on the dynamics near the critical points. This scan along the frequency is shown for various disorder strengths in Fig. 8.4.

The results obtained for large fixed amplitude $A \sim \Delta$ and fixed interactions $U = 4J$ from the experiment is shown in Fig. 8.4 **A** and for comparison the same is also shown as obtained from the matrix product based simulations in Fig. 8.4 **B**. On the x-axis is the high-frequency limit ($\Delta/\nu \to 0$), where we can expect the system to behave the same way as the undriven system. Hence, we also expect the transition to be the same as in the case of the undriven system with a critical disorder strength of $\Delta = 3J$. This is also where we see a sharp size of the imbalance. This region is the critical region and the analysis here of the precise critical point requires more care, and is separately described in Chapter 9. One can also see explicitly that the imbalance is non-zero at the disorder strength of $\Delta_c = 3J$ and hence, ask if this is already MBL. However, this is not accurate as near the critical point, there is (probably at least) one diverging length scale which causes finite time imbalance to be non-zero. A better way to understand this region is to consider the relaxation rates as explained in Chapter 9.

For larger disorder, on the x-axis one obtains a large imbalance in both theory and experiment which shows the localized nature in the high frequency limit. Decreasing the drive frequency generically causes the imbalance to decrease but it still persists at a non-zero value for a finite but high frequency. Further lowering the frequency, however, causes the system to completely delocalize, resulting in vanishing imbalance. This is shown in the form of an arrow from the MBL phase ② to the ergodic phase ①, black arrow. As described

in the introduction, the stroboscopic time evolution can be captured by a time-*independent* Floquet Hamiltonian, $\hat{H}_F$:

$$e^{-\frac{i}{\hbar}\hat{H}_F T} = \mathcal{T} e^{-\frac{i}{\hbar}\int_0^T \hat{H}(t)dt} \qquad (8.4)$$

which describes the unitary evolution over one period of the drive. Here, $\mathcal{T}$ is the time ordering operator and $\hbar$ is the reduced Planck's constant. Further, its statistical properties determine whether the quantum dynamics are ergodic or not [184]. For example, one can compute the level statistics of the quasi-energies ϵ_α, obtained from diagonalizing $\hat{H}_F$, and calculate the quasi-energies ϵ_α modulo h/T (due to the periodicity of the drive). The distribution $P(r)$ of the level statistics parameter, $r_\alpha = \min[\frac{\epsilon_{\alpha+1}-\epsilon_\alpha}{\epsilon_\alpha-\epsilon_{\alpha-1}}, \frac{\epsilon_\alpha-\epsilon_{\alpha-1}}{\epsilon_{\alpha+1}-\epsilon_\alpha}]$ helps one to identify the nature of the dynamics (ergodic or not). While the $P(r)$ in ergodic dynamics is expected to follow the circular orthogonal ensemble, a Poisson distribution is expected in the localized phase due to the absence of level repulsion. Typical plots for the distribution $P(r)$ are shown in the insets in Fig. 8.4 **B** and agree with these expectations. However, these numerics have been performed on systems of size $L = 8$, due to the finite amount of available computing resources. Hence, these results must be taken with caution. Nevertheless, they support the results obtained from the imbalance. Further, they show a crossover from the Poisson to the Gaussian distribution as one goes from the MBL phase ② to an ergodic phase ① along the black arrow, due to the finite system sizes.

Quantitative analysis of the frequency dependence

Fig. 8.5 **A** illustrates the contours of the phase diagram better by showing a cut at a constant disorder (vertical cut, along the black arrow). Here, we show the normalized imbalance for fixed $\Delta = 7.5J$ and interactions $U = 3J$ for large amplitude $A = \Delta$. The normalized imbalance is unity at high frequencies and continuously decreases upon decreasing the frequency, except for a small "bump" around $\Delta/(h\nu) \sim 1$. This is visible both in the experimental data (points) and the theoretical simulations (lines) and is connected to the nearest-neighbor energy level distribution of the quasi-periodic disorder. Upon lowering the frequency further, such that $\Delta/(h\nu) > 2$, we measure a vanishing imbalance signaling ergodic dynamics. The experimental data is typically slightly smaller than the theoretical data, likely due to the effects of the finite coupling to the environment [73].

8.3.3   Low amplitude regime and some open questions

Until now, we have focused primarily on the case of the large amplitude drive with $A = \Delta$. In Fig. 8.5 **B**, we show the imbalance after $50\,\tau$ as a function of the amplitude of the drive for a low frequency of $h\nu = \Delta/7.5 = 1J$ with fixed disorder $\Delta = 7.5J$ and interaction $U = 3J$. As noted earlier, the system delocalizes at large amplitudes $A \sim \Delta$. Upon decreasing the amplitude, we observe that the imbalance continuously increases, signaling that the system might no longer remain ergodic and might become MBL even at low frequencies, if the amplitude of the drive is not large enough. This implies that, despite the low-frequency drive, the system remains *exceedingly stable* for small drive amplitudes.
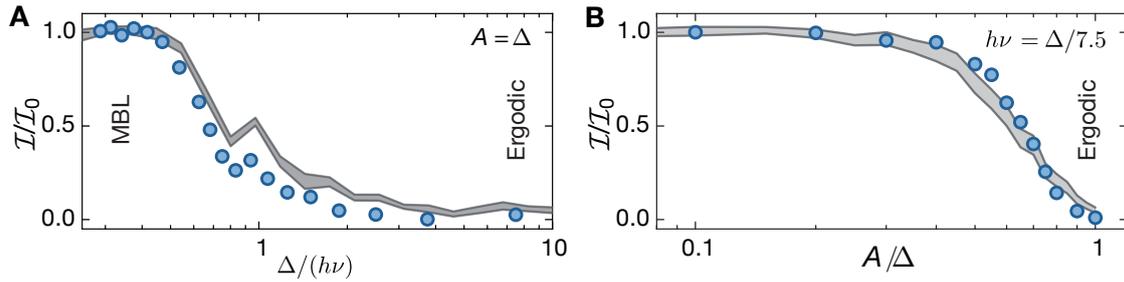
Figure 8.5: Amplitude and frequency cuts: The plot shows the asymptotic normalized imbalance for fixed disorder $\Delta = 7.5J$ and interaction $U = 3J$ for, **A**, fixed large amplitude $A = \Delta$, the frequency scan and **B**, fixed small frequency $\nu = \Delta/7.5$, the amplitude scan. The system appears to be stable at small amplitudes, but promptly delocalizes for large ones. The experimental data is shown as blue points and the gray lines denote the numerical simulation results. Error bars denote the error of the mean from six individual experimental realizations and are typically smaller than the data points. Thickness of the theoretical lines denotes one standard deviation of the data for different disorder realizations.

This is in stark contrast to many theoretical results, which argued that many-body systems must get delocalized at low frequencies. While it is unclear if this is a finite time result, further numerical simulations at least tend to support that the system might indeed strongly reduce the critical numbers to $A/(h\nu) \sim 10^{-5}$. Nonetheless, it is clear that an MBL system should be extremely robust in the case of the above-defined global drive at *all* frequencies. This could provide novel avenues for engineering new phases of matter. The ultimate fate of such a system for low drive amplitudes and low frequencies, however, remains an open question.

8.3.4 Conclusion

By periodically driving a many-body Hamiltonian, we have created and probed ergodic and non-ergodic phases. Periodic driving also provides a new tool to study the frequency-resolved measurements of the many-body system [185]. Further, we experimentally demonstrate that disorder can indeed protect driven systems from heating up. Even for highly non-perturbative drives with very large amplitudes, the MBL system is shown to undergo a finite-frequency localization-delocalization transition. Further, our experiment finds a novel regime of extreme stability at *any* drive frequency, providing exciting opportunities for engineering periodically driven phases of matter.

8.4 Discussions

We discuss, compare and contrast some important points to make the results mentioned above more concrete. Further, we think that these results can significantly add to the understanding of the microscopic picture and contribute to understand the various regimes. We will focus on numerics based results in this section, which are performed on the XXZ
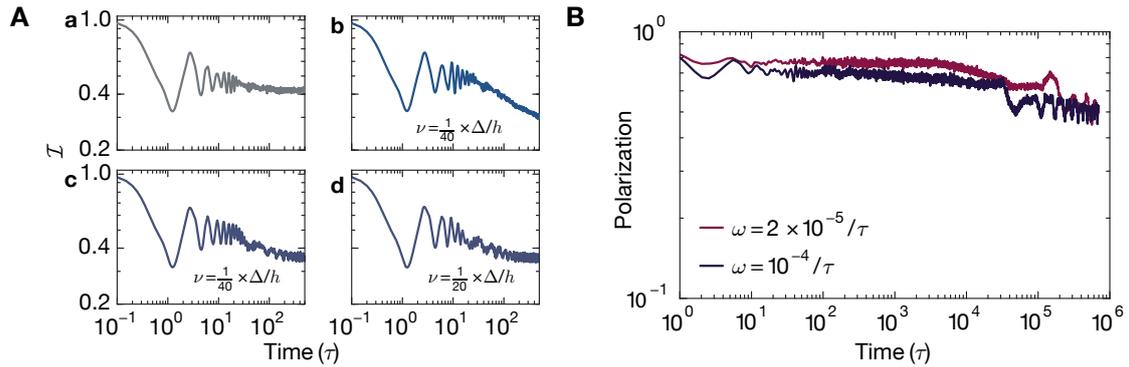
Figure 8.6: A quantitative comparison between the experimental global-drive and an electric-field gradient-drive. A: The time evolution of the imbalance is calculated using matrix-product-state techniques and is shown for a few illustrative cases: For no drive $A = 0$ in (**a**), a gradient drive with $A/\Delta = 0.2$ in (**b**) and the global drive for two low frequencies in (**c**) and (**d**). Compared to a static MBL system in (**a**), the driven system in (**b**) shows a clear power law relaxation of the imbalance. However, in case of driving with the global drive in (**c**) and (**d**), an unambiguous relaxation of the imbalance is not visible. The disorder strength is $\Delta = 5J$ and interaction $U = 4J$. **B:** A similar trend for the global drive can be captured by the relaxation of the spin polarization in the XXZ Hamiltonian, which also shows a large imbalance are very long times. The simulations are performed for disorder $\Delta = 5J_\perp$ and interaction $J_z = 1.0J_\perp$ and support that our observation of stability of MBL for the low-amplitude global-drive is also visible in other models of MBL. The simulations are performed by Prof. Michael Knap and are reported here with permission.

Hamiltonian as described in the initial chapters. The numerics in this section were necessitated out of discussions, and I thank Prof. Michael Knap for permission to share some unpublished results.

8.4.1   Global drive vs gradient drive and a Landau-Zener picture

Multiple theoretical studies [162–164, 166, 167, 186] on the MBL phase in the disordered XXZ Hamiltonian have studied the response of an MBL system at low frequencies and have pointed out that such a system must always delocalize. The reason for such a delocalization can be understood with a simple picture of Landau-Zener crossings [162], whereby the energy levels in the many-body spectrum have crossings which effectively get coupled at low frequencies. What is interesting in most theoretical studies is that even though the considered drives are macroscopically different, ranging from electric field gradient drive [167] to staggered hopping [166], they all find that MBL breaks down universally roughly for $A/(h\nu) \gtrsim 1$.

Since the drive we studied in this work was previously unexplored; we compared the relaxation of our system when driven by one of the above drives, where the system is modulated with a gradient potential. This is done for two reasons. One is for a direct comparison to check if the experimental results imply a *generic* result, expected in highly excites states of all disordered Hamiltonians, and more importantly, because of the low amplitude results in our system, where we already measured indications of non-universal behavior. To have such a comparative study, we show in Fig. 8.6 **A** four different time

A Experiment

B Theory
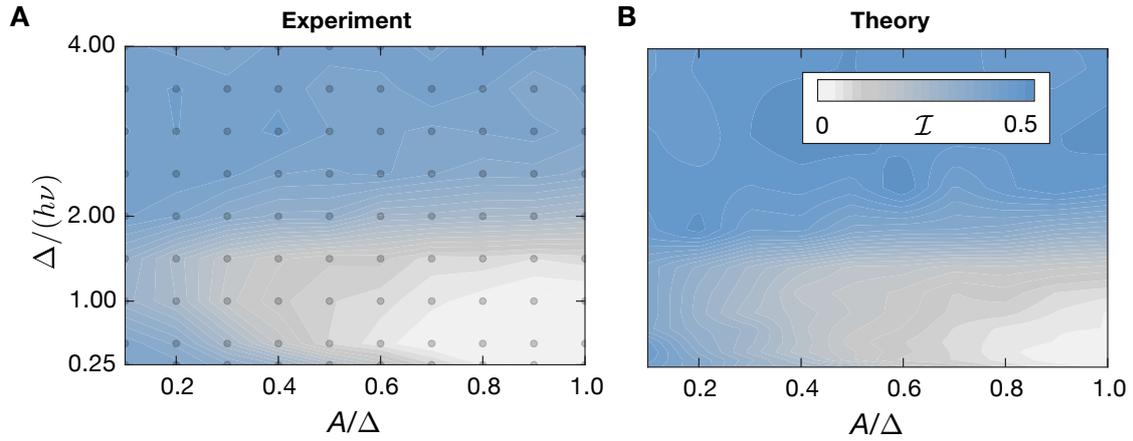
Figure 8.7: Dynamical phase diagram as a function of frequency and amplitude. We plot the imbalance after an evolution time of $50J$ for a disorder strength of $\Delta = 4J$ and an interaction strength of $U = 4J$ as a function of the drive frequency and the drive amplitude. We observe that the system remains localized for high frequencies for all amplitudes. At low frequencies, the system delocalizes for large amplitude. The system appears localized for low amplitudes and low frequencies.

evolutions. In Fig. 8.6 **A(a)** we show the imbalance for the case of no driving, where we observe a saturation of imbalance, signaling MBL. In Fig. 8.6 **A(b)**, we show the relaxation for a gradient drive, showing the predicted power law relaxation (and delocalization) of imbalance [167], for $A/(h\nu) = 8 \gg 1$. However, for the same parameter ratio, $A/(h\nu) = 8$, for the global drive studied in our system we see a relaxation to a new plateau behavior and no power law relaxation, as shown in Fig. 8.6 **A(c,d)**. However, it is not unambiguously clear that there cannot be further relaxation at longer times, and it is challenging to simulate even longer times in this case.

This limitation can be (up to a degree) circumvented by performing simulations with the disordered XXZ Hamiltonian, where it is possible to perform calculations for smaller frequencies and longer times. This is shown in Fig. 8.6 **B**. Here, we use a disorder strength $\Delta = 5J_\perp$ and an amplitude of $A = 0.16\Delta$ for a chain of length $L = 16$. We show the time evolution of a staggered Néel state (with a projected polarization of unity) for two very low frequencies $\nu = 2 \times 10^{-5}/\tau$ and $\nu = 10^{-4}/\tau$, which results in a large value of the parameter, $A/(h\nu)$. However, even for times as long as $10^6 \tau$, we do not observe a clear sign of delocalization. These results show that our observations are most likely generic and represent a case of extreme stability of the MBL state with respect to a small amplitude global-drive, in which the strength of the disorder is itself modulated. It remains an open challenge for both experimental and theoretical investigations, to infer the correct asymptotic description of the such in such regimes. Nonetheless, such results demonstrate novel avenues for engineering exceedingly stable driven phases of matter.
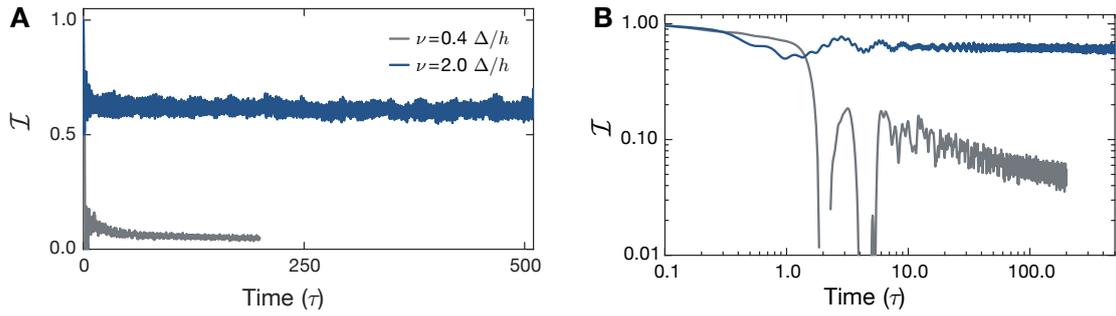
Figure 8.8: Long-time evolution of the imbalance with a large amplitude drive: We plot the theoretical imbalance $\mathcal{I}$ in the time traces in Fig. 8.3 to eacven longer times with disorder $\Delta = 7.5\,J$ and interaction $U = 4\,J$. This supports the result that the system remains localized for high frequency $\nu = 2.0\,\Delta/h$ but gets delocalized at low frequency $\nu = 0.4\,\Delta/h$. Part **A** and **B** show the same data, but on linear-linear and log-log plots, respectively. The linear plot is for the comparison to Fig. 8.3, while the log-log plot shows the slow power law decay of the small residual imbalance at low drive frequency.

Real-random disorder vs quasi-periodic disorder

One can ask if the non-interacting problem also delocalizes. There seems to be an important difference between the real-random (RR) and quasi-periodic (AA) disorder and that is the finiteness of the localization-delocalization point that changes the response at low frequencies, i.e. the critical disorder strength in the undriven non-interacting model is $\Delta_c^{\mathrm{RR}} = 0$, while it is $\Delta_c^{\mathrm{AA}} = 2J$ for the AA disorder. While it seems that the RR never delocalizes, indeed the localization length in the Floquet Hamiltonian can become arbitrarily large. On the other hand, it seems that indeed there is delocalization in the AA case. These results suggest that it is the finiteness of the critical point which is crucial and not the interactions. It would be interesting to realize driving protocols, where the driven non-interacting system (with finite undriven critical disorder strength) remains localized, but the driven interacting system delocalizes.

Role of interactions

One simple thing that interactions do is to move the localization-delocalization transition point to a finite value whether the system has RR or AA disorder. Hence, in this case, there is a finite value of the critical point, and hence, for any interactions, there still seems to be a localized and delocalized regime for the large amplitude global drive/gradient drive.

8.4.2   Amplitude-frequency phase diagram

We map out the amplitude-frequency phase diagram for disorder $\Delta = 4J$ and interaction $U = 4J$, as shown in Fig. 8.7. While the system shows vanishing imbalance for large amplitude and low frequency, it shows a persistent imbalance for high frequency and/or low amplitude. We expect the system to be MBL in these cases, though the fate of the system at low amplitude and low frequency, while it appears to be MBL, is unclear.
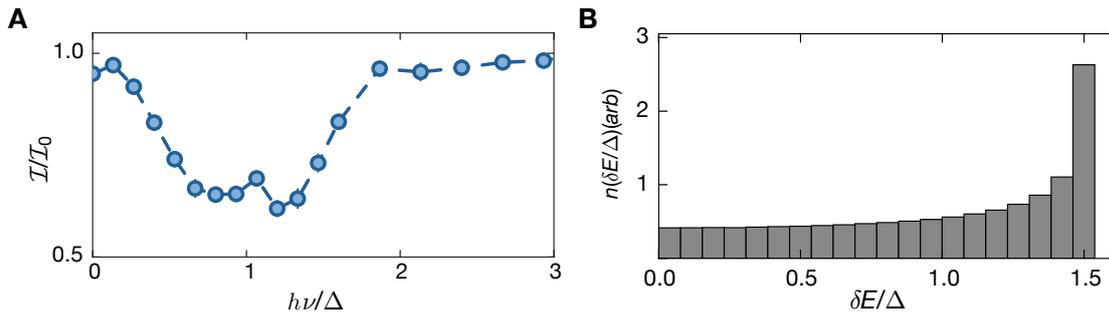
Figure 8.9: Frequency resolved spectrum of a localized state, A: We measure stationary imbalance for fixed disorder $\Delta = 7.5\,J$ and vanishing interactions for various modulation frequencies and find strong absorption signal for frequencies between 0.2-$2.0\Delta/h$. **Nearest-neighbor onsite energy differences in the quasi-periodic model, B:** The absorption can be understood as a result of a strong localized system and the nearest neighbor onsite energy differences δE in the Aubry-André model.

8.4.3 Asymptotic imbalance of the undriven system

The asymptotic value of the imbalance of the undriven system $\mathcal{I}_0$ is the value of the imbalance after an evolution of $40 - 50\,\tau$ for $A = 0$. For disorder $\Delta = 7.5\,J$ and $U = 4J$, we expect this value to be the imbalance of our system at infinite times. The undriven asymptotic value obtained in the experiment is $\mathcal{I}_0^{\text{exp}} = 0.56$ and its value for the theoretical case is $\mathcal{I}_0^{\text{theory}} = 0.66$. The discrepancy between theory and experiment is primarily attributed to the weak coupling of the experiment to the nearby tubes [73], which acts like a bath and to the lower value of the initial state imbalance of $\mathcal{I}^{\text{exp}}(t = 0) = 0.91$, compared to the numerical calculations which has unity imbalance for zero time evolution.

8.4.4 Longer-time dynamics of the strongly driven system

To further support the case of localization at high frequencies but delocalization at low frequencies, we theoretically evaluate the imbalance to even longer times than shown in Fig. 8.3 and this is shown in Fig. 8.8. The disorder is fixed to $\Delta = 7.5\,J$, the interaction to $U = 4J$ and the amplitude of the drive to $A = \Delta$. Part **A** and **B** show the same data, but the former is on a linear-linear plot and the latter on a log-log plot. The linear plot is to extend the earlier data to longer times showing a stable high-frequency phase. In the log-log plot, a very slow power-law decay of the imbalance is observed for the low-frequency drive. This supports the initial observation that the system is indeed in a Floquet-MBL phase for high-frequencies and is consistent with a Floquet-ETH phase for low-frequencies.

8.4.5 Frequency resolved spectrum

Lattice modulation spectroscopy is a powerful probe to characterize the excitation spectrum of a many-body state. This has been successfully used to characterize the low-temperature states such as the Mott-insulating and superfluid states and their low-energy

excitation spectrum [187]. Further, for ergodic excited states, one would expect a broad continuum of absorption. We can adapt this to our experiment and measure the absorption via imbalance loss as a function of modulation frequency for a small amplitude of modulation $A/\Delta = 0.2$. We perform this measurement for a strong disorder of $\Delta = 7.5\,J$ and interactions close to zero $U \approx 0$. This is shown in Fig. 8.9. The graph shows the residual normalized imbalance $(\mathcal{I}/\mathcal{I}_0)$ as a function of the drive frequency, and we observe strong absorption between frequencies $\nu \in [0.2, 2] \times \Delta/h$. The particular shape that we observe is a direct consequence of localization and the nearest-neighbor onsite energy differences in the quasi-periodic potential with Aubry-André type disorder potential (shown in Fig. 8.9 **B**) which features a peak $\sim 1.5\,\Delta$. This strongly peaked distribution of absorption is also visible in the phase diagram obtained in the main text. In the experiment, the measured absorption signal might be smoothened (especially near the maximum absorption point) due to the finite modulation amplitude (changes the Hamiltonian), the harmonic confinement and the averaging over multiple tubes [72], see Chapter 5.

Slow Relaxation and Many-Body Localization in 2D Quasi-Periodic Potentials

Short summary: MBL is probed in a model in two dimensions, with quasi-periodic potentials along both directions. The relaxation dynamics of the system near a possible MBL transition in two dimensions are revealed and described with phenomenological Griffiths-type arguments. The chapter closes with several open questions and the current status of the field.

9.1 Introduction

Whether and under which conditions MBL can occur in dimensions more than one remains an outstanding challenge for both experiment and theory. While a variety of numerical and analytical methods [22, 23, 40, 118, 188] have allowed us to understand and develop a physical picture for the MBL phase in one dimension, much less is evident in higher dimensions.

Simulations are expected to be reliable only deep in the MBL phase and cannot be easily extended to the regimes close to the MBL transition point. Consequently, despite intense interest [28–37], little is known with certainty about this regime. In particular, since the physical picture of the transition is unclear, the critical properties of the transition are unclear, and even basic notions are contested, such as whether the transition is continuous or discontinuous [41, 42]. For works which assume a continuous transition, critical exponents obtained from exact diagonalization studies of finite-sized systems ($\nu_{FS} \sim 1$) seem incompatible with the ones from renormalization group analysis [29, 30]($\nu_{RG} \sim 3.5$) and from some analytical considerations [189–191]($\nu_{\text{Harris}} \geq 2$) but are consistent with other analytical works [192] ($\nu \sim 1$). In comparison. the situation is even less certain in higher dimensions, which faces an acute scarcity of results [193–195]. Numerical calculations, for example, are extremely challenging in higher dimensions [196] due to small system sizes which are available.

Given the apparent conflict of the available results near the transition point and the inaccessibility of numerical simulations in higher dimensions, experiments stand to play a major role in illuminating the dynamics in these regimes. Previously, experiments have studied the possibility of MBL in three-dimensions [197] and in two dimensions [198] with short-ranged interactions and real-random disorder, by measuring mass transport.

While this provides some evidence for an MBL phase in higher dimensions, mass transport is probably the slowest relaxing observable in these systems, and hence, it becomes very hard to separate a slow, disorder induced timescale of transport [129]. Additionally, it has been argued that such an observable might not be able to capture the effects of rare regions in higher dimensions [199], which are expected to significantly affect the dynamics near the MBL transition point.

In this experiment, we probe a two-dimensional model with quasi-periodic potentials along both directions. The relaxation of a far-from-equilibrium state is captured with the imbalance, which relaxes very quickly in the absence of disorder and hence, allows capturing the longer relaxation timescales in disordered cases. Our results constitute benchmarks for theories which aim to capture the relaxation near a possible MBL transition point in higher dimensions.

9.2   Model

The model used to study the interplay of the interaction and the disorder in two dimensions is a direct generalization of the one-dimensional model described in Chapter 6. We load the fermionic Potassium-40 gas in a two-component spin mixture into a square lattice in two dimensions, as shown in Fig. 9.1 **A**. Atoms can tunnel between neighboring sites of this lattice and interact via on-site interactions. Different quasi-periodic potentials run along the orthogonal x and y-directions. This implies that the system is separable in the absence of interactions. The Hamiltonian of the system can be written as follows:

$$\hat{H} = -J \sum_{\langle \mathbf{i},\mathbf{j}\rangle,\sigma} (\hat{c}_{\mathbf{j},\sigma}^\dagger \hat{c}_{\mathbf{i},\sigma} + \text{h.c.}) + U \sum_{\mathbf{i}} \hat{n}_{\mathbf{i},\uparrow} \hat{n}_{\mathbf{i},\downarrow}$$
$$+ \Delta \sum_{\mathbf{i},\sigma} [\cos(2\pi\beta_x m) + \cos(2\pi\beta_y n)] \hat{n}_{\mathbf{i},\sigma}. \tag{9.1}$$

Here, $\hat{c}_{\mathbf{i},\sigma}^\dagger (\hat{c}_{\mathbf{i},\sigma})$ denotes the creation (annihilation) operator of a fermion with spin $\sigma \in \{|\uparrow\rangle, |\downarrow\rangle\}$ on a lattice site $\mathbf{i}$, characterized by its Cartesian coordinates $\mathbf{i} = (m, n)$. The number operator is denoted by $\hat{n}_{\mathbf{i},\sigma} = \hat{c}_{\mathbf{i},\sigma}^\dagger \hat{c}_{\mathbf{i},\sigma}$. The angle brackets in the first term $\langle,\rangle$ denote a restricted sum over nearest-neighbor sites. The tunneling matrix element along both the x-direction and the y-direction is the same and is set to $J \approx h \times 330\,\text{Hz}$. Here, h is Planck's constant. The on-site interaction strength between two spins is denoted by U and is tunable via a Feshbach resonance [140]. The disorder potential is characterized by the strength Δ and the lattice incommensurable wavelength ratios $\beta_x \approx 0.721$ along the x-direction and $\beta_y \approx 0.693$ along the y-direction. The incommensurable wavelength ratios are computed by the ratio between the main-lattice wavelength and the disorder-lattice wavelength. Therefore, in the x-direction, it is $\beta_x \approx 532\,\text{nm}/738.2\,\text{nm} \approx 0.721$ and in the y-direction, it is $\beta_y \approx 738.2\,\text{nm}/1064\,\text{nm} \approx 0.693$.

Atoms are selectively loaded on the even stripes to form a far-from-equilibrium state, and the relaxation dynamics is captured by monitoring the redistribution of atoms between the even and the odd stripes. In an ergodic time evolution, this density-wave pattern will quickly vanish, as the dynamics erase any visible microscopic details of the initial
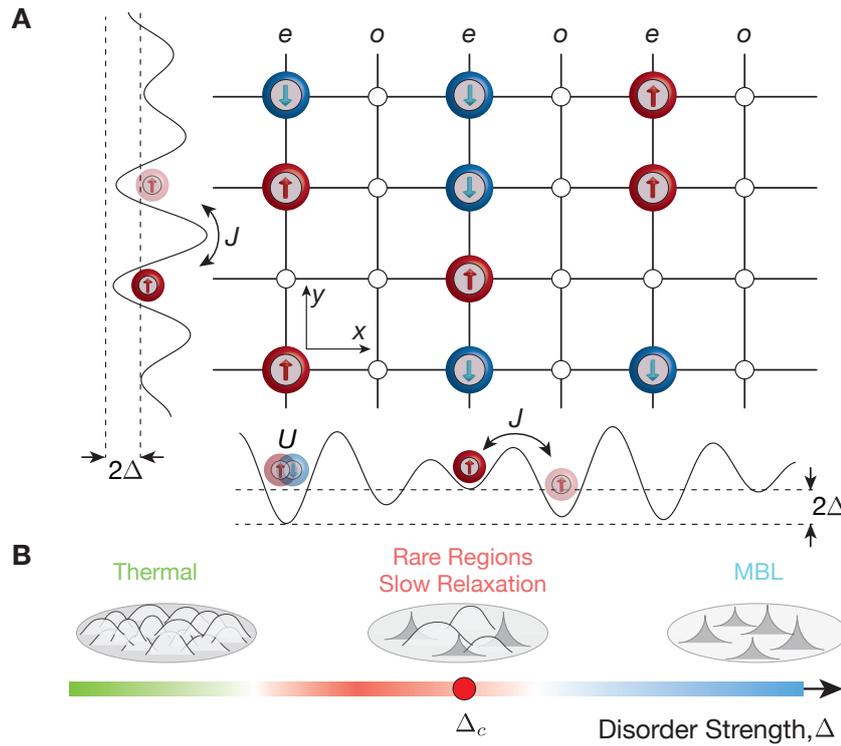
Figure 9.1: Schematic of the experiment, A: The two-dimensional system can be described by a square lattice with even stripes occupied by atoms in the initial state. The spin at each site is not controlled and is expected to be random. The hopping along both the x-direction and the y-direction is the same and is given by J. The interaction U is present only between atoms of different spin states located on the same site. The disorder is characterized by the quasi-periodic potential of strength Δ and the incommensurable numbers β_x and β_y. The size of the system in the central plane is approximately 200×100 sites containing several thousand atoms. **Expected phase diagram, B:** One expected phase diagram would be a thermal-ETH phase for low-disorders which relaxes very quickly (green area) and an MBL phase at large disorders which violates ETH (red-area). If there is a transition between the two, dynamics near it can be strongly dictated by regions which have anomalous characteristics, such as extremely long relaxation times arising due to strong local disorder or unusually few interaction partners.

conditions. If this does not happen, and the system remembers its initial state, this directly indicates the breakdown of ergodicity. The memory of the initial conditions can be measured by the normalized atom number difference between the even stripes (N_e) and the odd stripes (N_o), defined as the imbalance $\mathcal{I} = (N_e - N_o)/(N_e + N_o)$. Like in the one-dimensional case, this serves as our dynamical order parameter. The imbalance exhibits fast relaxation in the absence of disorder and thereby, facilitates identification of a possible slow relaxation timescale, introduced due to the addition of disorder. This must be contrasted with the mass transport studied in Refs. [197, 198], which is a slow process even in clean ergodic systems, without any disorder [129]. Furthermore, the imbalance is argued to capture effects stemming from Griffiths-type relaxation mechanisms, even in higher dimensions [199].
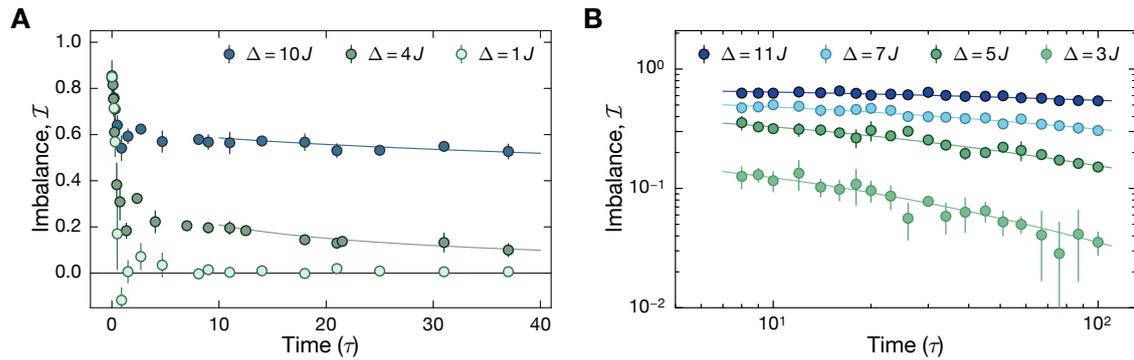
Figure 9.2: Time evolution of imbalance in two dimensions: We fix the interaction to $U = 5J$ and measure the imbalance after different evolution times for several disorder strengths starting from an initial state with the imbalance close to unity. **A:** Shown on a linear plot, one can directly observe that the imbalance relaxes to zero very quickly in case of low disorder strength $\Delta = 1J$, signaling ergodic behavior. At intermediate disorder strength $\Delta = 4J$, the imbalance appears to show slow relaxation. For a strong disorder strength $\Delta = 10J$, the system appears to relax at a vanishingly small rate. **B:** The imbalance relaxation is shown for additional disorder strengths on a logarithmic plot and shows a continuous slowing down of relaxation with increasing disorder strength. Solid lines are fits $\propto t^{-\zeta \log(t)}$, where ζ is the relaxation exponent, as described in the main text. Each point is a mean of six individual experimental realizations, and error bars denote the error of the mean. All times are given in units of the hopping time, $\tau = h/(2\pi J)$.

9.3   Results

9.3.1   Slowing down of thermalization

To exemplify the relaxation dynamics in such a Hamiltonian, we fix the interaction to $U = 5J$ and explore the dynamics for a variety of disorder strengths, as shown in Fig. 9.2. Since the initial state contains almost all atoms on the even stripes, the imbalance is close to unity at zero evolution times for all cases. During the time evolution, however, the relaxation strongly depends on the underlying disorder strength. In Fig. 9.2 **A**, this is plotted on a linear scale. For a low disorder strength, $\Delta = 1J$, we see the imbalance relaxes to zero in a few tunneling times. This signals that the system is ergodic for small disorders. On the other hand, upon increasing the disorder strength to intermediate values, $\Delta = 4J$, we see that the imbalance does not quickly vanish, but instead shows a slow relaxation. This becomes even weaker for larger disorder values, $\Delta = 10J$. To see this slow relaxation at intermediate disorders clearly, we plot it for several additional values in Fig. 9.2 **B** on a double logarithmic scale, which shows the continuous slowing down of relaxation as the disorder strength is increased.

9.3.2   Locally in the other phase

Here, we that the theoretical understanding of the mechanism behind the observed relaxation in two dimensions is currently unclear. It appears intimately connected to the nature of two very challenging problems: firstly, on the possibility of an MBL phase itself
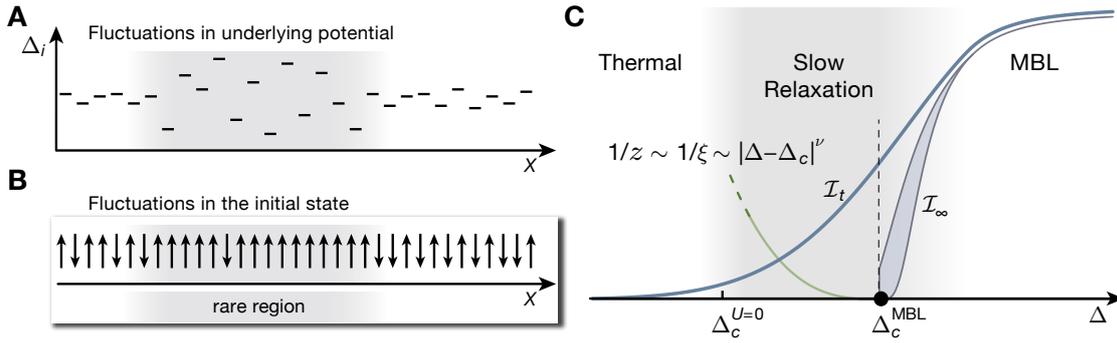
Figure 9.3: Rare-region schematic: The diagram shows two possible mechanisms which are expected to dominate the relaxation of the system. **A:** If the on-site potentials are distributed truly randomly, local fluctuations of the disorder can result in the creation of regions with an usually large amount of effective disorder, resulting in a long timescale of local relaxation. However, as depicted in **B**, regions with unusually large total spin might mimic such effects, at least to intermediate times. **Effect on the relaxation dynamics and imbalance, C:** Since different regions are disordered differently, their relaxation also has different characteristic timescales, and such a distribution can result in the relaxation of the imbalance dominated at time t with some characteristic region of length scale l_t. The system would completely relax after very long times and the value of the imbalance $\mathcal{I}_\infty$ distinguishes the localized system from a delocalized system. This relaxation can be captured with some universal rate $1/z$ near the MBL transition disorder strength Δ_c with an exponent ν. In the graph, Δ denotes the disorder strength, Δ_c^{MBL} is the MBL critical point whereas Δ_c^{AL} denotes the AL critical disorder strength, below which slow relaxation is not expected. Whether or not $\mathcal{I}_\infty$ can be discontinuous at the transition point is currently unclear [42].

in two dimensions and secondly, on the dynamical signatures of universality near critical points of the MBL transition. The solution might or might not further possess two or more classes of universality, depending on the underlying disorder being deterministic like quasi-periodic or real-random [152].

Even in one dimension, the dynamical signatures of universality near the MBL critical point are unclear. In systems with quenched real-random disorder, Refs. [30, 199] predicted relaxation to be dominated by anomalous regions with unusually strong local disorder, resulting in sub-diffusive transport near the MBL transition. Numerical calculations of Ref. [116] supported such a phenomenology. However, recent results [77, 200] show the same signatures even in the absence of any such quenched disorder, and per say, the relaxation appears strikingly similar to the case of relaxation in a system with a real-random disorder. In two dimensions, the experimental results presented here provide the first results on such relaxation in this regime, as shown in Fig. 9.2. Nevertheless, not too close to the MBL transition and at intermediate times, another type of Griffiths effects might explain the observed phenomena, as described next.

Phenomenological Griffith-type arguments

Consider a microscopic picture of the initial conditions. There are two features which could be relevant, see Fig. 9.3 . In a system with true randomness, regions with unusually

large local disorder can exist, with a probability which is exponentially small in their volume (L^d):

$$p(L) \sim e^{-(L/l_0)^d} \tag{9.2}$$

where, $l_0 \sim 1$ is some number which depends on the exact distribution of the real-random disorder (e.g. box or Gaussian). Such a region is shown pictorially in Fig. 9.3 **A**. On the other hand, the surroundings near it have effectively very low disorder strength and hence, a high mobility of particles. On short timescales, this anomalously strongly disordered region would be effectively detuned away from its surroundings and appear localized, showing incomplete relaxation of a density wave (i.e. this region would seem localized at intermediate times, even though the entire system would eventually thermalize). Subsequently, on a longer timescale, it would couple with its surroundings and assuming that the surroundings are thermal, it would eventually relax completely. Since there is a *distribution* of such locally *insulating volumes*, they would relax with a distribution of characteristic timescales.

Importantly, even if there are no strong fluctuations in the local disorder (for example in quasi-periodic systems), as shown in Fig. 9.3 **B**, there could instead be large local fluctuations in how an infinite temperature state is constituted locally. With an exponentially small probability in its size, the initial state might contain a large region with predominantly a single spin component. The gray shaded region, in this case, has a very large total spin **S**. Even though the total spin is globally a fixed quantity, it can fluctuate locally. Such regions with a large total spin interact very weakly (or not at all) since interactions in our system exist between atoms with different spins. Even a small amount of disorder can *localize* such an isolated single-spin region. Local distributions of the total spin can result in distributions of local relaxation timescales, which would result in some characteristic global relaxation. Such an argument would suggest that perhaps *each* globally conserved quantity which can fluctuate locally, for example, the average density, the disorder strength, the total spin, etc. would contribute to a distribution of relaxation timescales.

Such distribution of relaxation timescales would imply that the imbalance would reach its infinite time value I_∞ by relaxing via many characteristic timescales. While these locally anomalous regions should occur with a probability which is exponentially small in their volume, *how* they relax in time and *what* their characteristic relaxation timescale is, would depend strongly on the process which dominates their relaxation. This itself can crossover from one to another as different processes can dominate the relaxation at various times. As shown in Fig. 9.3 **C**, this results in the imbalance at finite times $\mathcal{I}_t$ relaxing slowly through many channels until it reaches its final value $\mathcal{I}_\infty$, which would be zero and non-zero in the delocalized and the localized phases, respectively.

Within this coarse-graining assumption with a hierarchy of timescales, each dominating at a characteristic time, the process which relaxes the system still has to be determined, to understand the relaxation dynamics of our system. This can occur in two ways as it depicted in Fig. 9.4. First, an anomalous region could relax via tunneling out of the region, which would take exponentially long in the *linear size* of the region. Secondly, such an
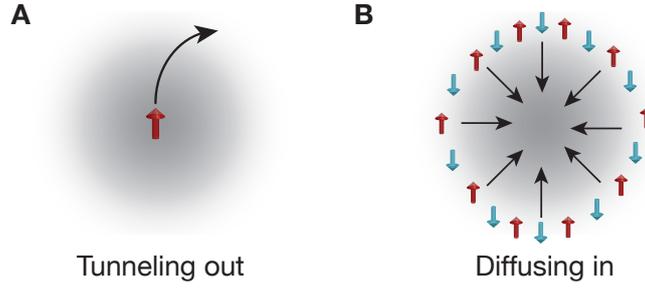
Figure 9.4: Two-mechanisms for relaxation: Two mechanisms could relax a localized region, **A**, tunneling out, whereby the particle tunnels out of the region and **B**, where the thermal surroundings of the inclusion diffuses in, evaporating the region from outside. Red and blue arrows denote two different spins and the shaded region is an anomalously strongly localized region.

inclusion could relax via the neighborhood spins diffusing in the region via second-order tunneling processes and thereby, rendering the region highly interacting and initiating higher-order rearrangement processes to relax the region. This kind of relaxation should then scale polynomially in the length of the system. The initial relaxation could be dominated by the tunneling mechanism as the second-order spin diffusion is too slow, whereas, at later times, it could crossover to the diffusive case. In both cases, the relaxation should become extremely slow for increasing disorder strength. These two cases would give rise to the following types of relaxation:

$$t(L) \sim \begin{cases} e^{L/\xi} & \text{Tunneling out} \\ \frac{1}{s} L^a & \text{Diffusing in} \end{cases} \tag{9.3}$$

where, ξ is some length scale given by the total spin of the region and the amount of fluctuation of the local disorder and $s \ll 1$ is the spin diffusion rate, which for intermediate disorder strengths is expected to be a second-order process and therefore, small in magnitude. Additionally, the tunneling mechanism suggests that at some time t, the regions which contribute the imbalance relaxation are of characteristic size $\log(t)$.

Currently, this analysis and in general, the effect of conserved quantities is incompletely understood, and it is unclear, how the polynomial type relaxation would affect the dynamics. The tunneling mechanism is considered in Ref. [199] and assuming this to be also true in our system, at least to intermediate times, the following relaxation form is obtained in two dimensions:

$$\mathcal{I}_t \sim t^{-\zeta \log(t)} \tag{9.4}$$

Fits to this function are shown by the solid lines in the time traces in Fig. 9.2 and show remarkable agreement with the observed data for all disorders, and hence, can be used to capture the relaxation rate of imbalance, at least at these timescales.

9.3.3 Relaxation exponents and the critical disorder strength

To quantitatively analyze this relaxation, we model it with the following form:
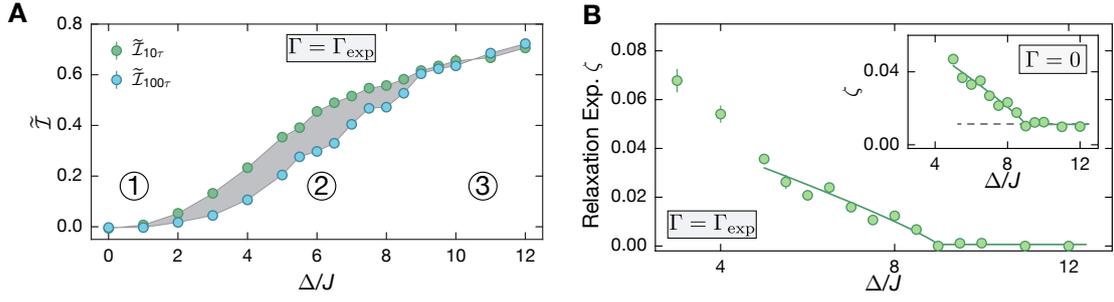
Figure 9.5: Closed-system imbalance, A: We mark the three possible regimes observed in the experiment. In the low disorder regime ①, we observe identical and vanishing closed-system imbalance, $\tilde{\mathcal{I}}$ at short ($10\,\tau$) and longer times ($100\,\tau$). Upon increasing the disorder strength, we observe a regime ②, wherein a clear relaxation between the short and long time data is visible, and imbalance remains non-zero. Finally, in regime ③, the short and long time value of $\tilde{\mathcal{I}}$ match, implying that the relaxation is absent up to a known bath-like coupling. Error bars denote error of the mean. **Relaxation exponents ζ, B:** Assuming a known coupling to the environment $\Gamma = \Gamma_{\mathrm{exp}}$, this rate of relaxation can be captured by relaxation exponents ζ, which continuously decrease until a critical value of the disorder strength $\Delta_c^{2D} = 9J$, where they appear to completely vanish, indicating an MBL phase in the isolated limit. A piecewise fit $\zeta \propto \{|\Delta - \Delta_c|^\nu, 0\}$ restricted around the critical regimes $\Delta \in \{5, 12\}$ yields $\nu = 0.9$. The inset shows the same evaluation assuming zero coupling to the environment, also exhibiting a sharp change in the relaxation exponents at the same critical disorder strength Δ_c. Error bars denote the fit errors. Solid line is a fit near the critical disorder strength, as described in the main text.

$$\mathcal{I} = \tilde{\mathcal{I}} \times f(t) \tag{9.5}$$

Here, $\tilde{\mathcal{I}}$ is called the closed-system imbalance, and $f(t)$ is a weak coupling to the environment, present in all real systems such that, it eventually always thermalizes the system. We model this coupling as $f(t) = e^{-(\Gamma t)^\beta}$, where $1 \gg \Gamma > 0$ and β configure the weak coupling to the external environment that happens in the experiment due to coupling between identical two-dimensional planes along the z-direction. This weak coupling can be attributed to a non-zero hopping along the z-direction and its value in the experiment is roughly given by $\Gamma = \Gamma_{\mathrm{exp}} = 10^{-3}\,\tau^{-1}$ with the stretching exponent $\beta \approx 0.6$. This allows us to separate the slow relaxation of an isolated system from relaxation due to a dissipative external coupling, which is small but non-zero. We also perform the data analysis assuming that the system was perfectly isolated by taking $\Gamma = 0$, and show that the central features of the experiment remain unchanged.

The closed-system imbalance $\tilde{\mathcal{I}}$ is shown after a short evolution time of $10\,\tau$ and after a longer evolution time of $100\,\tau$ in Fig. 9.5 **A**. Here, three different regimes can be identified. For weak disorder strengths $\Delta < 2J$, marked by ①, $\tilde{\mathcal{I}}$ is almost zero and matches for both short and long times. The short time data can be thought to be dominated by single-particle dynamics and since all eigenstates are delocalized in this region, the particles delocalize quickly, resulting in a vanishing imbalance. Upon tuning the disorder strength to even higher values, marked in ② with $2J < \Delta < 9J$, the $\tilde{\mathcal{I}}$ is non-zero and also decreases

from the short time value to the longer time value, showing that this region relaxes slowly. All the single-particle states are strongly localized for these disorder strengths, and the dynamics are frozen in the absence of interactions. Finally, upon increasing the strength of the disorder potential, we observe a large residual $\tilde{\mathcal{I}}$ and a negligible difference between the short and long time value of $\tilde{\mathcal{I}}$. This absence of relaxation on the observed timescale would indicate an MBL phase in the isolated limit. However, caution must be taken with this statement. It is fundamentally unknown if such a regime exists as a distinct phase in the thermodynamic sense or simply has extremely long relaxation timescales, see Appendix B.

To quantify the rate of relaxation of the system, the time evolution of $\tilde{\mathcal{I}}$ is fitted with $\tilde{\mathcal{I}} \sim t^{-\zeta \log(t)}$, and the extracted relaxation exponents ζ are shown in Fig. 9.5 B. The relaxation exponents are observed to continuously decrease showing slowing down of the relaxation with increasing disorder, until a critical disorder strength of $\Delta_c = 9J$ is reached, where the relaxation exponent appears to vanish completely. Following the observation in one dimension [77, 117], where this vanishing of the critical exponents indicates the emergence of an MBL phase in the isolated limit, this would indicate the appearance of an MBL phase in the isolated system limit in two dimensions. Near this critical disorder strength, a piecewise fit of $\zeta \propto \{|\Delta - \Delta_c|^\nu, 0\}$ in the restricted regime of $\Delta \in \{5, 12\}$ (solid lines) gives $\nu = 0.9$. However, as the regime where critical scaling is expected to hold is unknown, the critical exponent has an unknown uncertainty. Additionally, in the inset of the figure, the relaxation exponents are shown by taking zero coupling $\Gamma = 0$ in the analysis. Here also, the exponents decrease continuously and reach a constant offset at the same critical disorder strength $\Delta_c = 9J$. The offset is consistent with the background coupling effects, marked by the dashed black line. A significant ground for future work would be to understand this region with a controlled bath-like coupling [73, 76].

9.3.4 Role of interactions on the relaxation dynamics

In the absence of interactions $U = 0$, our system becomes separable along the two directions and is effectively a scalar product of the solutions along the two individual directions. This implies that both the x-direction and the y-direction get individually localized around $\Delta = 2J$ and remain uncoupled. This allows good characterization of the system in the non-interacting case, where numerical calculations are feasible. Afterward, the interacting Hamiltonian can be examined by tuning the magnetic field, which probes the full two-dimensional interacting system.

To check these expectations, we first load a single component gas and set the magnetic field such that the interaction strength is approximately zero. We fix the disorder strength to $\Delta = 5J$. For this disorder strength, we expect the system to be strongly localized with the single-particle localization length to be approximately a single site [72]. The imbalance is expected to saturate to a non-zero value in just a few tunneling times and show no further relaxation. This is indeed what we measure, as shown in Fig. 9.6. The plot also shows the atom numbers as a function of time, indicating that atom losses are negligible during these timescales.
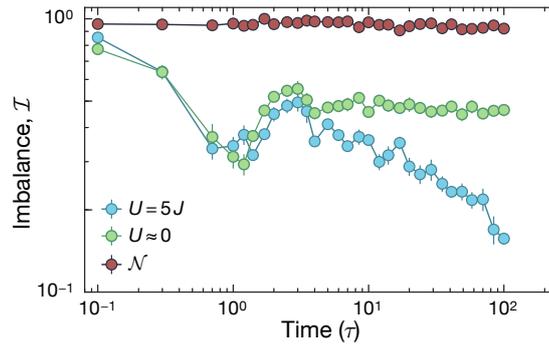
Figure 9.6: Time evolution in the interacting and the non-interacting Hamiltonians: The figure shows the time evolution of the imbalance at fixed disorder $\Delta = 5J$ with interaction $U = 5J$, and without interaction $U \approx 0$. While the non-interacting system is known to be localized and shows a plateau with no visible dynamics, the interacting Hamiltonian clearly exhibits slow relaxation. This demonstrates that the observed slow relaxation at intermediate disorders is inherently an interacting feature and absent in the non-interacting Hamiltonian. Each point is averaged over six individual experimental realizations, and error bars denote the error of the mean. Atom numbers, $\mathcal{N}$, are also shown as a function of time, showing that there are typically less than 10 % losses during the entire time evolution.

The time evolution of imbalance in the interacting case is also shown for comparison. At very short times ($\sim 1\,\tau$), the physics is dominated by single particle relaxation to nearest-neighbor sites, and the non-interacting and interacting data are close to each other. However, within a few tunneling times, interaction effects become clear, generating a slow relaxation only in the interacting case, showing that the observed relaxation is a clear feature of the interacting system in two dimensions.

To explore the thermalization rates as a function of interaction strength, the imbalance at an intermediate evolution time of $50\,\tau$ is shown for various disorders in Fig. 9.7 A. We observe that tuning from weak $U \sim 0$ to intermediate interactions $U \sim 5J$ significantly reduces the imbalance for intermediate disorder strengths. This trend stops upon further increasing the interactions $U > 10J$, where the imbalance approximately saturates and increases only by a small amount even for very strong interactions $U > 20J$. This is strikingly different to one dimension. There, the imbalance for infinite interaction strength is the same as the case of zero interaction strength in the absence of doublons because of an exact mapping between the two cases [72, 106]. On the other hand, in two dimensions, such a mapping does not exist and the system remains interacting even in the hard-core limit, as demonstrated in the experiment.

Finally, the impact of the energy density on the relaxation dynamics is shown in Fig. 9.7 B. The energy density of the initial state is changed by loading states with different doublon fractions: if the system is interacting, there is an energy cost associated with each doublon and hence, the energy density of the overall state depends on its doublon fraction. In Fig. 9.7 B, the imbalance after an intermediate evolution time of $50\,\tau$ is shown for a fixed disorder strength of $\Delta = 6J$ for two different doublon fractions: $D_i \approx 5\%$ and $D_i \approx 30\%$. These results can be divided into three distinct regimes:
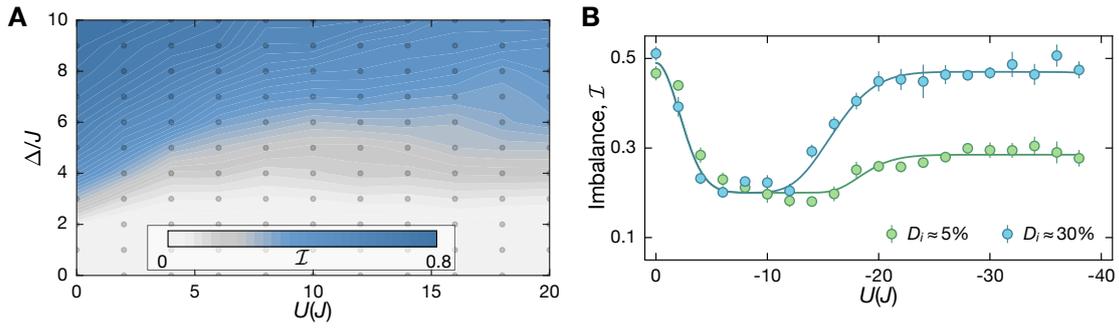
Figure 9.7: Interaction effect at intermediate evolution times, A: To see the effect of the interaction and the disorder strength, we plot the residual imbalance after an evolution time of $50\,\tau$. Generally, interactions tend to delocalize the system and disorder tends to cause localization. In contrast to one dimension, where the imbalance of the hard-core interacting system could be mapped to the non-interacting case, the imbalance for strong interactions in two dimensions is strikingly different from the non-interacting case. Experimental data are measured at the gray points. **Effect of the energy-density on the relaxation dynamics, B:** We show the imbalance for two different doublon fractions in the initial state of $D_i \approx 5\%, 30\%$ but at fixed disorder strength $\Delta = 6J$. Each point is an average of twelve individual experimental realizations. Solid lines are guides to the eye.

1. **Weak interactions, $U \lesssim 8J$:** The non-interacting case shows a large imbalance of about 0.5 and is strongly localized. Upon turning on the interactions, the separability of the system is broken and we observe that interactions tend to delocalize the system, a indicated by a sharp reduction in the imbalance. This trend is identical for both the initial states. This response is understandable because the energy density changes negligibly for weak interactions upon changing the doublon fraction by 30%. While qualitatively this trend is similar to the one-dimensional case as explained in Chapter 6, there is a vast difference in the quantitative amount of delocalization for weak interactions in two dimensions.

2. **Intermediate interactions, $8J \lesssim U \lesssim 16J$:** Upon increasing the strength of interactions, the imbalance does not decrease. In the absence of doublons, the imbalance plateaus. In contrast, the case with many doublons now shows an even higher imbalance since, at these interactions, doublons begin to act like new quasi-particles with much heavier weight.

3. **Strong interactions, $U > 16J$:** For strong interactions, one can observe two important behaviors. Firstly, in the case of almost no doublons, the strongly interacting system does not have the same imbalance as the non-interacting system but rather shows a strong delocalization effect even with hard-core interactions. This behavior is strikingly different compared to the one-dimensional case, where hard-core interactions were ineffective in causing any delocalization, as discussed in Chapter 6. Secondly, there is a vast difference between the imbalance of the two initial states. This is because we are probing very different energy densities and this has a clear impact on their relaxation dynamics. Beyond the bandwidth of two non-interacting particles

($\sim 16J$), the doublons effectively have a reduced mobility $J_D \approx J^2/U$ and hence, see higher effective disorder strength resulting in a larger imbalance. The case with 30% doublons happens to measure the same imbalance as the non-interacting case. In general, we expect that increasing the doublon fraction results in a larger imbalance, at least at intermediate times.

9.3.5 Conclusion

We have observed an extended regime of slow relaxation in two-dimensional quasi-periodic potentials. In this regime, the observed relaxation becomes extremely slow, even though the interactions, disorder and the single-particle bandwidth are all comparable to each other. After accounting for a weak coupling between multiple 2D planes, the relaxation is observed to vanish completely beyond a critical disorder strength. While our results already provide important benchmarks for theories of MBL in higher-dimensions, many important features of the critical regime remain to be explored. Isolating the system further would allow us to distinguish different forms of relaxations, and hence, identify the nature of the relaxation processes.

On the theoretical front, *if*, MBL indeed does not exist as a distinct *phase* in higher dimensions, it would be reminiscent of non-thermal integrable interacting systems, also known to exist only in one dimension. This would also imply that all interacting systems in higher dimensions thermalize. In practice, however, there will be an enormous separation of timescales of thermalization in MBL systems in comparison to other two-dimensional thermal systems. One simple case would be to consider the one-dimensional Fermi-Hubbard model which is non-thermal and integrable for all interactions [112]. This changes as soon as the corresponding two-dimensional model is constructed by coupling the one-dimensional systems. The resulting timescales for local thermalization are then of a few tunneling times [73]. This is very different from the way thermalization of two-dimensional "MBL" systems would happen, wherein the involved timescales would be colossal. This distinction necessarily separates the two kinds of systems.

Secondly, it is currently unclear what the central differences between quasi-periodic and real-random systems are. While real-random systems can support rare-regions from disorder, multiple recent studies have shown relaxation which appears qualitatively and quantitatively similar, even with deterministic potentials, such as quasi-periodic potentials [152, 200], and the reason behind this is currently unclear. We hope such interesting questions are resolved in future.

9.4 Discussions

9.4.1 Effect of "ergodic grains" in a localized bulk

One of the major obstacles with testing the possibility of an MBL phase in experiments in higher dimensions is the absence of a theory that describes the dynamics or explores the MBL transition in higher dimensions. One theory proposed by De Roeck and Huve-
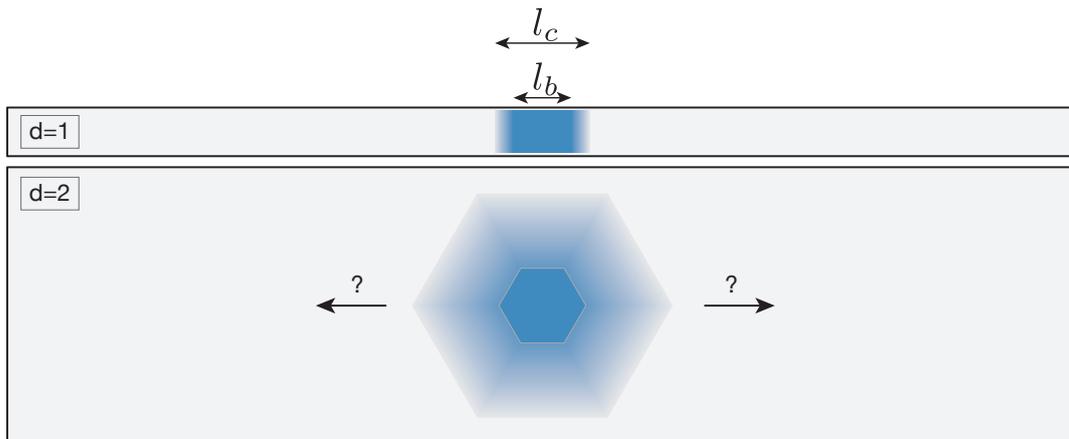
Figure 9.8: Effect of "ergodic" grains in an otherwise MBL "phase" in one and two dimensions: It is currently unclear whether MBL can occur in systems with true disorder in $d > 1$ as a distinct phase. The central argument against the existence of an MBL phase in $d = 2$ is the destabilizing mechanism of small ergodic grains (blue areas). These grains, however, are argued not to destabilize the MBL phase in one dimension. If these arguments are correct, then the delocalization *timescales* are predicted to be very long even for moderate disorder strengths. The fate of the system is unclear in two dimensions in the absence of real-random disorder (like in the current experiment). In the picture, l_b denotes a small ergodic grain, and l_c denotes the size of the region it can delocalize.

neers [194] argues that MBL can only exist as a phase in one dimension and only for interactions which decay faster than exponential. Their arguments are briefly described and extended to estimate the delocalization timescales using the microscopic parameters of the Hamiltonian. This is useful as it brings testability to the theory. To the best of my knowledge, these are unpublished calculations and hence, must be taken with caution. They are summarized here, see Appendix B for additional details.

We consider a spin model. The starting point is to locate a region in the space of linear size l_b with a low amount of disorder, as shown in Fig. 9.8. This can occur as the disorder is random and hence, there is a non-zero probability of finding such regions in a large system. We call this region an ergodic grain. Additionally, the rest of the spins are assumed to be perfectly localized [40].

The theory assumes that the grain is as ergodic as it can be and anything delocalized by the original grain will be completely amalgamated in the grain. While this assumption is crucial for obtaining the results, it is not entirely clear if this is indeed fully accurate, since a feedback from the MBL phase can also change the spectral properties of the system [201]. Nevertheless, assuming that the grain remains as ergodic as possible, upon interacting with the nearest spin, it can completely absorb it and half its level spacing. The coupling of this grain to the rest of the spins of the system is assumed to be decreasing exponentially with the distance. Naively, this process of absorption would continue indefinitely, completely delocalizing all the localized bits. However, this is not true in one dimension as the growth of the grain will be halted due to an exponential decrease of the

coupling. One can estimate the cut-off length scale l_c by equating the level space with the coupling. Assume that the level spacing of the grain is given by $\alpha = 2^{-l_b}$. Then,

$$\alpha/2^{l_c} = e^{-l_c/\xi} \tag{9.6}$$

where ξ is some localization length which is close to unity. This is because after absorbing l_c spins the grain's level spacing is reduced by 2^{l_c} but the coupling has also decreased. This leads to two competing scales, and after l_c exceeds a certain distance, the grain cannot delocalize the next bit. This distance is given by:

$$l_c = \frac{\log(2)}{\log(2) - 1/\xi} l_b \tag{9.7}$$

Note that there might be factors of 2 which are different here and in Ref. [194], because of how the length of the grain ($2l_b$ vs. l_b) is defined. Importantly, in $d = 2$, this grain will eventually always delocalize the whole system because the level spacing decreases super-exponentially as $2^{-l_c^2}$, while the coupling decreases exponentially. Hence, even a *single* grain can delocalize the entire system.

Obviously, it will take an infinite amount of time for a single grain to delocalize an infinite system. However, in a truly large system, one will have a *finite density* of these grains and hence, each grain only has to delocalize a small volume of the full system. To estimate the time it takes for the grain to do so, consider that all grains in a small area are within a small $\sim \delta \times \Delta$ energy spacing with each other and the size of the grain is l_b, where Δ is the overall strength of the disorder in the Hamiltonian. The probability for the existence of this grain is then given by $\sim (\delta)^{l_b^d}$ in d dimensions. Further, there will be a density of such regions ρ and hence, each of them only has to thermalize a finite region around them. The timescale of this thermalization is assumed to be exponential in the region size which it has to thermalize (since the coupling goes down exponentially). This region is roughly of size $1/\rho$. Hence, the time taken to delocalize the region around the grain is given by

$$\tau_{\text{deloc}} \sim e^{\frac{1}{d \times \xi} \delta^{l_b^{-d}}} \tag{9.8}$$

Note that the choice of l_b, δ and ξ are all dependent on d. This timescale is enormous and would be a very challenging task for the experiments to measure. To get a rough estimate of this, one can take the grain to be of a rather small length, $l_b = 3$, assume that the fluctuations of the disorder are $\delta = 0.2$ and $\xi = 1$. This evaluates to $\tau_{\text{deloc}} \approx e^{10^6} \tau$, where τ is the hopping time. One can see that this is extremely long.

These results are derived for real-random systems, which can contain such rare-regions of the underlying disorder, which might be absent in systems with deterministic disorders. The implications of this are unclear because the primary argument requires traveling only a linear distance l_c to gain l_c^{d-1} more atoms to obtain degeneracy still holds and the original proof might be generalizable to systems with deterministic disorders. However, a counter argument might be that in quasi-periodic systems there might not be any ergodic grain at all since there are no rare-regions and therefore, it might support an MBL phase. Answers to such questions are currently not known.
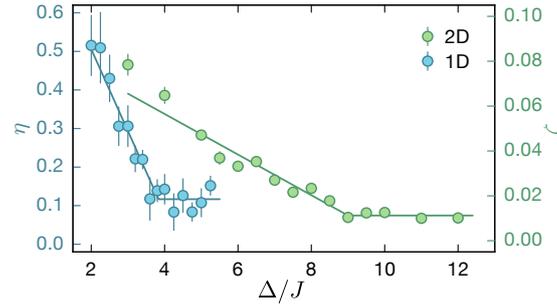
Figure 9.9: Relaxation exponents in one and two dimensions: We plot the relaxation exponents in one and two dimensions for comparison, highlighting the effect of dimensionality in delocalizing the system. η denotes the relaxation exponents extracted in one dimension from the imbalance relaxation of the form $\mathcal{I} \sim t^{-\eta}$ for fixed interaction $U = 4J$, as described in Ref. [77]. ζ denotes the relaxation exponents in two dimensions obtained from the imbalance relaxation of the form $\mathcal{I} \sim t^{-\zeta \log(t)}$ for a fixed interaction strength of $U = 5J$. Error bars denote the fit error, and solid lines are guides to the eye. The one-dimensional exponents approach an offset value at $\Delta_c^{1D} = 4J$, while in two dimensions this happens at a disorder strength of $\Delta_c^{2D} = 9J$. The localization transition for the single particle $\Delta_c^{U=0} = 2J$ is identical in both 1D and 2D.

9.4.2 Dimensionality effect on the relaxation dynamics

Higher dimensions provide additional delocalization routes and interaction partners, which can result in much faster delocalization, and perhaps an MBL phase can only exist for even larger disorder strengths. We can observe this effect of dimensionality by tuning the hopping along the y-direction to almost zero, thereby leaving only the hopping along the x-direction appreciable. This was reported in Ref. [77], and provides evidence for such slow dynamics also in one dimension. The crucial difference in one dimension is that the relaxation is expected to follow a power law $\mathcal{I} \sim t^{-\eta}$, where η is the relaxation exponent. A systematic comparison of the relaxation exponents between one and two dimensions is shown in Fig. 9.9, assuming $\Gamma = 0$ (i.e. no background calibration).

Here, one can see that the relaxation exponents approach the background value in one dimension at $\Delta_c^{1D} = 4J$, while in two dimensions they approach the background value at $\Delta_c^{2D} = 9J$. Hence, the two-dimensional system has a much larger critical disorder strength, even though the single particle localization strength $\Delta_c^{U=0} = 2J$ is identical in both cases. This highlights the role of dimensionality in the ensuing dynamics, since more interactions partners allow for additional delocalization, as compared to the one-dimensional system (since no additional paths for delocalization are created in the two-dimensional crossed quasi-periodic potentials).

9.4.3 Experimental sequence

After the preparation of an ultracold gas of a two component mixture of ^{40}K gas at a temperature of $T/T_F \approx 0.2$, where T_F is the Fermi temperature, we load them into deep lattices. These are $50\,E_r^{738\,\text{nm}}$ along the z-direction, $36\,E_r^{738\,\text{nm}}$ along the y-direction and $20\,E_r^{1064\,\text{nm}}$ along the x-direction. We add $20\,E_r^{532\,\text{nm}}$ of $532\,\text{nm}$ lattice along the x-direction
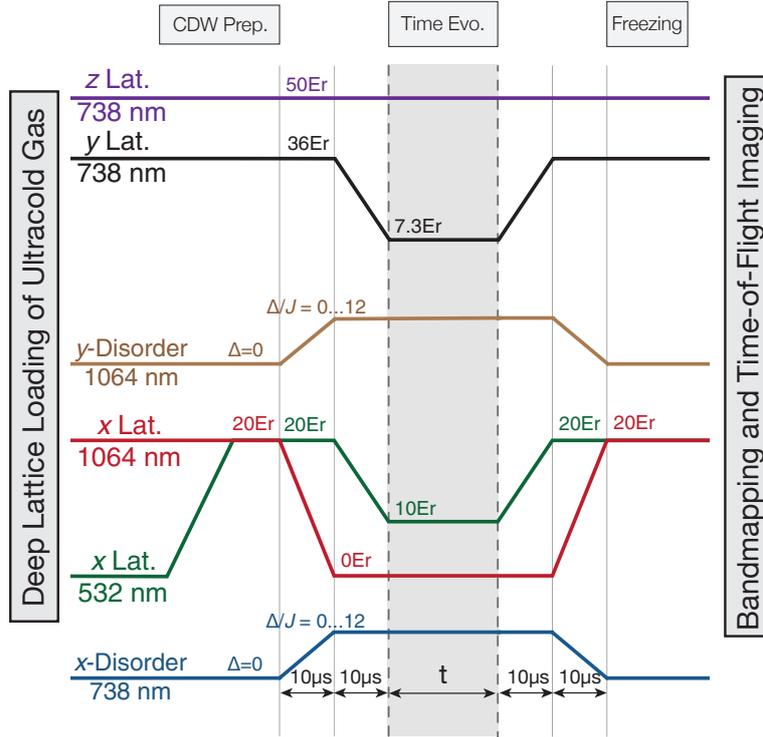
Figure 9.10: Experimental sequence: A schematic showing the lattice ramps after loading the ultracold atom cloud into deep lattices. Further details are provided in the main text.

with a phase difference of $\pi/3$ to the 1064 nm lattice. This finishes the preparation of the initial state with almost all atoms on the even stripes. A Feshbach resonance is utilized [140] to set the interaction strength U/J for the time of evolution. Additionally, we decrease the intensity of five lattice lasers: the 532 nm laser along the x-direction to $10\,E_r^{532\,nm}$, the 1064 nm lattice laser along the x-direction to $0\,E_r^{1064\,nm}$ and the 738 nm lattice laser along the y-direction to $7.3\,E_r^{738\,nm}$ and the disorder lasers along the two directions. Since the lattice lasers have difference wavelengths along the two directions, we choose their intensities so that the hopping J is the same along the x-direction and y-direction. At the same time, the disorder lasers along x-direction and y-direction are ramped to different intensities, so that we can obtain the same Δ/J along the two directions. A schematic of this is shown in Fig. 9.10. The conversion from the lattice depth and the recoil energy to the disorder strength is given by $\Delta/J = \alpha s_d$, where s_d is the depth of the respective disorder lattice in its recoil energy. The value of α in the x-direction is 11.11 and in the y-direction is 5.21. Further details on this are provided in Chapter 5 and Appendix A.

9.4.4   Coupling identical 2D planes

We investigate whether coupling the different two-dimensional planes can indeed cause a faster delocalization. We fix the disorder strength to $\Delta = 8J$ and the interaction to $U = 5J$, and the measure the imbalance after an evolution time of $\sim 50\,\tau$ for various
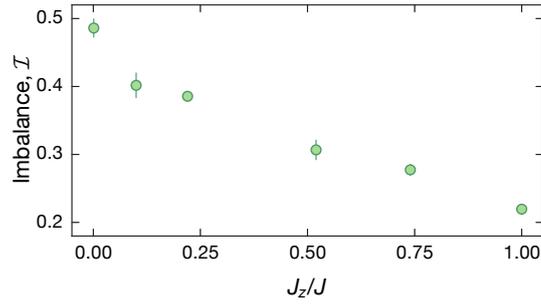
Figure 9.11: Coupling identical planes in two dimensions: To experimentally check that coupling along the z-direction can affect the dynamics along the plane, we measure the imbalance after an evolution time of $50\,\tau$ for fixed interaction strength of $U = 5J$ and disorder strength $\Delta = 8J$ as a function of different values of hopping along the z-direction, J_z. The smallest value is $J_z/J = 10^{-3}$. The figure shows that indeed hopping along the z-direction can delocalize the system faster. Each point is an average of nine individual experimental realizations and error bars denote the error of the mean.
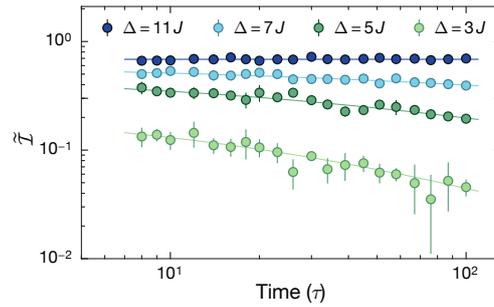
Figure 9.12: Closed-system imbalance $\widetilde{\mathcal{I}}$ time evolution: We plot the closed-system imbalance $\widetilde{\mathcal{I}}$ inferred from the time traces in Fig. 9.2. The slight bending on a log-log plot supports the fact that system relaxes slightly faster than power-law as described in the main text. Solid lines are fits.

hopping strengths along the z-direction. This is shown in Fig. 9.11. Note that this is not the *lifetime* measurement as done in Chapter 7. We observe that increasing the hopping along the z-direction indeed results in a lower imbalance, indicating faster delocalization.

9.4.5   Closed-system imbalance time evolution

The coherent imbalance $\tilde{\mathcal{I}}$ is plotted as a function of evolution time on a log-log plot as shown in Fig. 9.12. This is deduced from the time traces in Fig. 9.2 by assuming a coupling constant of $\Gamma = \Gamma_{\text{exp}}$ as previously described. We observe that the relaxation is slightly faster than a power law, and supports the logarithmic correction in two dimensions.

9.4.6   Relative relaxation rates from power-law fits in $d = 1, 2$

Our system allows a direct comparison between the rate of relaxation between the one and two dimensions. To show this, the relaxation exponents from the same power-law fit $\sim t^{-\eta}$ are shown in Fig. 9.13. While these power law fits describe the behavior suboptimally (about 40% worse on a χ^2 test as compared to the ones described earlier), they are nevertheless useful to make a direct comparison between the two cases. The relaxation exponents shown in Fig. 9.13 should be interpreted as the relative rates of relaxation. This also shows that the two-dimensional system has higher relaxation rates, which is attributed to the greater number of interaction partners. Further, as far as localization is concerned, except for a renormalized critical disorder strength, the system appears as localized in two dimensions as it does in one dimension. The critical disorder strength remains the same even with this power-law fit, $\Delta_c^{2D} = 9 J$, demonstrating that the experimental results are not fine tuned and are largely model independent.
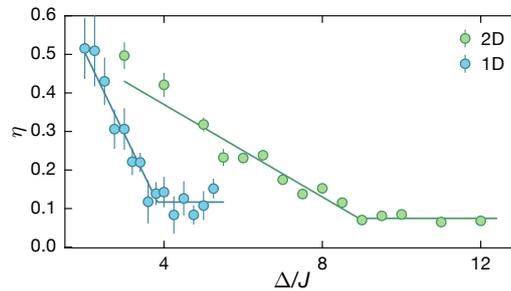
Figure 9.13: Relative relaxation rate in $d = 1, 2$**:** To capture a relative relaxation rate in one and two dimensions, we fit the time traces in Fig. 9.2 with a power-law type relaxation, $\sim t^{-\eta}$. This allows a direct comparison with the exponents in one dimension. The plot shows that except for the renormalized disorder strength, MBL in $d = 2$ appears as much accurate as MBL in $d = 1$. Further, the critical point in 2D is obtained at the same disorder strength as in the main text, demonstrating that its extraction is not fine tuned. Error bars denote the fit error, and solid lines are guides to the eye. The data for the one-dimensional case is taken from Ref. [77].

Quantum Dynamics in Localized Systems

While the defining property of MBL is the survival of localization in interacting systems at finite energy-densities [21, 104, 202], many additional features in such an MBL phase were discovered. In particular, even when the system is perfectly localized, with no dynamics visible in the time evolution of observables such as the imbalance, quantities such as entanglement entropy were found to exhibit an unbounded growth [119]. Surprisingly, this growth was only visible in the interacting phase, and was present despite any mass transport of classical quantities, Fig. 4.4. Such a growth was then phenomenologically explained via effects stemming weak dephasing due to interactions [127, 128]. Having access to such an observable, especially in two dimensions, can, therefore, reveal insights into the ensuing dynamics invisible to transport. However, it has proven hard to measure such a quantity, except in small systems ($N < 10$) [203], as it requires either full tomography of the system [78] or multiple identical copies [203]. Recently, an out-of-time-ordered correlation function (OTOC) was proposed to capture similar behavior like an entanglement entropy and argued to be able to distinguish between the quantum dynamics in the Anderson-localized case and the many-body localized phase [204–207].

An OTOC provides an estimate of scrambling of two operators which initially commute, but over time stop to commute due to the time evolution generated by the Hamiltonian. To illustrate these properties, we consider the XXZ Hamiltonian, $\hat{H}$ in the MBL $J_z > 0$ or the AL $J_z = 0$ case. Let $\hat{U} = e^{-i\hat{H}t}$ be the evolution unitary. The initial state is the Néel state $|\phi\rangle = |... \uparrow\downarrow\uparrow\downarrow ...\rangle$. Let the operators whose commutation we want to probe be $\hat{V} = \hat{X}_1$ and $\hat{W} = \hat{X}_8$, where $\hat{X}_i$ is the x-Pauli matrix for a spin $1/2$ particle on site i. Further, let $\hat{V}_t$ and $\hat{W}_t$ be their corresponding Heisenberg operators. The OTOC is defined as:

$$\text{OTOC} = \langle\phi|\hat{W}_t^\dagger\hat{V}^\dagger\hat{W}_t V|\phi\rangle \tag{10.1}$$

Physically, this implies that one perturbs the system at a site $i = 1$ and lets the perturbation grow, and perturbs again at a site $i = 8$, at a later time t. The time evolution is then reversed with the opposite order of the operators and the overlap with the original state is calculated. These operations in the forward and backward time evolution commute at zero time. Hence, the OTOC is unity at zero times. However, as the perturbations propagate, the original operators do not commute anymore, since the effect of a perturbation from one site reaches the other and only a reversal of the time can no longer be expected to undo the time evolution. This makes the OTOC decay. Experimentally measuring this generically seems very hard as well, since it requires having *two* identical copies of the
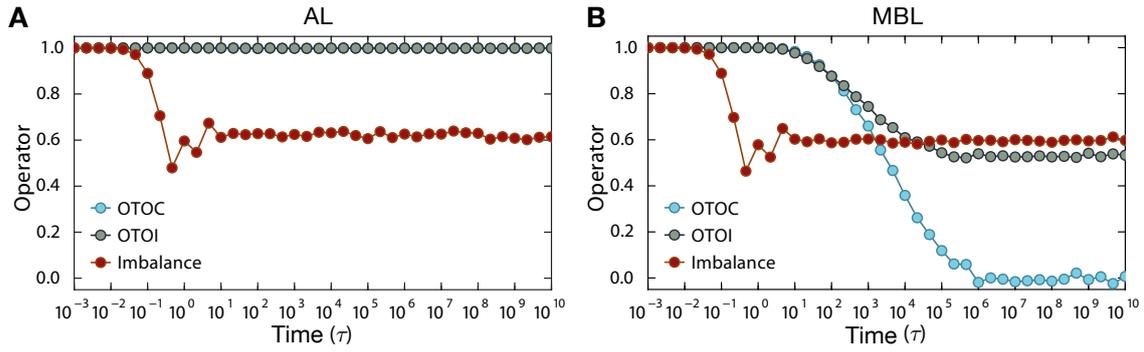
Figure 10.1: Ordered vs. out-of-time ordered measurements: We show the evolution of the normal imbalance, an OTOC and an OTOI for(**A**) an AL system and for (**B**) an MBL system. Like an OTOC, an OTOI can also capture the quantum dynamics invisible to normal imbalance. The simulations are performed for the XXZ Hamiltonian, with $L = 8$, $J_\perp = 1$, $\Delta = 4$. For the AL case, $J_z = 0$ and for the MBL case, $J_z = 0.2$.

system or a carefully chosen initial state [208]. This is because after applying the sequence of operators $W_t^\dagger V^\dagger W_t V$ on the initial state of the system $|\phi\rangle$ the system is in a state $|\psi\rangle = W_t^\dagger V^\dagger W_t V |\phi\rangle$ and an overlap with the initial state is required. However, one can make a small modification, by measuring the spin-imbalance in the final state. We call this an out-of-time ordered imbalance (OTOI) since it requires only one copy of the system and an expectation value of a simple observable in the final state.

$$\text{OTOI} = \langle\psi|\mathcal{I}|\psi\rangle \qquad (10.2)$$

i.e. one can apply the sequence of operations and just measure the imbalance in the final system. To show that such an OTOC/OTOI can indeed capture the behavior and show the different dynamics in the AL and the MBL cases, we show their time evolution in Fig. 10.1. In Fig. 10.1 **A**, one sees that in the AL phase, the normal imbalance, an OTOC and an OTOI show the same behavior. After a few tunneling times, they saturate and show no further dynamics. In contrast, in the MBL phase, shown in Fig. 10.1 **A**, while the normal imbalance saturates, the OTOC/OTOI continue to show the quantum dynamics to extremely long times. While an OTOI appears to be easier measurable than OTOC as it does not require two copies of the system, it is still a challenging task, as it also required the reversal of the sign of the Hamiltonian (to implement time-reversal). But perhaps with a Feshbach resonance [140] (allowing $U \to -U$), disorder phase control [72] (giving $\cos(2\pi\beta i + \phi) \to -\cos(2\pi\beta i + \phi)$) and lattice phase modulation [209] (changing $J \to -J$), it might be possible to measure such quantum dynamics in the near future via an OTOI.

Conclusions and outlook

The goal of this thesis was to introduce how ultracold atoms can be utilized to probe many-body (and single particle) disordered systems via monitoring the relaxation dynamics of a far-from-equilibrium state. Within this context, we designed new experimental setups and observables. We probed the effect of localization, controlled bath-like coupling and higher dimensions, unveiling several genuinely new regimes.

The initial chapters introduced the theories that underline the experimental studies. We presented them in a manner useful for developing an intuition for the experiments and, hence, they were described more by their features and the experimental implications and less by their formal mathematics. Chapter 2 described thermalization in isolated quantum systems, focusing on the aspect of the loss of the memory of the initial conditions. Chapter 3 introduced the concept of localization of single-particle eigenstates, which has direct implications on the dynamics of the expansion and the imbalance. This was generalized to many-body localization in Chapter 4 wherein, despite interactions, thermalization breaks down. This could be captured from the even-odd imbalance. To finish the introduction, we described the experimental components required to realize many-body disordered systems with interacting fermions in optical lattices, in Chapter 5.

Having introduced the necessary background, Chapter 6 presented the results on MBL in one dimension and demonstrated the effects of interactions, energy-density, and disorder on the ensuing dynamics. We inferred this by monitoring the relaxation of a high-energy-density state, which revealed a drastic departure from ergodic behavior. Deep in the MBL phase, the results in one dimension were further shown to be quantitatively and qualitatively well captured by high-performance numerical simulations based on Matrix product states [210]. Hence, the experiment was set to stand at an excellent starting point for exploring regimes not accessible to numerical simulations.

The effects of the environment on the experimental system were explored in Chapter 7, leading to several striking observations. Firstly, it provided a technical way to explore a *controlled* bath-like coupling, which could be understood as a dephasing mechanism, systematically uncovering the effect of external bath-like coupling in regimes where numerical simulations were not possible. Secondly, we found that even non-thermal systems can act as a collective bath for each other and provided a valuable tool to distinguish interacting non-thermal systems like MBL systems from non-interacting, non-thermal systems such as AL systems.

Next, Chapter 8 explored the regime of periodically driven systems, also known as Floquet systems. While the conventional wisdom would suggest that such systems should heat up to an infinite temperature featureless state, the experiment retained a memory of the initial state, even for highly non-perturbative drives. Moreover, a new regime was found, which was realized to be unexpectedly stable for all drive frequencies. These results demonstrated the possibility of creating novel driven phases of matter.

We probe the two-dimensional case in Chapter 9. We observed an extended regime of slow relaxation in which the single-particle bandwidth, the interaction strength, and the disorder strength were all comparable to each other. The results demonstrated a clear interplay of dimensionality, interactions, and disorder. The experimental results revealed regimes and dynamics, not readily available to classical numerical simulations.

Outlook

A variety of numerical and analytical techniques have been developed to address the questions of thermalization and localization in isolated quantum systems. These include perturbative calculations [21], numerical methods such as exact-diagonalization, matrix-product-state calculations and Krylov-space techniques [118], adapted renormalization group (RG) analysis [23, 29, 30] and formal mathematical works [40, 143, 202]. At the same time, experiments have revealed dynamics in regimes difficult to access using above techniques, thus complementing theoretical results. These regimes include relaxation in higher dimensions [75, 198], bath-like effects [73, 76] and dynamics close to possible MBL transition points [75, 77]. The techniques and methods developed and utilized in this thesis should also be useful for understanding many other systems, such as relaxation due to external mechanisms in dipolar [211] and Coulomb [212] interacting systems. In addition to such exciting results, several intriguing future directions can be pointed out:

- The mechanism(s) of relaxation in $d = 1, 2, 3$: Probing the non-dissipative dynamics to even longer times in the experiments could reveal many important features, including stronger bounds on relaxation behavior and the microscopic mechanisms of relaxation. These could also allow us to address the interplay of spin and charge sectors and on the role of resonances such as due to the SU(2) symmetry and plaquette resonances on charge delocalization in one and two dimensions [75, 153, 213]. Additionally, it should also be possible to probe the dynamics in three dimensions and investigate the role of dimensionality.

- The critical region and configurational vs. quenched Griffith-type effects: An interesting question would be to compare and contrast the nature of slow relaxation approaching the MBL critical point when the underlying disorder is truly random instead of quasi-periodic [152]. This should reveal the different kinds of relaxation that control the regions on the ergodic side of the transition and the change in transport properties upon approaching the MBL transition [214].

- Quantum dynamics in the absence of transport: While the entanglement entropy has been measured in small systems [203], and has been shown to reveal additional

information on the dynamics, it would be exciting to probe such an observable in an experiment with a large number of particles. One way to do this might be to use the idea of out-of-time ordered measurements, which has been shown to capture such behavior [204–207].

- Mixing localized and delocalized states: In an experiment with single-site resolution, one can design a region of low disorder in the system to probe the delocalizing effects of an ergodic grain. Such a scenario and similar questions on the fate of a quantum system with localized and delocalized regions [215–219] are poorly understood. Furthermore, these are closely related to the idea of the many-body localization proximity effect [220], whereby an MBL system can not only be robust against a small bath but can even destroy it.

- MBL-SSB and protection of topologically-ordered Floquet states: Several Floquet-MBL studies have shown the possibility of realizing novel phases of matter based on symmetry-breaking and disorder can be used to protect these systems from heating [176–182], as demonstrated in Chapter 8. Such protection can be useful as many of the topological phenomena observed in ultracold atoms require an effective Floquet-Hamiltonian which always shows heating [169–175]. An interesting case would be to use disorder to protect ultracold atoms from heating up due to the drive, but at the same time utilizing the drive to transform the system to a topologically non-trivial state.

The list of such exciting regimes is currently exploding, and in many ways, experiments are beginning to investigate them. I hope in the coming times, many of these new areas will be explored and at the same time, many of the incomplete stories of this thesis will be further developed.

Relation between lattice depths and Hamiltonian parameters

Tunneling matrix element, J

The hopping strength can be evaluated by calculating the Wannier function overlap between a single site and its neighbor [221], which for our system was reported in Ref. [136]. Such functions form a basis in the real-space and hence, form a useful basis for calculating the onsite interaction strength, the disorder strength and the tunneling matrix element in our system. For this thesis, we only need to consider the lowest band, and hence, each Wannier state can be labeled with a single index, $w_i(x)$. This allows the calculation of the hopping J between two sites i, j. For the lattices used in this thesis, only the hopping between the nearest-neighbor sites is appreciable, and its tunneling matrix element can be calculated as:

$$J = \int dx \, w_i^*(x) \left(-\frac{\hbar^2}{2m} \frac{\partial^2}{\partial x^2} + V_{\text{latt}}(x) \right) w_{i+1}(x) \tag{A.1}$$

where, x is the directional coordinate along which the hopping has to be calculated, m is the mass of ^{40}K and V_{text} is the optical lattice potential. J decreases strongly ($\sim$ exponentially [44]) with the lattice depth. The important values of the tunneling matrix element J and the corresponding hopping time τ, employed in the various experiments are as follows:

Lattice Wavelength (nm)	Lattice Depth	J/h(Hz)	$\tau = h/(2\pi J)$ (ms)	Chapter
532	$8\,E_{\text{r}}^{532\,\text{nm}}$	550	0.293	6,7,8
738	$5.4\,E_{\text{r}}^{738\,\text{nm}}$	550	0.293	7
532	$10\,E_{\text{r}}^{532\,\text{nm}}$	330	0.5	9
738	$7.3\,E_{\text{r}}^{738\,\text{nm}}$	330	0.5	9
738	$36\,E_{\text{r}}^{738\,\text{nm}}$	1.72	90	6,7
738	$45\,E_{\text{r}}^{738\,\text{nm}}$	0.5	320	7,8

Interaction strength, U

Interactions between ^{40}K spins are point-like. Hence, two particles of opposite spin must be on the same site to have appreciable interaction strength. Using the Wannier functions, the interaction strength can be calculated as:

$$U = \frac{4\pi\hbar^2 a}{m} \int d^3\mathbf{r}\, |w(\mathbf{r})|^4 \tag{A.2}$$

where, a is the scattering length, controllable via a Feshbach resonance [140]. Unlike the hopping, this depends on the full overlap along the three directions and hence requires the three-dimensional coordinate $\mathbf{r}$ and the corresponding Wannier functions. The interactions decrease upon decreasing the depth of the lattice since the width of the Wannier functions increases, and hence their overlap on a given site decreases. When the hopping along the y-direction was continuously changed in Chapter 7, the scattering length was also continuously changed to maintain the same interaction strength.

Disorder strength, Δ

The calculation of the disorder strength holds under the approximation of a large main-lattice depth and small disorder-lattice depth [222]. The disorder strength Δ depends on *both* the depth of the primary lattice, $V_p = s_p E_{\mathrm{r}}^{p\,\mathrm{nm}}$ with wavelength $\lambda_p = 2\pi/k_p$ and the depth of the disorder lattice $V_d = s_d E_{\mathrm{r}}^{d\,\mathrm{nm}}$. Further, it depends on the ratio of the main to primary lattice wavelength $\beta = \lambda_p/\lambda_d$. It can be calculated as:

$$\Delta = \frac{s_d \beta^2}{2} k_p E_{\mathrm{r}}^{p} \int dx \cos(2\beta k_p x |w(k_p x)|^2) \tag{A.3}$$

Typically, the disorder lattice is about $0.5\,E_{\mathrm{r}}^{d\,\mathrm{nm}}$ and the main lattice is about 8-10 $E_{\mathrm{r}}^{p\,\mathrm{nm}}$. Some exemplary values are shown below, along with the effective disorder then produce for $1\,E_{\mathrm{r}}^{\mathrm{nm}}$ of the disorder lattice depth:

Main Lattice Depth	J/h (Hz)	Disorder Lattice Depth	Δ/J	Chapter
$8\,E_{\mathrm{r}}^{532\,\mathrm{nm}}$	550	$1\,E_{\mathrm{r}}^{738\,\mathrm{nm}}$	6.7	6,7,8
$10\,E_{\mathrm{r}}^{532\,\mathrm{nm}}$	330	$1\,E_{\mathrm{r}}^{738\,\mathrm{nm}}$	11.0	9
$7.3\,E_{\mathrm{r}}^{738\,\mathrm{nm}}$	330	$1\,E_{\mathrm{r}}^{1064\,\mathrm{nm}}$	5.2	9

Delocalization due to an ergodic grain in 2D

In this section, we calculate the timescales at which an ergodic bubble can delocalize an MBL system in two dimensions. I thank W. D. Roeck for discussions on these calculations. The central ideas are taken from Ref. [194]. There can exist small areas, called ergodic grains, in a large system which are delocalized in the small region, e.g. due to anomalously low disorder in that region. In higher dimensions, $d > 1$, these regions then can grow indefinitely and delocalize the entire system. A single grain will naturally require an infinite amount of time to delocalize an infinite system, $\lim_{L\to\infty} L^d$. However, in a truly large system, a finite density ρ of such regions will exist. Each of these delocalized regions has to then delocalize a region roughly of a size l_c^d. The sum of all these regions can then tile the entire system, see Fig. B.1. In such a case, in finite time, each grain would have delocalized a part of the system but together they would delocalize the entire system. In this section, we would like to estimate the timescales of such a case, according to the theory of Ref. [194].

First, the grain has to be ergodic, and for this, the effective disorder in this grain has to be small enough. Let the disorder Δ of the Hamiltonian be extremely large, so that all the single-particle states have a small localization length ξ. Due to the random nature of the onsite energies, there can exist a region of size l_b, which has a much smaller effective disorder, $\delta \times \Delta$, such that $\delta \ll 1$. The probability of finding such grains will be exponentially small in its volume:

$$p = (\delta)^{l_b^d} \tag{B.1}$$

Further, the density of such grains will be given approximately by the inverse of the volume of the average region it has to delocalize:

$$\rho = (1/l_c)^d \implies l_c = (1/\rho)^{1/d} \tag{B.2}$$

Moreover, the density of the grain is just the inverse probability of their occurrence,

$$1/\rho = \delta^{l_b^d} \tag{B.3}$$

To delocalize the entire system, the gain must grow to delocalize a region of size l_c^d. We assume that this will take exponentially long in the region length and the coupling decreases exponentially with the distance divided by the non-interacting localization length:
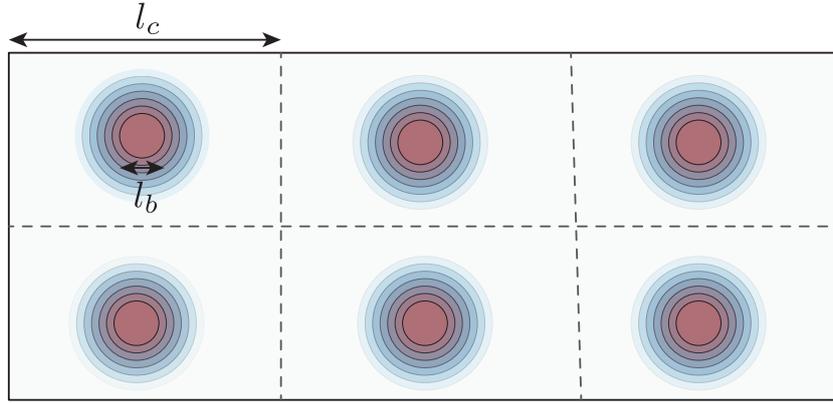
Figure B.1: Ergodic grain delocalization in two-dimensions: Schematic for an ergodic gain of size l_b (brown) growing (to fading blue) and delocalizing a finite region of size $l_c \gg l_b$. The regions of size $l_c \times l_c$ tile the entire system of size $L \times L$, and each of these regions contain one ergodic grain. The resulting timescales of delocalization are finite, but can be enormously large, exceeding the lifetimes of the universe by several orders of magnitude.

$$\tau_{\text{deloc}} = e^{l_c/\xi} \tag{B.4}$$

Together, these assumptions lead to the following timescale of delocalization:

$$\tau_{\text{deloc}} = e^{\frac{\left[\delta\left(l_b\right)^d\right]^{1/d}}{\xi}} = e^{\frac{1}{d \times \xi}\delta^{l_b^{-d}}} \tag{B.5}$$

In order to get an estimate this, one needs to assume some basic scales of the system, the hardest of which is the estimation the grain length, l_b. For one estimate, we take it to be rather small, with the grain length of three sites. We will see, that even this gives enormous timescales. In two dimensions, a rather conservative estimate would be:

$$d = 2, \xi = 1.0, \delta = 0.2, l_b = 3 \tag{B.6}$$

Plugging these number results in:

$$\tau_{\text{deloc}} = e^{1000000}\,\tau \tag{B.7}$$

where, $\tau = 300\,\mu\text{s}$ is the hopping times. For comparison, we can compute the lifetime of the universe:

$$\tau_{\text{universe}} \approx 10\,\text{billion years} \approx e^{50}\,\tau \tag{B.8}$$

Hence, within this theory of delocalization, for experiments, two-dimensional MBL can be treated exactly like a phase with infinite lifetimes, since its lifetime exceeds the lifetime of the universe by several orders of magnitude. In reality, the lifetime of the system would be governed by other factors, such as coupling to the environment.

References

[1] P. W. Anderson. *More Is Different*. Science **177**, 393–396 (1972). Referenced on page: 1

[2] H. Kamerlingh Onnes. *Further experiments with liquid helium. G. On the electrical resistance of pure metals, etc. VI. On the sudden change in the rate at which the resistance of mercury disappears*. Comm. Phys. Lab. Univ. Leiden **No. 124c** (1911). Referenced on page: 1

[3] P. Kapitza. *Viscosity of Liquid Helium Below the lambda-Point*. Nature **141**, 74 (1938). Referenced on page: 1

[4] J. F. Allen and A. D. Misener. *Flow of Liquid Helium II*. Nature **142**, 643 (1938). Referenced on page: 1

[5] D. D. Osheroff, R. C. Richardson, and D. M. Lee. *Evidence for a New Phase of Solid He^3*. Phys. Rev. Lett. **28**, 885–888 (1972). Referenced on page: 1

[6] K. v. Klitzing, G. Dorda, and M. Pepper. *New Method for High-Accuracy Determination of the Fine-Structure Constant Based on Quantized Hall Resistance*. Phys. Rev. Lett. **45**, 494–497 (1980). Referenced on page: 1

[7] D. C. Tsui, H. L. Stormer, and A. C. Gossard. *Two-Dimensional Magnetotransport in the Extreme Quantum Limit*. Phys. Rev. Lett. **48**, 1559–1562 (1982). Referenced on pages: 1, 25

[8] M. H. Anderson, J. R. Ensher, M. R. Matthews, C. E. Wieman, and E. A. Cornell. *Observation of Bose-Einstein Condensation in a Dilute Atomic Vapor*. Science **269**, 198–201 (1995). Referenced on page: 1

[9] K. B. Davis, M. O. Mewes, M. R. Andrews, N. J. van Druten, D. S. Durfee, D. M. Kurn, and W. Ketterle. *Bose-Einstein Condensation in a Gas of Sodium Atoms*. Phys. Rev. Lett. **75**, 3969–3973 (1995). Referenced on page: 1

[10] C. C. Bradley, C. A. Sackett, J. J. Tollett, and R. G. Hulet. *Evidence of Bose-Einstein Condensation in an Atomic Gas with Attractive Interactions [Phys. Rev. Lett. 75, 1687 (1995)]*. Phys. Rev. Lett. **79**, 1170–1170 (1997). Referenced on page: 1

[11] P. W. Anderson. *Basic Notions in Condensed Matter Physics*. Westview Press, Boulder, CO (1997). Referenced on page: 1

[12] M. Z. Hasan and C. L. Kane. *Colloquium: Topological insulators*. Rev. Mod. Phys. **82**, 3045–3067 (2010). Referenced on page: 1

[13] X.-L. Qi and S.-C. Zhang. *Topological insulators and superconductors*. Rev. Mod. Phys. **83**, 1057–1110 (2011). Referenced on page: 1

[14] X.-G. Wen. *Topological Order: From Long-Range Entangled Quantum Matter to a Unified Origin of Light and Electrons*. ISRN Condensed Matter Physics **2013**, 198710 (2013). Referenced on page: 1

[15] P. C. Hohenberg. *Existence of Long-Range Order in One and Two Dimensions*. Phys. Rev. **158**, 383–386 (1967). Referenced on page: 1

[16] N. D. Mermin and H. Wagner. *Absence of Ferromagnetism or Antiferromagnetism in One- or Two-Dimensional Isotropic Heisenberg Models*. Phys. Rev. Lett. **17**, 1133–1136 (1966). Referenced on page: 1

[17] S. Coleman. *There are no Goldstone bosons in two dimensions*. Comm. Math. Phys. **31**, 259–264 (1973). Referenced on page: 1

[18] S. Sachdev. *Quantum Phase Transitions, Second Edition*. Cambridge University press (2011). Referenced on pages: 1, 2

[19] S. L. Sondhi, S. M. Girvin, J. P. Carini, and D. Shahar. *Continuous quantum phase transitions*. Rev. Mod. Phys. **69**, 315–333 (1997). Referenced on page: 1

[20] M. P. A. Fisher, P. B. Weichman, G. Grinstein, and D. S. Fisher. *Boson localization and the superfluid-insulator transition*. Phys. Rev. B **40**, 546–570 (1989). Referenced on pages: 1, 60

[21] D. Basko, I. Aleiner, and B. Altshuler. *Metal-insulator transition in a weakly interacting many-electron system with localized single-particle states*. Ann. Phys. **321**, 1126 – 1205 (2006). Referenced on pages: 1, 2, 27, 30, 45, 50, 107, 110

[22] R. Nandkishore and D. A. Huse. *Many-Body Localization and Thermalization in Quantum Statistical Mechanics*. Annu. Rev. Condens. Matter Phys. **6**, 15–38 (2015). Referenced on pages: 1, 2, 28, 29, 59, 89

[23] E. Altman and R. Vosk. *Universal Dynamics and Renormalization in Many-Body-Localized Systems*. Annu. Rev. Condens. Matter Phys. **6**, 383–409 (2015). Referenced on pages: 1, 2, 28, 89, 110

[24] P. W. Anderson. *Absence of Diffusion in Certain Random Lattices*. Phys. Rev. **109**, 1492–1505 (1958). Referenced on pages: 1, 4, 15, 17, 27

[25] D. A. Huse, R. Nandkishore, V. Oganesyan, A. Pal, and S. L. Sondhi. *Localization-protected quantum order*. Phys. Rev. B **88**, 014206 (2013). Referenced on page: 2

[26] A. Chandran, V. Khemani, C. R. Laumann, and S. L. Sondhi. *Many-body localization and symmetry-protected topological order*. Phys. Rev. B **89**, 144201 (2014). Referenced on page: 2

[27] Y. Bahri, R. Vosk, E. Altman, and A. Vishwanath. *Localization and topology protected quantum coherence at the edge of hot matter*. Nat. Commun. **6**, 7341 EP – (2015). Referenced on page: 2

[28] A. Pal and D. A. Huse. *Many-body localization phase transition*. Phys. Rev. B **82**, 174411 (2010). Referenced on pages: 2, 31, 89

[29] R. Vosk, D. A. Huse, and E. Altman. *Theory of the Many-Body Localization Transition in One-Dimensional Systems*. Phys. Rev. X **5**, 031032 (2015). Referenced on pages: 2, 89, 110

[30] A. C. Potter, R. Vasseur, and S. A. Parameswaran. *Universal Properties of Many-Body Delocalization Transitions*. Phys. Rev. X **5**, 031033 (2015). Referenced on pages: 2, 89, 93, 110

[31] L. Zhang, B. Zhao, T. Devakul, and D. A. Huse. *Many-body localization phase transition: A simplified strong-randomness approximate renormalization group*. Phys. Rev. B **93**, 224201 (2016). Referenced on pages: 2, 89

[32] P. T. Dumitrescu, R. Vasseur, and A. C. Potter. *Scaling Theory of Entanglement at the Many-Body Localization Transition*. (2017). arXiv:1701.04827. Referenced on pages: 2, 89

[33] M. Serbyn, Z. Papić, and D. A. Abanin. *Criterion for Many-Body Localization-Delocalization Phase Transition*. Phys. Rev. X **5**, 041047 (2015). Referenced on pages: 2, 89

[34] T. Devakul and R. R. P. Singh. *Early Breakdown of Area-Law Entanglement at the Many-Body Delocalization Transition*. Phys. Rev. Lett. **115**, 187201 (2015). Referenced on pages: 2, 89

[35] E. J. Torres-Herrera and L. F. Santos. *Dynamics at the many-body localization transition*. Phys. Rev. B **92**, 014208 (2015). Referenced on pages: 2, 89

[36] M. Serbyn and J. E. Moore. *Spectral statistics across the many-body localization transition*. Phys. Rev. B **93**, 041424 (2016). Referenced on pages: 2, 89

[37] X. Yu, D. J. Luitz, and B. K. Clark. *Bimodal entanglement entropy distribution in the many-body localization transition*. Phys. Rev. B **94**, 184202 (2016). Referenced on pages: 2, 89

[38] D. J. Luitz and Y. Bar Lev. *Anomalous Thermalization in Ergodic Systems*. Phys. Rev. Lett. **117**, 170404 (2016). Referenced on pages: 2, 33

[39] J. Lux, J. Müller, A. Mitra, and A. Rosch. *Hydrodynamic long-time tails after a quantum quench*. Phys. Rev. A **89**, 053608 (2014). Referenced on pages: 2, 13, 45

[40] J. Z. Imbrie, V. Ros, and A. Scardicchio. *Review: Local Integrals of Motion in Many-Body Localized systems*. (2016). arXiv:1609.08076. Referenced on pages: 2, 28, 33, 89, 101, 110

[41] T. Grover. *Certain General Constraints on the Many-Body Localization Transition* (2014). arXiv:1405.1471. Referenced on pages: 2, 34, 89

[42] V. Khemani, S. P. Lim, D. N. Sheng, and D. A. Huse. *Critical Properties of the Many-Body Localization Transition*. Phys. Rev. X **7**, 021013 (2017). Referenced on pages: 2, 34, 89, 93

[43] N. F. Mott. *Conduction in non-crystalline systems*. Philos. Mag. **17**, 1259–1268 (1968). Referenced on pages: 2, 27

[44] I. Bloch, J. Dalibard, and W. Zwerger. *Many-body physics with ultracold gases*. Rev. Mod. Phys. **80**, 885–964 (2008). Referenced on pages: 2, 113

[45] C. Nayak, S. H. Simon, A. Stern, M. Freedman, and S. Das Sarma. *Non-Abelian anyons and topological quantum computation*. Rev. Mod. Phys. **80**, 1083–1159 (2008). Referenced on page: 2

[46] Z.-L. Xiang, S. Ashhab, J. Q. You, and F. Nori. *Hybrid quantum circuits: Superconducting circuits interacting with other quantum systems*. Rev. Mod. Phys. **85**, 623–653 (2013). Referenced on page: 2

[47] M. W. Doherty, N. B. Manson, P. Delaney, F. Jelezko, J. Wrachtrup, and L. C. Hollenberg. *The nitrogen-vacancy colour centre in diamond*. Physics Reports **528**, 1 – 45 (2013). Referenced on page: 2

[48] I. M. Georgescu, S. Ashhab, and F. Nori. *Quantum simulation*. Rev. Mod. Phys. **86**, 153–185 (2014). Referenced on page: 2

[49] J. M. Deutsch. *Quantum statistical mechanics in a closed system*. Phys. Rev. A **43**, 2046–2049 (1991). Referenced on pages: 2, 11, 25, 26

[50] M. Srednicki. *Chaos and quantum thermalization*. Phys. Rev. E **50**, 888–901 (1994). Referenced on pages: 2, 11

[51] M. Rigol, V. Dunjko, and M. Olshanii. *Thermalization and its mechanism for generic isolated quantum systems*. Nature **452**, 854–858 (2008). Referenced on pages: 2, 11

[52] N. Linden, S. Popescu, A. J. Short, and A. Winter. *Quantum mechanical evolution towards thermal equilibrium*. Phys. Rev. E **79**, 061103 (2009). Referenced on pages: 2, 9

[53] S. Chu. *Nobel Lecture: The manipulation of neutral particles*. Rev. Mod. Phys. **70**, 685–706 (1998). Referenced on page: 3

[54] C. N. Cohen-Tannoudji. *Nobel Lecture: Manipulating atoms with photons*. Rev. Mod. Phys. **70**, 707–719 (1998). Referenced on page: 3

[55] W. D. Phillips. *Nobel Lecture: Laser cooling and trapping of neutral atoms*. Rev. Mod. Phys. **70**, 721–741 (1998). Referenced on page: 3

[56] A. J. Leggett. *Bose-Einstein condensation in the alkali gases: Some fundamental concepts*. Rev. Mod. Phys. **73**, 307–356 (2001). Referenced on page: 3

[57] B. DeMarco and D. S. Jin. *Onset of Fermi Degeneracy in a Trapped Atomic Gas*. Science **285**, 1703–1706 (1999). Referenced on page: 3

[58] D. Jaksch, C. Bruder, J. I. Cirac, C. W. Gardiner, and P. Zoller. *Cold Bosonic Atoms in Optical Lattices*. Phys. Rev. Lett. **81**, 3108–3111 (1998). Referenced on page: 3

[59] M. Greiner, O. Mandel, T. Esslinger, T. W. Hansch, and I. Bloch. *Quantum phase transition from a superfluid to a Mott insulator in a gas of ultracold atoms*. Nature **415**, 39–44 (2002). Referenced on page: 3

[60] R. Jördens, N. Strohmaier, K. Günter, H. Moritz, and T. Esslinger. *A Mott insulator of fermionic atoms in an optical lattice*. Nature **455**, 204–207 (2008). Referenced on page: 3

[61] U. Schneider, L. Hackermüller, S. Will, T. Best, I. Bloch, T. A. Costi, R. W. Helmes, D. Rasch, and A. Rosch. *Metallic and Insulating Phases of Repulsively Interacting Fermions in a 3D Optical Lattice*. Science **322**, 1520–1525 (2008). Referenced on page: 3

[62] J. Dalibard, F. Gerbier, G. Juzeliūnas, and P. Öhberg. *Colloquium*. Rev. Mod. Phys. **83**, 1523–1543 (2011). Referenced on page: 3

[63] G. Roati, C. D'Errico, L. Fallani, M. Fattori, C. Fort, M. Zaccanti, G. Modugno, M. Modugno, and M. Inguscio. *Anderson localization of a non-interacting Bose-Einstein condensate*. Nature **453**, 895–898 (2008). Referenced on pages: 3, 34, 45, 47

[64] J. Billy, V. Josse, Z. Zuo, A. Bernard, B. Hambrecht, P. Lugan, D. Clement, L. Sanchez-Palencia, P. Bouyer, and A. Aspect. *Direct observation of Anderson localization of matter waves in a controlled disorder*. Nature **453**, 891–894 (2008). Referenced on pages: 3, 34, 45, 47

[65] V. Gurarie, L. Pollet, N. V. Prokof'ev, B. V. Svistunov, and M. Troyer. *Phase diagram of the disordered Bose-Hubbard model*. Phys. Rev. B **80**, 214519 (2009). Referenced on page: 3

[66] B. Deissler, M. Zaccanti, G. Roati, C. D'Errico, M. Fattori, M. Modugno, G. Modugno, and M. Inguscio. *Delocalization of a disordered bosonic system by repulsive interactions*. Nat. Phys. **6**, 354–358 (2010). Referenced on page: 3

[67] C. D'Errico, E. Lucioni, L. Tanzi, L. Gori, G. Roux, I. P. McCulloch, T. Giamarchi, M. Inguscio, and G. Modugno. *Observation of a Disordered Bosonic Insulator from Weak to Strong Interactions*. Phys. Rev. Lett. **113**, 095301 (2014). Referenced on page: 3

[68] C. Meldgin, U. Ray, P. Russ, D. Chen, D. M. Ceperley, and B. DeMarco. *Probing the Bose glass-superfluid transition using quantum quenches of disorder*. Nat. Phys. **12**, 646–649 (2016). Referenced on page: 3

[69] R. P. Feynman. *Simulating physics with computers*. International Journal of Theoretical Physics **21**, 467–488 (1982). Referenced on page: 3

[70] D. M. Ceperley and B. J. Alder. *Ground State of the Electron Gas by a Stochastic Method*. Phys. Rev. Lett. **45**, 566–569 (1980). Referenced on page: 3

[71] U. Schollwöck. *The density-matrix renormalization group*. Rev. Mod. Phys. **77**, 259–315 (2005). Referenced on page: 3

[72] M. Schreiber, S. S. Hodgman, P. Bordia, H. P. Lüschen, M. H. Fischer, R. Vosk, E. Altman, U. Schneider, and I. Bloch. *Observation of many-body localization of interacting fermions in a quasirandom optical lattice*. Science **349**, 842–845 (2015). Referenced on pages: 6, 34, 46, 49, 51, 56, 62, 71, 88, 97, 98, 108

[73] P. Bordia, H. P. Lüschen, S. S. Hodgman, M. Schreiber, I. Bloch, and U. Schneider. *Coupling Identical one-dimensional Many-Body Localized Systems*. Phys. Rev. Lett. **116**, 140401 (2016). Referenced on pages: 6, 59, 82, 87, 97, 100, 110

[74] P. Bordia, H. Luschen, U. Schneider, M. Knap, and I. Bloch. *Periodically driving a many-body localized quantum system*. Nat. Phys. **13**, 460–464 (2017). Referenced on page: 6

[75] P. Bordia, H. Lüschen, S. Scherg, S. Gopalakrishnan, M. Knap, U. Schneider, and I. Bloch. *Probing Slow Relaxation and Many-Body Localization in Two-Dimensional Quasi-Periodic Systems*. (2017). arXiv:1704.03063. Referenced on pages: 6, 110

[76] H. P. Lüschen, P. Bordia, S. S. Hodgman, M. Schreiber, S. Sarkar, A. J. Daley, M. H. Fischer, E. Altman, I. Bloch, and U. Schneider. *Signatures of Many-Body Localization in a Controlled Open Quantum System*. Phys. Rev. X **7**, 011034 (2017). Referenced on pages: 6, 59, 64, 97, 110

[77] H. P. Lüschen, P. Bordia, S. Scherg, F. Alet, E. Altman, U. Schneider, and I. Bloch. *Evidence for Griffiths-Type Dynamics near the Many-Body Localization Transition in Quasi-Periodic Systems*. (2016). arXiv:1612.07173. Referenced on pages: 6, 60, 93, 97, 103, 106, 110

[78] D. Lu, T. Xin, N. Yu, Z. Ji, J. Chen, G. Long, J. Baugh, X. Peng, B. Zeng, and R. Laflamme. *Tomography is Necessary for Universal Entanglement Detection with Single-Copy Observables*. Phys. Rev. Lett. **116**, 230501 (2016). Referenced on pages: 10, 107

[79] A. M. Kaufman, M. E. Tai, A. Lukin, M. Rispoli, R. Schittko, P. M. Preiss, and M. Greiner. *Quantum thermalization through entanglement in an isolated many-body system*. Science **353**, 794–800 (2016). Referenced on pages: 10, 34

[80] C. Neill, P. Roushan, M. Fang, Y. Chen, M. Kolodrubetz, Z. Chen, A. Megrant, R. Barends, B. Campbell, B. Chiaro, A. Dunsworth, E. Jeffrey, J. Kelly, J. Mutus, P. J. J. O'Malley, C. Quintana, D. Sank, A. Vainsencher, J. Wenner, T. C. White, A. Polkovnikov, and J. M. Martinis. *Ergodic dynamics and thermalization in an isolated quantum system*. Nat. Phys. **12**, 1037–1041 (2016). Referenced on page: 10

[81] J. R. Garrison and T. Grover. *Does a single eigenstate encode the full Hamiltonian?* (2015). arXiv:1503.00729. Referenced on pages: 10, 13

[82] M. Rigol and M. Srednicki. *Alternatives to Eigenstate Thermalization*. Phys. Rev. Lett. **108**, 110601 (2012). Referenced on page: 11

[83] H. Kim, T. N. Ikeda, and D. A. Huse. *Testing whether all eigenstates obey the eigenstate thermalization hypothesis*. Phys. Rev. E **90**, 052105 (2014). Referenced on page: 11

[84] M. Rigol, V. Dunjko, V. Yurovsky, and M. Olshanii. *Relaxation in a Completely Integrable Many-Body Quantum System: An Ab Initio Study of the Dynamics of the Highly Excited States of 1D Lattice Hard-Core Bosons*. Phys. Rev. Lett. **98**, 050405 (2007). Referenced on page: 13

[85] S. Aubry and G. André. *Analyticity breaking and Anderson localization in incommensurate lattices*. Ann. Israel Phys. Soc. **3** (1980). Referenced on pages: 17, 47, 55

[86] J. Sokoloff. *Unusual band structure, wave functions and electrical conductance in crystals with incommensurate periodic potentials*. Physics Reports **126**, 189 – 244 (1985). Referenced on pages: 17, 47

[87] A. Y. Gordon, S. Jitomirskaya, Y. Last, and B. Simon. *Duality and singular continuous spectrum in the almost Mathieu equation*. Acta Math. **178**, 169–183 (1997). Referenced on pages: 17, 47

[88] S. Y. Jitomirskaya. *Metal-insulator transition for the almost Mathieu operator*. Ann. Math. **150**, 1159–1175 (1999). Referenced on pages: 17, 47

[89] J. Biddle and S. Das Sarma. *Predicted Mobility Edges in One-Dimensional Incommensurate Optical Lattices: An Exactly Solvable Model of Anderson Localization*. Phys. Rev. Lett. **104**, 070601 (2010). Referenced on page: 18

[90] S. Ganeshan, J. H. Pixley, and S. Das Sarma. *Nearest Neighbor Tight Binding Models with an Exact Mobility Edge in One Dimension*. Phys. Rev. Lett. **114**, 146601 (2015). Referenced on page: 18

[91] E. Abrahams, P. W. Anderson, D. C. Licciardello, and T. V. Ramakrishnan. *Scaling Theory of Localization: Absence of Quantum Diffusion in Two Dimensions*. Phys. Rev. Lett. **42**, 673–676 (1979). Referenced on pages: 19, 20

[92] P. A. Lee and T. V. Ramakrishnan. *Disordered electronic systems*. Rev. Mod. Phys. 57, 287–337 (1985). Referenced on page: 19

[93] F. Andraschko, T. Enss, and J. Sirker. *Purification and Many-Body Localization in Cold Atomic Gases*. Phys. Rev. Lett. 113, 217201 (2014). Referenced on pages: 22, 48

[94] M. Cramer, A. Flesch, I. P. McCulloch, U. Schollwöck, and J. Eisert. *Exploring Local Quantum Many-Body Relaxation by Atoms in Optical Superlattices*. Phys. Rev. Lett. 101, 063001 (2008). Referenced on page: 22

[95] P. Barmettler, M. Punk, V. Gritsev, E. Demler, and E. Altman. *Relaxation of Antiferromagnetic Order in Spin-1/2 Chains Following a Quantum Quench*. Phys. Rev. Lett. 102, 130603 (2009). Referenced on pages: 22, 48

[96] S. Trotzky, Y.-A. Chen, A. Flesch, I. P. McCulloch, U. Schollwöck, J. Eisert, and I. Bloch. *Probing the relaxation towards equilibrium in an isolated strongly correlated one-dimensional Bose gas*. Nat. Phys. 8, 325–330 (2012). Referenced on pages: 22, 48

[97] S. Raghu, X.-L. Qi, C. Honerkamp, and S.-C. Zhang. *Topological Mott Insulators*. Phys. Rev. Lett. 100, 156401 (2008). Referenced on page: 25

[98] N. Y. Yao, C. R. Laumann, S. Gopalakrishnan, M. Knap, M. Müller, E. A. Demler, and M. D. Lukin. *Many-Body Localization in Dipolar Systems*. Phys. Rev. Lett. 113, 243002 (2014). Referenced on page: 26

[99] Z. Papić, E. M. Stoudenmire, and D. A. Abanin. *Many-body localization in disorder-free systems: The importance of finite-size constraints*. Ann. Phys. 362, 714 – 725 (2015). Referenced on page: 26

[100] N. Y. Yao, C. R. Laumann, J. I. Cirac, M. D. Lukin, and J. E. Moore. *Quasi-Many-Body Localization in Translation-Invariant Systems*. Phys. Rev. Lett. 117, 240601 (2016). Referenced on page: 26

[101] M. Rigol. *Breakdown of Thermalization in Finite One-Dimensional Systems*. Phys. Rev. Lett. 103, 100403 (2009). Referenced on page: 26

[102] T. Grover and M. P. A. Fisher. *Quantum disentangled liquids*. J. Stat. Mech. Theor. Exp. 2014, P10010 (2014). Referenced on page: 26

[103] N. F. Mott. *Conduction in glasses containing transition metal ions*. Journal of Non-Crystalline Solids 1, 1 – 17 (1968). Referenced on pages: 27, 59

[104] I. V. Gornyi, A. D. Mirlin, and D. G. Polyakov. *Interacting Electrons in Disordered Wires: Anderson Localization and Low-T Transport*. Phys. Rev. Lett. 95, 206603 (2005). Referenced on pages: 27, 30, 45, 107

[105] V. Oganesyan and D. A. Huse. *Localization of interacting fermions at high temperature*. Phys. Rev. B 75, 155111 (2007). Referenced on pages: 28, 33

[106] P. Jordan and E. Wigner. *Über das Paulische Äquivalenzverbot*. Zeitschrift für Physik **47**, 631–651 (1928). Referenced on pages: 28, 98

[107] T. Prosen. *Open XXZ Spin Chain: Nonequilibrium Steady State and a Strict Bound on Ballistic Transport*. Phys. Rev. Lett. **106**, 217206 (2011). Referenced on page: 30

[108] M. Žnidarič. *Spin Transport in a One-Dimensional Anisotropic Heisenberg Model*. Phys. Rev. Lett. **106**, 220601 (2011). Referenced on page: 30

[109] T. Kinoshita, T. Wenger, and D. S. Weiss. *A quantum Newton's cradle*. Nature **440**, 900–903 (2006). Referenced on page: 30

[110] B. Paredes, A. Widera, V. Murg, O. Mandel, S. Folling, I. Cirac, G. V. Shlyapnikov, T. W. Hansch, and I. Bloch. *Tonks-Girardeau gas of ultracold atoms in an optical lattice*. Nature **429**, 277–281 (2004). Referenced on page: 30

[111] J. P. Ronzheimer, M. Schreiber, S. Braun, S. S. Hodgman, S. Langer, I. P. McCulloch, F. Heidrich-Meisner, I. Bloch, and U. Schneider. *Expansion Dynamics of Interacting Bosons in Homogeneous Lattices in One and Two Dimensions*. Phys. Rev. Lett. **110**, 205301 (2013). Referenced on pages: 30, 34, 65, 68, 71

[112] B. S. Shastry. *Exact Integrability of the One-Dimensional Hubbard Model*. Phys. Rev. Lett. **56**, 2453–2455 (1986). Referenced on pages: 30, 47, 100

[113] I. L. Aleiner, B. L. Altshuler, and G. V. Shlyapnikov. *A finite-temperature phase transition for disordered weakly interacting bosons in one dimension*. Nat. Phys. **6**, 900–904 (2010). Referenced on page: 30

[114] D. Pekker, G. Refael, E. Altman, E. Demler, and V. Oganesyan. *Hilbert-Glass Transition: New Universality of Temperature-Tuned Many-Body Dynamical Quantum Criticality*. Phys. Rev. X **4**, 011052 (2014). Referenced on page: 30

[115] Y. Bar Lev and D. R. Reichman. *Dynamics of many-body localization*. Phys. Rev. B **89**, 220201 (2014). Referenced on page: 30

[116] D. J. Luitz, N. Laflorencie, and F. Alet. *Extended slow dynamical regime close to the many-body localization transition*. Phys. Rev. B **93**, 060201 (2016). Referenced on pages: 31, 93

[117] D. J. Luitz, N. Laflorencie, and F. Alet. *Many-body localization edge in the random-field Heisenberg chain*. Phys. Rev. B **91**, 081103 (2015). Referenced on pages: 31, 97

[118] D. J. Luitz and Y. B. Lev. *The Ergodic Side of the Many-Body Localization Transition* (2016). arXiv:1610.08993. Referenced on pages: 31, 89, 110

[119] J. H. Bardarson, F. Pollmann, and J. E. Moore. *Unbounded Growth of Entanglement in Models of Many-Body Localization*. Phys. Rev. Lett. **109**, 017202 (2012). Referenced on pages: 32, 33, 107

[120] J. Eisert, M. Cramer, and M. B. Plenio. *Colloquium : Area laws for the entanglement entropy*. Rev. Mod. Phys. **82**, 277–306 (2010). Referenced on pages: 31, 32

[121] M. B. Hastings. *An area law for one-dimensional quantum systems*. J. Stat. Mech. **2007**, P08024 (2007). Referenced on page: 32

[122] P. Calabrese and J. Cardy. *Evolution of entanglement entropy in one-dimensional systems*. J. Stat. Mech. **2005**, P04010 (2005). Referenced on pages: 33, 53

[123] G. D. Chiara, S. Montangero, P. Calabrese, and R. Fazio. *Entanglement entropy dynamics of Heisenberg chains*. J. Stat. Mech. **2006**, P03001 (2006). Referenced on page: 33

[124] H. Kim and D. A. Huse. *Ballistic Spreading of Entanglement in a Diffusive Nonintegrable System*. Phys. Rev. Lett. **111**, 127205 (2013). Referenced on pages: 33, 53

[125] D. N. Page. *Average entropy of a subsystem*. Phys. Rev. Lett. **71**, 1291–1294 (1993). Referenced on page: 33

[126] M. Žnidarič, T. Prosen, and P. Prelovšek. *Many-body localization in the Heisenberg XXZ magnet in a random field*. Phys. Rev. B **77**, 064426 (2008). Referenced on pages: 33, 54

[127] M. Serbyn, Z. Papić, and D. A. Abanin. *Universal Slow Growth of Entanglement in Interacting Strongly Disordered Systems*. Phys. Rev. Lett. **110**, 260601 (2013). Referenced on pages: 33, 107

[128] D. A. Huse, R. Nandkishore, and V. Oganesyan. *Phenomenology of fully many-body-localized systems*. Phys. Rev. B **90**, 174202 (2014). Referenced on pages: 33, 107

[129] U. Schneider, L. Hackermuller, J. P. Ronzheimer, S. Will, S. Braun, T. Best, I. Bloch, E. Demler, S. Mandt, D. Rasch, and A. Rosch. *Fermionic transport and out-of-equilibrium dynamics in a homogeneous Hubbard model with ultracold atoms*. Nat. Phys. **8**, 213–218 (2012). Referenced on pages: 34, 51, 71, 90, 91

[130] J. P. Ronzheimer. *Non-equilibrium dynamics of ultracold atoms in optical lattices*. PhD thesis, Faculty of Physics, Ludwig-Maximilians-Universität, Munich (2014). Referenced on page: 35

[131] S. Braun. *Negative absolute temperature and the dynamics of quantum phase transitions*. PhD thesis, Faculty of Physics, Ludwig-Maximilians-Universität, Munich (2014). Referenced on page: 35

[132] M. Schreiber. *In prep.* PhD thesis, Faculty of Physics, Ludwig-Maximilians-Universität, Munich (). Referenced on pages: 35, 38, 40, 49

[133] R. Grimm, M. Weidemüller, and Y. B. Ovchinnikov. *Optical Dipole Traps for Neutral Atoms*. **42**, 95 – 170 (2000). Referenced on page: 36

[134] N. Ashcroft and N. Mermin. *Solid State Physics*. Saunders College, Philadelphia (1976). Referenced on page: 36

[135] D. Jaksch. *Bose-Einstein Condensation and Applications*. PhD thesis, Leopold-Franzens-Universität Innsbruck, Austria (1999). Referenced on page: 38

[136] F. Görg. *Ultracold Fermionic Atoms in Optical Superlattices*. Master's thesis, Technical University Munich, Germany (2014). Referenced on pages: 38, 41, 113

[137] M. Köhl, H. Moritz, T. Stöferle, K. Günter, and T. Esslinger. *Fermionic Atoms in a Three Dimensional Optical Lattice: Observing Fermi Surfaces, Dynamics, and Interactions*. Phys. Rev. Lett. **94**, 080403 (2005). Referenced on page: 41

[138] J. Sebby-Strabley, M. Anderlini, P. S. Jessen, and J. V. Porto. *Lattice of double wells for manipulating pairs of cold atoms*. Phys. Rev. A **73**, 033605 (2006). Referenced on page: 40

[139] S. Folling, S. Trotzky, P. Cheinet, M. Feld, R. Saers, A. Widera, T. Muller, and I. Bloch. *Direct observation of second-order atom tunnelling*. Nature **448**, 1029–1032 (2007). Referenced on page: 40

[140] C. A. Regal, C. Ticknor, J. L. Bohn, and D. S. Jin. *Creation of ultracold molecules from a Fermi gas of atoms*. Nature **424** (2003). Referenced on pages: 43, 47, 48, 50, 62, 90, 104, 108, 114

[141] T. Köhler, K. Góral, and P. S. Julienne. *Production of cold molecules via magnetically tunable Feshbach resonances*. Rev. Mod. Phys. **78**, 1311–1361 (2006). Referenced on page: 43

[142] L. Hackermüller, U. Schneider, M. Moreno-Cardoner, T. Kitagawa, T. Best, S. Will, E. Demler, E. Altman, I. Bloch, and B. Paredes. *Anomalous Expansion of Attractively Interacting Fermionic Atoms in an Optical Lattice*. Science **327**, 1621–1624 (2010). Referenced on page: 43

[143] J. Z. Imbrie. *Diagonalization and Many-Body Localization for a Disordered Quantum Spin Chain*. Phys. Rev. Lett. **117**, 027201 (2016). Referenced on pages: 45, 110

[144] D. S. Wiersma, P. Bartolini, A. Lagendijk, and R. Righini. *Localization of light in a disordered medium*. Nature **390**, 671–673 (1997). Referenced on page: 45

[145] T. Schwartz, G. Bartal, S. Fishman, and M. Segev. *Transport and Anderson localization in disordered two-dimensional photonic lattices*. Nature **446**, 52–55 (2007). Referenced on page: 45

[146] S. S. Kondov, W. R. McGehee, J. J. Zirbel, and B. DeMarco. *Three-Dimensional Anderson Localization of Ultracold Matter*. Science **334**, 66–68 (2011). Referenced on page: 45

[147] M. Ovadia, D. Kalok, I. Tamir, S. Mitra, B. Sacépé, and D. Shahar. *Evidence for a Finite-Temperature Insulator*. Scientific Reports **5**, 13503 EP – (2015). Referenced on page: 45

[148] S. Iyer, V. Oganesyan, G. Refael, and D. A. Huse. *Many-body localization in a quasiperiodic system*. Phys. Rev. B **87**, 134202 (2013). Referenced on pages: 46, 77

[149] V. Mastropietro. *Localization of Interacting Fermions in the Aubry-André Model*. Phys. Rev. Lett. **115**, 180401 (2015). Referenced on page: 46

[150] V. Mastropietro. *Interacting spinning fermions with quasi-random disorder* (2016). arXiv:1611.00748. Referenced on page: 46

[151] V. Mastropietro. *Localization in the Ground State of an Interacting Quasi-Periodic Fermionic Chain*. Communications in Mathematical Physics **342**, 217–250 (2016). Referenced on page: 46

[152] V. Khemani, D. N. Sheng, and D. A. Huse. *Two universality classes for the many-body localization transition*. arXiv:1702.03932 (2017). Referenced on pages: 46, 93, 100, 110

[153] P. Prelovšek, O. S. Barišić, and M. Žnidarič. *Absence of full many-body localization in the disordered Hubbard chain*. Phys. Rev. B **94**, 241104 (2016). Referenced on pages: 53, 110

[154] S. A. Gurvitz. *Delocalization in the Anderson Model due to a Local Measurement*. Phys. Rev. Lett. **85**, 812–815 (2000). Referenced on page: 59

[155] B. Nowak, J. J. Kinnunen, M. J. Holland, and P. Schlagheck. *Delocalization of ultracold atoms in a disordered potential due to light scattering*. Phys. Rev. A **86**, 043610 (2012). Referenced on page: 59

[156] R. Nandkishore, S. Gopalakrishnan, and D. A. Huse. *Spectral features of a many-body-localized system weakly coupled to a bath*. Phys. Rev. B **90**, 064203 (2014). Referenced on page: 59

[157] S. Johri, R. Nandkishore, and R. N. Bhatt. *Many-Body Localization in Imperfectly Isolated Quantum Systems*. Phys. Rev. Lett. **114**, 117401 (2015). Referenced on page: 59

[158] D. A. Huse, R. Nandkishore, F. Pietracaprina, V. Ros, and A. Scardicchio. *Localized systems coupled to small baths: From Anderson to Zeno*. Phys. Rev. B **92**, 014203 (2015). Referenced on page: 59

[159] E. Levi, M. Heyl, I. Lesanovsky, and J. P. Garrahan. *Robustness of Many-Body Localization in the Presence of Dissipation*. Phys. Rev. Lett. **116**, 237203 (2016). Referenced on page: 59

[160] M. H. Fischer, M. Maksymenko, and E. Altman. *Dynamics of a Many-Body-Localized System Coupled to a Bath*. Phys. Rev. Lett. **116**, 160401 (2016). Referenced on pages: 59, 64

[161] P. Ponte, A. Chandran, Z. Papić, and D. A. Abanin. *Periodically driven ergodic and many-body localized quantum systems*. Ann. Phys. **353**, 196–204 (2015). Referenced on pages: 76, 78

[162] P. Ponte, Z. Papić, F. m. c. Huveneers, and D. A. Abanin. *Many-Body Localization in Periodically Driven Systems*. Phys. Rev. Lett. **114**, 140401 (2015). Referenced on pages: 76, 78, 84

[163] A. Lazarides, A. Das, and R. Moessner. *Fate of Many-Body Localization Under Periodic Driving*. Phys. Rev. Lett. **115**, 030402 (2015). Referenced on pages: 76, 78, 84

[164] D. A. Abanin, W. D. Roeck, and F. Huveneers. *Theory of many-body localization in periodically driven systems*. Ann. Phys. **372**, 1 – 11 (2016). Referenced on pages: 76, 78, 84

[165] M. Kozarzewski, P. Prelovšek, and M. Mierzejewski. *Distinctive response of many-body localized systems to a strong electric field*. Phys. Rev. B **93**, 235151 (2016). Referenced on pages: 76, 78

[166] J. Rehn, A. Lazarides, F. Pollmann, and R. Moessner. *How periodic driving heats a disordered quantum spin chain*. Phys. Rev. B **94**, 020201 (2016). Referenced on pages: 76, 78, 84

[167] S. Gopalakrishnan, M. Knap, and E. Demler. *Regimes of heating and dynamical response in driven many-body localized systems*. Phys. Rev. B **94**, 094201 (2016). Referenced on pages: 76, 78, 84, 85

[168] D. A. Abanin, W. De Roeck, and F. m. c. Huveneers. *Exponentially Slow Heating in Periodically Driven Many-Body Systems*. Phys. Rev. Lett. **115**, 256803 (2015). Referenced on page: 76

[169] T. Oka and H. Aoki. *Photovoltaic Hall effect in graphene*. Phys. Rev. B **79**, 081406 (2009). Referenced on pages: 76, 111

[170] T. Kitagawa, E. Berg, M. Rudner, and E. Demler. *Topological characterization of periodically driven quantum systems*. Phys. Rev. B **82**, 235114 (2010). Referenced on pages: 76, 111

[171] N. H. Lindner, G. Refael, and V. Galitski. *Floquet topological insulator in semiconductor quantum wells*. Nat. Phys. **7**, 490–495 (2011). Referenced on pages: 76, 111

[172] M. Aidelsburger, M. Atala, M. Lohse, J. T. Barreiro, B. Paredes, and I. Bloch. *Realization of the Hofstadter Hamiltonian with Ultracold Atoms in Optical Lattices*. Phys. Rev. Lett. **111**, 185301 (2013). Referenced on pages: 76, 111

[173] H. Miyake, G. A. Siviloglou, C. J. Kennedy, W. C. Burton, and W. Ketterle. *Realizing the Harper Hamiltonian with Laser-Assisted Tunneling in Optical Lattices*. Phys. Rev. Lett. **111**, 185302 (2013). Referenced on pages: 76, 111

[174] G. Jotzu, M. Messer, R. Desbuquois, M. Lebrat, T. Uehlinger, D. Greif, and T. Esslinger. *Experimental realization of the topological Haldane model with ultracold fermions*. Nature **515**, 237–240 (2014). Referenced on pages: 76, 111

[175] M. Aidelsburger, M. Lohse, C. Schweizer, M. Atala, J. T. Barreiro, S. Nascimbene, N. R. Cooper, I. Bloch, and N. Goldman. *Measuring the Chern number of Hofstadter bands with ultracold bosonic atoms*. Nat. Phys. **11**, 162–166 (2015). Referenced on pages: 76, 111

[176] V. Khemani, A. Lazarides, R. Moessner, and S. L. Sondhi. *Phase Structure of Driven Quantum Systems*. Phys. Rev. Lett. **116**, 250401 (2016). Referenced on pages: 76, 111

[177] D. V. Else and C. Nayak. *Classification of topological phases in periodically driven interacting systems*. Phys. Rev. B **93**, 201103 (2016). Referenced on pages: 76, 111

[178] C. W. von Keyserlingk and S. L. Sondhi. *Phase structure of one-dimensional interacting Floquet systems. I. Abelian symmetry-protected topological phases*. Phys. Rev. B **93**, 245145 (2016). Referenced on pages: 76, 111

[179] C. W. von Keyserlingk and S. L. Sondhi. *Phase structure of one-dimensional interacting Floquet systems. II. Symmetry-broken phases*. Phys. Rev. B **93**, 245146 (2016). Referenced on pages: 76, 111

[180] A. C. Potter, T. Morimoto, and A. Vishwanath. *Classification of Interacting Topological Floquet Phases in One Dimension*. Phys. Rev. X **6**, 041001 (2016). Referenced on pages: 76, 111

[181] D. V. Else, B. Bauer, and C. Nayak. *Floquet Time Crystals*. Phys. Rev. Lett. **117**, 090402 (2016). Referenced on pages: 76, 111

[182] C. W. von Keyserlingk, V. Khemani, and S. L. Sondhi. *Absolute stability and spatiotemporal long-range order in Floquet systems*. Phys. Rev. B **94**, 085112 (2016). Referenced on pages: 76, 111

[183] A. Lazarides, A. Das, and R. Moessner. *Equilibrium states of generic quantum systems subject to periodic driving*. Phys. Rev. E **90**, 012110 (2014). Referenced on page: 76

[184] L. D'Alessio and M. Rigol. *Long-time Behavior of Isolated Periodically Driven Interacting Lattice Systems*. Phys. Rev. X **4**, 041048 (2014). Referenced on page: 82

[185] S. Gopalakrishnan, M. Müller, V. Khemani, M. Knap, E. Demler, and D. A. Huse. *Low-frequency conductivity in many-body localized systems*. Phys. Rev. B **92**, 104202 (2015). Referenced on page: 83

[186] V. Khemani, R. Nandkishore, and S. L. Sondhi. *Nonlocal adiabatic response of a localized system to local manipulations*. Nat. Phys. **11**, 560–565 (2015). Referenced on page: 84

[187] T. Esslinger. *Fermi-Hubbard Physics with Atoms in an Optical Lattice*. Annu. Rev. Condens. Matter Phys. **1**, 129–152 (2010). Referenced on page: 88

[188] K. Agarwal, E. Altman, E. Demler, S. Gopalakrishnan, D. A. Huse, and M. Knap. *Rare-region effects and dynamics near the many-body localization transition*. Ann. Phys. (Berlin) (2017). Referenced on page: 89

[189] J. T. Chayes, L. Chayes, D. S. Fisher, and T. Spencer. *Finite-Size Scaling and Correlation Lengths for Disordered Systems*. Phys. Rev. Lett. **57**, 2999–3002 (1986). Referenced on page: 89

[190] A. B. Harris. *Effect of random defects on the critical behaviour of Ising models*. Journal of Physics C: Solid State Physics **7**, 1671 (1974). Referenced on page: 89

[191] A. Chandran, C. R. Laumann, and V. Oganesyan. *Finite size scaling bounds on many-body localized phase transitions*. (2015). arXiv:1509.04285. Referenced on page: 89

[192] C. Monthus. *Many-Body-Localization Transition in the Strong Disorder Limit: Entanglement Entropy from the Statistics of Rare Extensive Resonances*. Entropy **18** (2016). Referenced on page: 89

[193] S. Inglis and L. Pollet. *Accessing Many-Body Localized States through the Generalized Gibbs Ensemble*. Phys. Rev. Lett. **117**, 120402 (2016). Referenced on page: 89

[194] W. De Roeck and F. m. c. Huveneers. *Stability and instability towards delocalization in many-body localization systems*. Phys. Rev. B **95**, 155129 (2017). Referenced on pages: 89, 101, 102, 115

[195] A. Chandran, A. Pal, C. R. Laumann, and A. Scardicchio. *Many-body localization beyond eigenstates in all dimensions*. Phys. Rev. B **94**, 144203 (2016). Referenced on page: 89

[196] Y. Bar Lev and D. R. Reichman. *Slow dynamics in a two-dimensional Anderson-Hubbard model*. Europhys Lett. **113**, 46001 (2016). Referenced on page: 89

[197] S. S. Kondov, W. R. McGehee, W. Xu, and B. DeMarco. *Disorder-Induced Localization in a Strongly Correlated Atomic Hubbard Gas*. Phys. Rev. Lett. **114**, 083002 (2015). Referenced on pages: 89, 91

[198] J.-y. Choi, S. Hild, J. Zeiher, P. Schauß, A. Rubio-Abadal, T. Yefsah, V. Khemani, D. A. Huse, I. Bloch, and C. Gross. *Exploring the many-body localization transition in two dimensions*. Science **352**, 1547–1552 (2016). Referenced on pages: 89, 91, 110

[199] S. Gopalakrishnan, K. Agarwal, E. A. Demler, D. A. Huse, and M. Knap. *Griffiths effects and slow dynamics in nearly many-body localized systems*. Phys. Rev. B **93**, 134206 (2016). Referenced on pages: 90, 91, 93, 95

[200] Y. B. Lev, D. M. Kennes, C. Klöckner, D. R. Reichman, and C. Karrasch. *Transport in quasiperiodic interacting systems: from superdiffusion to subdiffusion* (2017). arXiv:1702.04349. Referenced on pages: 93, 100

[201] S. Banerjee and E. Altman. *Solvable model for a dynamical quantum phase transition from fast to slow scrambling*. Phys. Rev. B **95**, 134302 (2017). Referenced on page: 101

[202] J. Z. Imbrie. *On Many-Body Localization for Quantum Spin Chains*. Journal of Statistical Physics **163**, 998–1048 (2016). Referenced on pages: 107, 110

[203] R. Islam, R. Ma, P. M. Preiss, M. Eric Tai, A. Lukin, M. Rispoli, and M. Greiner. *Measuring entanglement entropy in a quantum many-body system*. Nature **528**, 77–83 (2015). Referenced on pages: 107, 110

[204] Y. Huang, Y.-L. Zhang, and X. Chen. *Out-of-time-ordered correlators in many-body localized systems*. Ann. Phys. (Berlin) (2016). Referenced on pages: 107, 111

[205] R.-Q. He and Z.-Y. Lu. *Characterizing many-body localization by out-of-time-ordered correlation*. Phys. Rev. B **95**, 054201 (2017). Referenced on pages: 107, 111

[206] R. Fan, P. Zhang, H. Shen, and H. Zhai. *Out-of-time-order correlation for many-body localization*. Science Bulletin **62**, 707 – 711 (2017). Referenced on pages: 107, 111

[207] X. Chen, T. Zhou, D. A. Huse, and E. Fradkin. *Out-of-time-order correlations in many-body localized and thermal phases*. Ann. Phys. (Berlin) (2016). Referenced on pages: 107, 111

[208] B. Swingle, G. Bentsen, M. Schleier-Smith, and P. Hayden. *Measuring the scrambling of quantum information*. Phys. Rev. A **94**, 040302 (2016). Referenced on page: 108

[209] A. Eckardt, C. Weiss, and M. Holthaus. *Superfluid-Insulator Transition in a Periodically Driven Optical Lattice*. Phys. Rev. Lett. **95**, 260404 (2005). Referenced on page: 108

[210] G. Vidal. *Efficient Simulation of One-Dimensional Quantum Many-Body Systems*. Phys. Rev. Lett. **93**, 040502 (2004). Referenced on page: 109

[211] G. Kucsko, S. Choi, J. Choi, P. C. Maurer, H. Sumiya, S. Onoda, J. Isoya, F. Jelezko, Eugene, N. Y. Yao, and M. D. Lukin. (2016). arXiv:1609.08216. Referenced on page: 110

[212] J. Smith, A. Lee, P. Richerme, B. Neyenhuis, P. W. Hess, P. Hauke, M. Heyl, D. A. Huse, and C. Monroe. *Many-body localization in a quantum simulator with programmable random disorder*. Nat. Phys. **12**, 907–911 (2016). Referenced on page: 110

[213] I. V. Protopopov, W. W. Ho, and D. A. Abanin. *The effect of SU(2) symmetry on many-body localization and thermalization* (2016). arXiv:1612.01208. Referenced on page: 110

[214] M. Žnidarič, A. Scardicchio, and V. K. Varma. *Diffusive and Subdiffusive Spin Transport in the Ergodic Phase of a Many-Body Localizable System*. Phys. Rev. Lett. **117**, 040601 (2016). Referenced on page: 110

[215] X. Li, S. Ganeshan, J. H. Pixley, and S. Das Sarma. *Many-Body Localization and Quantum Nonergodicity in a Model with a Single-Particle Mobility Edge*. Phys. Rev. Lett. **115**, 186601 (2015). Referenced on page: 111

[216] R. Modak and S. Mukerjee. *Many-Body Localization in the Presence of a Single-Particle Mobility Edge*. Phys. Rev. Lett. **115**, 230401 (2015). Referenced on page: 111

[217] X. Li, J. H. Pixley, D.-L. Deng, S. Ganeshan, and S. Das Sarma. *Quantum nonergodicity and fermion localization in a system with a single-particle mobility edge*. Phys. Rev. B **93**, 184204 (2016). Referenced on page: 111

[218] Y. Bar Lev, D. R. Reichman, and Y. Sagi. *Many-body localization in system with a completely delocalized single-particle spectrum*. Phys. Rev. B **94**, 201116 (2016). Referenced on page: 111

[219] K. Hyatt, J. R. Garrison, A. C. Potter, and B. Bauer. *Many-body localization in the presence of a small bath*. Phys. Rev. B **95**, 035132 (2017). Referenced on page: 111

[220] R. Nandkishore. *Many-body localization proximity effect*. Phys. Rev. B **92**, 245141 (2015). Referenced on page: 111

[221] N. Marzari, A. A. Mostofi, J. R. Yates, I. Souza, and D. Vanderbilt. *Maximally localized Wannier functions: Theory and applications*. Rev. Mod. Phys. **84**, 1419–1475 (2012). Referenced on page: 113

[222] M. Modugno. *Exponential localization in one-dimensional quasi-periodic optical lattices*. New J. Phys page 033023 (2009). Referenced on page: 114

Acknowledgments

My journey from Udaipur to Munich has been a long one, and there are a LOT of people who have defined my years. In this little space, it would only be appropriate to thank people with whom I have interacted academically.

First and foremost, I would like to thank my supervisor, Prof. Immanuel Bloch, who gave me the opportunity to learn and grow in this group in 2010 and again from 2013. He has continued to inspire me every single day, directly via discussions and indirectly, by his approach to experimental physics. He has been tremendously kind to me, and despite his very busy schedule, has *always* managed to take time out. I am indebted.

I am also thankful to Dr. Ulich Schneider for frequent discussions and in particular, for the help with many basic questions during the initial stages of my graduate time. I would also like to thank all my collaborators and in particular, Prof. Ehud Altman and Prof. Michael Knap for many useful discussions and explanations. I am grateful to Michael Schreiber and Sean Hodgman for having taught me almost everything that I know in the lab with so much energy and enthusiasm. Henrik Lüschen has been around for my entire time in Munich, and we have shared a great amount of time in the lab. I particularly enjoyed our complementary approaches to the experiment. I am also grateful to two very smart people who did their Master's thesis in my lab, Frederik Görg and Pau Gomez, for many fun times and for explaining me their results.

Outside my lab, I am grateful to Tracy Li and Ahmed Omran for numerous weekend discussions on all sorts of topics, ranging from the genus of the torus to the choices in life. Your absence was felt during the last year. I would also like to thank people at LMU, especially Sebastian Scherg, Thomas Kohlert, Martin Reitter, Michael Lohse, Christian Schweizer, Monika Aidelsburger and Simon Fölling for various discussions, Berlin, optics and coffee complaints. I am sure such traditions would continue with the new graduate students. On many afternoons and conferences, I have also thoroughly enjoyed discussing with MPQ people, and I am thankful to Christian Gross, Johannes Zeiher, Jaeyoon Choi, Sebastian Hild, Martin Boll and Timon Hilker. I acknowledge Bodo Hecker's technical assistances, with always a big smile on the face. I am grateful for the invaluable help from Ildiko Kecskesi, Marianne Kargl, and Kristina Schuldt. With Ildiko especially on my side, German bureaucracy seems vincible.

It takes a village to raise a child. My Ph.D. was a result of my community of people in Munich who are very dear to me. I thank them from the bottom of my heart. Far away from me are also the people who have lost the most for my gain. I don't know how to fill my absence on Holi and Diwali and how I will make up for all the important times I could not be with them. To thank them, I would not even know where to begin. Today, I will not attempt the impossible.